

FAULT-TOLERANT CAPABILITY OF STAR-
CONNECTED SYMMETRICAL SIX-PHASE INDUCTION
MACHINE WITH SINGLE AND TWO
ISOLATED NEUTRALS

WAN NORAISHAH WAN ABDUL MUNIM

INSTITUTE FOR ADVANCED STUDIES
UNIVERSITY OF MALAYA
KUALA LUMPUR

2020

**FAULT-TOLERANT CAPABILITY OF STAR-
CONNECTED SYMMETRICAL SIX-PHASE
INDUCTION MACHINE WITH SINGLE AND TWO
ISOLATED NEUTRALS**

WAN NORAISHAH WAN ABDUL MUNIM

**THESIS SUBMITTED IN FULFILMENT OF THE
REQUIREMENTS FOR THE DEGREE OF
DOCTOR OF PHILOSOPHY**

**INSTITUTE FOR ADVANCED STUDIES
UNIVERSITY OF MALAYA
KUALA LUMPUR**

2020

UNIVERSITY OF MALAYA
ORIGINAL LITERARY WORK DECLARATION

Name of Candidate: WAN NORAISHAH WAN ABDUL MUNIM

Matric No: HHD140006

Name of Degree: DOCTOR OF PHILOSOPHY

Title of Thesis ("this Work"): FAULT-TOLERANT CAPABILITY OF STAR-
CONNECTED SYMMETRICAL SIX-PHASE INDUCTION MACHINE
WITH SINGLE AND TWO ISOLATED NEUTRALS

Field of Study: MACHINES AND DRIVES

I do solemnly and sincerely declare that:

- (1) I am the sole author/writer of this Work;
- (2) This Work is original;
- (3) Any use of any work in which copyright exists was done by way of fair dealing and for permitted purposes and any excerpt or extract from, or reference to or reproduction of any copyright work has been disclosed expressly and sufficiently and the title of the Work and its authorship have been acknowledged in this Work;
- (4) I do not have any actual knowledge nor do I ought reasonably to know that the making of this work constitutes an infringement of any copyright work;
- (5) I hereby assign all and every rights in the copyright to this Work to the University of Malaya ("UM"), who henceforth shall be owner of the copyright in this Work and that any reproduction or use in any form or by any means whatsoever is prohibited without the written consent of UM having been first had and obtained;
- (6) I am fully aware that if in the course of making this Work I have infringed any copyright whether intentionally or otherwise, I may be subject to legal action or any other action as may be determined by UM.

Candidate's Signature

Date:

Subscribed and solemnly declared before,

Witness's Signature

Date:

Name:

Designation:

**FAULT-TOLERANT CAPABILITY OF STAR-CONNECTED SYMMETRICAL
SIX-PHASE INDUCTION MACHINE WITH SINGLE AND TWO
ISOLATED NEUTRALS**

ABSTRACT

Traditionally, electrical machines have been designed to operate with single- or three-phase power supplies. In the early stage of power electronics development, three-phase machine suffers problems such as high torque ripple due to low order harmonics during six-step switching and limited current handling capacity of the power switches. This has motivated the use of multiphase machines which is capable of mitigating the aforementioned issues. The revival of multiphase machine research is mainly motivated by the need for more reliable drive systems. The vector space decomposition (VSD) model is used for a healthy multiphase machine as the basis for control to transform the phase variables to the decoupled stationary-frame variables, which consist of flux and torque producing α - β components and loss producing x - y and zero sequence components. For normal operation, the machine is controlled by regulating the α - β current components while keeping the x - y and zero sequence components to zero. The discussed control structure become invalid when the machine suffers from fault, such as when one of the phase connection is open-circuited. However, the multiphase machine is capable to continue operation during fault with smooth torque if proper post-fault control is applied. This research presents a study of fault-tolerant of star-connected symmetrical six-phase induction machine (S6-IM) by evaluating the capability of S6-IM in terms of current and voltage limits. This thesis proposes the comparison between single (1N) and two isolated neutral points (2N) considering up to three simultaneous open-circuit faults. Indirect rotor field-oriented control (IRFOC) is used to generate the α , β , x , y , θ_+ and θ_- reference voltages. Vector control separately regulates the torque and flux producing components

of the stator current and hence requires accurate current control which can be achieved using a linear current regulation. Meanwhile, reconfiguration of the controller is minimized when transiting from pre-fault to post-fault operation based on normal decoupling transformation without changing the machine parameter. Two modes of post-fault operation namely minimum loss (ML) and maximum torque (MT) are further analyzed. The maximum torque is expected to be the same as the optimal amplitude. Moreover in post-fault operation, the voltage limit analysis plays an important element for post-fault control as the voltage limit has a direct impact on the speed limit. Hence, machine voltage equations require accurate knowledge of the machine parameters, especially for the rotor time constant in IRFOC. The machine equation in the $\alpha\beta$ frame is used to perform machine parameter estimation. The accuracy of the estimated machine parameter is crucial to determine the maximum line-to-line voltages. Hence, a test rig capable of implementing and evaluating the fault-tolerant operation of an S6-IM is developed. The simulation and experimental results obtained confirm the validity and efficiency of the most suitable proposed method for the fault-tolerant capability of star-connected S6-IM with single and two isolated neutrals.

Keywords: Fault-tolerant drives, field-oriented control, six-phase machines, machine parameter, voltage limit.

**KEUPAYAAN TOLERANSI KEROSAKAN MESIN ARUHAN ENAM FASA
BERSIMETRI SAMBUNGAN BINTANG DENGAN SATU DAN
DUA NEUTRAL**

ABSTRAK

Secara tradisinya, mesin elektrik telah direka untuk beroperasi dengan bekalan kuasa fasa tunggal atau bekalan kuasa tiga fasa. Pada peringkat awal pembangunan elektronik kuasa, mesin tiga fasa mengalami masalah seperti riak tork yang tinggi disebabkan oleh harmonik aras rendah semasa pensuisan enam langkah dan arus yang terhad untuk mengendali kapasiti suis kuasa. Ini telah mendorong penggunaan mesin berbilang fasa yang mampu mengurangkan isu-isu yang telah disebutkan di atas. Kebangkitan semula penyelidikan mesin berbilang fasa didorong terutamanya oleh keperluan sistem pemacu yang lebih dipercayai. Ruang vektor penguraian (VSD) model digunakan oleh mesin berbilang fasa yang sempurna keadaannya yakni tidak rosak sebagai asas kawalan untuk mengubah pembolehubah fasa kepada pembolehubah kerangka-bergerak yang dipisahkan, yakni yang terdiri daripada fluks dan tork dimana ia menghasilkan komponen α - β dan elemen kehilangan menghasilkan x - y dan jujukan komponen sifar. Untuk operasi biasa, mesin dikawal dengan mengawal komponen arus α - β sambil mengekalkan komponen x - y dan jujukan komponen sifar kepada sifar. Struktur kawalan yang dibincangkan menjadi tidak sah apabila mesin mengalami kerosakan, contohnya apabila satu sambungan fasa di litar buka. Walau bagaimanapun, mesin berbilang fasa mampu untuk meneruskan operasi dengan tork yang lancar jika berlaku kerosakan; tetapi dengan syarat kawalan selepas kerosakan yang betul digunakan. Cadangan penyelidikan ini membincangkan tentang kajian toleransi kerosakan mesin aruhan enam-fasa bersimetri (S6-IM) sambungan bintang menerusi penilaian keupayaan mesin aruhan enam-fasa bersimetri dari segi had arus dan voltan. Kertas cadangan ini mencadangkan perbandingan di antara satu (1N) dan dua titik neutral terpencil (2N) merangkumi

sehingga tiga kerosakan litar terbuka. Kawalan berorientasikan bidang rotor secara tidak langsung (IRFOC) digunakan untuk mengawal voltan rujukan α , β , x , y , θ_+ and θ_- . Kawalan vektor mengawal secara berasingan tork dan fluks; yakni elemen yang menghasilkan komponen-komponen arus stator dan oleh yang demikian, ia memerlukan kawalan arus yang tepat yang boleh dicapai dengan menggunakan kawalan arus linear. Sementara itu, konfigurasi semula pengawal dapat dikurangkan apabila ia transit dari operasi pra-kerosakan kepada operasi pasca-kerosakan berdasarkan kepada transformasi nyahgandingan yang biasa. Dua mod operasi pasca-kerosakan seperti kehilangan minimum (ML) dan tork maksimum (MT) akan dianalisis. Tork maksimum dijangka memberi keputusan yang sama dengan amplitud yang optimum. Selain itu dalam operasi pasca-kerosakan, analisis had voltan memainkan elemen penting untuk kawalan pasca-kerosakan kerana had voltan mempunyai kesan langsung pada had laju. Oleh itu, persamaan voltan mesin memerlukan pengetahuan yang tepat tentang parameter mesin, terutamanya untuk pemalar masa rotor di dalam IRFOC. Persamaan mesin dalam kerangka α - β digunakan untuk melaksanakan anggaran parameter mesin. Ketepatan parameter mesin yang dianggarkan adalah penting untuk menentukan maksimum voltan dari satu fasa ke fasa yang lain. Oleh itu, ujian-kaji yang mampu melaksana dan menilai operasi toleransi kerosakan mesin aruhan enam-fasa bersimetri akan dilakukan. Keputusan simulasi yang diperolehi akan mengesahkan kesahihan dan keberkesanan kaedah yang paling sesuai dicadangkan untuk keupayaan toleransi kerosakan mesin aruhan enam fasa bersimetri sambungan bintang dengan satu dan dua neutral.

Kata kunci: Pemacu toleransi kerosakan, Kawalan berorientasikan bidang rotor, mesin enam-fasa, parameter mesin, had voltan.

ACKNOWLEDGEMENTS

First and foremost, I would like to express my gratitude to Allah, the Almighty for His blessing and guidance during preparing this thesis. Genuinely, I would like to record my appreciation and grateful thanks towards the late Professor Dr. Ir. Hew Wooi Ping and Dr. Che Hang Seng, my supervisors in Power Energy Dedicated Advanced Centre (UMPEDAC), University of Malaya, for their constructive ideas, guidance and supervision throughout completing this thesis. I was very lucky to have the opportunity to be supervised with an extraordinary person who is knowledgeable and expert in this field. I especially appreciate the contribution of Dr. Che Hang Seng for his inspiration and assistance. He is a very passionate with his work and personally, I was driven by his motivation to be a good researcher. Discussions with Dr. Che Hang Seng had been tremendously helpful and contributed to a big part of my thesis.

I also would like to express my gratitude to Dr. Mahdi Tousizadeh for the useful advice, comments and suggestions which has facilitated the completion of my research. My warmest thanks goes to my friends and colleagues in UMPEDAC, it was truly a pleasure to work with you guys.

I would like to acknowledge University of Teknologi MARA (UiTM) and Kementerian Pendidikan Tinggi (KPT) for sponsoring my study in UM and providing the financial support.

Last and most importantly, I owe my deepest appreciation and special thanks to my family members for all their support. To my beloved husband, Faizan, my kids, Faqih Naufal, Ammar Fahim and baby Faseeha Aulya, thank you for your endless love, infinite patience and encouragement. To my dearest parents, Wan Abdul Munim and Wan Ainun, my mother in law, Che Siah thank you for your support, prayers and care. This thesis would not be possible without you all.

TABLE OF CONTENTS

Abstract	iii
Abstrak	v
Acknowledgements	vii
Table of Contents	viii
List of Figures	xii
List of Tables	xvi
List of Symbols and Abbreviations	xvii
List of Appendices	xx
CHAPTER 1: INTRODUCTION	1
1.1 Background of Study	1
1.2 Problem Statements	4
1.3 Research Objectives	4
1.4 Scope of Study	5
1.5 Thesis Novelty and Originality	5
1.6 Thesis Structure	5
CHAPTER 2: LITERATURE REVIEW	7
2.1 Introduction	7
2.2 Operation of Healthy Multiphase Machine	8
2.2.1 Control of S6 Machine based on Vector Space Decomposition Approach	9
2.2.2 Current Limits	11
2.2.3 Voltage Limits	11
2.3 Operation of Post-fault Multiphase Machine	12
2.3.1 Fault-tolerant Control based on Vector Space Decomposition Approach	15

2.3.2	Current Limits	18
2.3.2.1	Operation with Minimum Loss (ML).....	20
2.3.2.2	Operation with Maximum Torque (MT).....	21
2.3.2.3	Optimization of Post-Fault Currents	21
2.3.3	Voltage Limits	22
2.4	Conclusion	23

CHAPTER 3: POST-FAULT CURRENT LIMITS OF SYMMETRICAL SIX-PHASE INDUCTION MACHINE24

3.1	Introduction.....	24
3.2	Types of Open-Phase Fault and Machine Equations.....	27
3.2.1	S6-IM under One Phase Loss - Single Isolated Neutral (1 OPF-1N)	28
3.2.2	S6-IM under One Phase Loss - Two Isolated Neutrals (1 OPF-2N).....	29
3.2.3	S6-IM under Two Phases Loss - Single Isolated Neutral (2 OPFs-1N)...	31
3.2.4	S6-IM under Two Phases Loss -Two Isolated Neutrals (2 OPFs-2N)	32
3.2.5	S6-IM under Three Phases Loss - Single Isolated Neutral (3 OPFs-1N).34	
3.2.6	S6-IM under Three Phases Loss - Two Isolated Neutrals (3 OPFs-2N)..35	
3.3	Simulation Results for the S6-IM under 1 OPF to 3 OPFs	37
3.4	Experimental Results and Discussion.....	42
3.4.1	Verification of Current Limits.....	42
3.4.2	Fault-tolerant Performance Comparison with A6 and D3.....	45
3.5	Conclusion	47

CHAPTER 4: MACHINE PARAMETERS ESTIMATION USING CLOSED-LOOP CONTROL SIGNALS CURVE FITTING49

4.1	Introduction.....	49
4.2	Existing Machine Parameter Estimation Methods for Multiphase Machines	49

4.3	Proposed Machine Parameters Estimation Method.....	51
4.3.1	Effect of Inverter Non-idealities and Parasitic Impedance.....	53
4.3.2	Selection of Machine Equation Reference Frame.....	55
4.4	Theoretical Voltage Equations for S6 Induction Machine.....	55
4.4.1	Voltage Equations in α - β Subspace.....	56
4.4.2	Parameter Estimation in x - y and θ - Subspaces.....	57
4.5	Parameter Estimation Process	58
4.6	Results and Discussions.....	61
4.6.1	Experimental Validation of the Proposed Method.....	61
4.6.2	Verification of Estimated Parameters under Different Operating Points.....	64
4.7	Conclusions	67
 CHAPTER 5: POST-FAULT VOLTAGE LIMITS OF SYMMETRICAL SIX-PHASE INDUCTION MACHINE		68
5.1	Introduction.....	68
5.2	Line-to-Line Voltages of Symmetrical Six-phase Induction Machine.....	71
5.3	Line-to-Line Voltages of Symmetrical Six-phase Induction Machine under Different Operating Points.....	74
5.4	Results and Discussions.....	75
5.4.1	Voltage against Synchronous Frequency, ω_s	76
5.4.2	Voltage against Slip Frequency, ω_{slip}	81
5.5	Conclusions	91
 CHAPTER 6: CONCLUSIONS AND FUTURE WORKS		93
6.1	Conclusions	93
6.2	Future Works	95
	References	97

List of Publications and Papers Presented	105
Journal Paper	105
Conference Paper	105
Appendix A	106
Appendix B	117
Appendix C	122
Appendix D	135

University of Malaya

LIST OF FIGURES

Figure 1.1: Three mainstream six-phase machines: (a) D3: Dual three-phase machine ($\gamma = 0^\circ$) (b) A6: Asymmetrical six-phase machine ($\gamma = 30^\circ$) and (c) S6: Symmetrical six-phase machine ($\gamma = 60^\circ$)	2
Figure 2.1: (a) Single and two neutrals connection (b) six-phase induction motor with a generic spatial shifting γ between three-phase windings	9
Figure 2.2: Vector representation of S6 under different fault scenarios. Note: Dotted line indicates open-circuited phase windings.....	15
Figure 2.3: Dual-PI controllers	17
Figure 3.1: Fault-tolerant control scheme with DSRF (dual PI) controllers in the x-y current loop	25
Figure 3.2: Dual PI current control of x-y currents	25
Figure 3.3: Dual PI current control of $0+0-$ currents.....	25
Figure 3.4: Stator phase currents in 1 OPF with 1N	37
Figure 3.5: Stator phase currents in 2 OPFs (case 2a) with 1N	38
Figure 3.6: Stator phase currents in 2 OPFs (case 2b) with 1N	38
Figure 3.7: Stator phase currents in 2 OPFs (case 2c) with 1N	38
Figure 3.8: Stator phase currents in 2 OPFs (case 2d) with 1N	39
Figure 3.9: Stator phase currents in 3 OPFs (case 3a) with 1N	39
Figure 3.10: Stator phase currents in 3 OPFs (case 3b) with 1N	39
Figure 3.11: Stator phase currents in 3 OPFs (case 3c) with 1N	40
Figure 3.12: Stator phase currents in 3 OPFs (case 3d) with 1N	40
Figure 3.13: Stator phase currents in 1 OPF with 2N	40
Figure 3.14: Stator phase currents in 2 OPFs (case 2a) with 2N	41
Figure 3.15: Stator phase currents in 2 OPFs (case 2b) with 2N	41
Figure 3.16: Stator phase currents in 2 OPFs (case 2d) with 2N	41

Figure 3.17: Stator phase currents in 3 OPFs (case 3a) with 2N	42
Figure 3.18: Test 1 (scenario 1) for S6-2N. From top to bottom: (a) Motor speed; (b) d - q currents; (c) phase currents of winding 1 and (d) phase currents of winding 2.	43
Figure 3.19: Test 2 (scenario 2a) for S6-1N. From top to bottom: (a) Motor speed; (b) d - q currents; (c) phase currents of winding 1 and (d) phase currents of winding 2.	44
Figure 3.20: Test 3 (scenario 3a) for S6-1N. From top to bottom: (a) Motor speed; (b) d - q currents; (c) phase currents of winding 1 and (d) phase currents of winding 2.	45
Figure 4.1: Typical six-phase machine	52
Figure 4.2: Ideal six-phase induction machine	52
Figure 4.3: Fault-tolerant control scheme with DSRF (dual PI) controllers in the x - y current loop	53
Figure 4.4: Disturbance added with additional impedance becomes an effective impedance	54
Figure 4.5: Flowchart showing the overall parameter estimation process	59
Figure 4.6: Theoretical V_{xy} and experimental V_{xy} after optimized for 1 OPF-1N	62
Figure 4.7: Theoretical V_{0-} and experimental V_{0-} after optimized for 1 OPF-1N	62
Figure 4.8: Theoretical $V_{\alpha\beta}$ and experimental $V_{\alpha\beta}$ after optimized for 1 OPF-1N	63
Figure 4.9: Machine parameters based on tests 1, 3, 5 (1400 rpm) and tests 2, 4, 6 (350 rpm) for healthy S6 machine. From top to bottom: (a) L_m ; (b) $L_{ls\alpha\beta}$; (c) R_r ; (d) $L_{lr\alpha\beta}$	63
Figure 4.10: Comparison of experimental V_{line} with theoretical V_{line} calculated using estimated machine parameters under 1 OPF-1N.....	64
Figure 4.11: Percentage average error of estimated machine parameter under different operating points and i_{qs} in healthy operation.....	65
Figure 4.12: Percentage average error of estimated machine parameter under different operating points and ω_{slip} in healthy operation	65
Figure 4.13: Maximum line-to-line voltages under different ω_{slip} at rated ω_s in healthy operation.....	66
Figure 4.14: Maximum line-to-line voltages under different ω_{slip} at rated ω_s in 1OPF with 2N operation.....	66

Figure 4.15: Maximum line-to-line voltages under different ω_{slip} at rated ω_s in 1OPF with 1N operation.....	67
Figure 5.1: Maximum line voltage constraint for S6-1N, where $V_{dc} = V_{LLpeak}$	68
Figure 5.2: Voltage limit for S6-IM configured with 1N and 2N.....	69
Figure 5.3: Magnitude of phase voltage and line-to-line voltage of symmetrical six-phase induction machine	72
Figure 5.4: Line-to-line voltage representation of symmetrical six-phase induction machine under healthy operation	73
Figure 5.5: Voltage limit under different ω_s at rated ω_{slip} and rated current in healthy operation.....	77
Figure 5.6: Voltage limit under different ω_s at rated ω_{slip} and rated current in 1 OPF with 2N operation.....	78
Figure 5.7: Voltage limit under different ω_s at rated ω_{slip} and rated current in 1 OPF with 1N operation.....	78
Figure 5.8: Voltage limit under different ω_s at rated ω_{slip} and rated current in 2 OPFs (case 2a) with 2N operation	78
Figure 5.9: Voltage limit under different ω_s at rated ω_{slip} and rated current in 2 OPFs (case 2a) with 1N operation	79
Figure 5.10: Voltage limit under different ω_s at rated ω_{slip} and rated current in 2 OPFs (case 2b) with 2N operation	79
Figure 5.11: Voltage limit under different ω_s at rated ω_{slip} and rated current in 2 OPFs (case 2b) with 1N operation	79
Figure 5.12: Voltage limit under different ω_s at rated ω_{slip} and rated current in 2 OPFs (case 2c) with 1N operation	80
Figure 5.13: Voltage limit under different ω_s at rated ω_{slip} and rated current in 3 OPFs (case 3a) with 2N operation	80
Figure 5.14: Voltage limit under different ω_s at rated ω_{slip} and rated current in 3 OPFs (case 3a) with 1N operation	80
Figure 5.15: Voltage limit under different ω_{slip} at rated ω_s and rated current in healthy operation.....	82

Figure 5.16: Voltage limit under different ω_{slip} at rated ω_s and rated current in 1 OPF with 2N operation.....	83
Figure 5.17: Voltage limit under different ω_{slip} at rated ω_s and rated current in 1 OPF with 1N operation.....	83
Figure 5.18: Voltage limit under different ω_{slip} at rated ω_s and rated current in 2 OPFs (case 2a) with 2N operation	83
Figure 5.19: Voltage limit under different ω_{slip} at rated ω_s and rated current in 2 OPFs (case 2a) with 1N operation	84
Figure 5.20: Voltage limit under different ω_{slip} at rated ω_s and rated current in 2 OPFs (case 2b) with 2N operation	84
Figure 5.21: Voltage limit under different ω_{slip} at rated ω_s and rated current in 2 OPFs (case 2b) with 1N operation	84
Figure 5.22: Voltage limit under different ω_{slip} at rated ω_s and rated current in 2 OPFs (case 2c) with 1N operation	85
Figure 5.23: Voltage limit under different ω_{slip} at rated ω_s and rated current in 3 OPFs (case 3a) with 2N operation	85
Figure 5.24: Voltage limit under different ω_{slip} at rated ω_s and rated current in 3 OPFs (case 3a) with 1N operation	85
Figure 5.25: Healthy (left plot) and 1 OPF (right plot) for S6-2N. From top to bottom: (a) phase currents; (b) line voltages.....	86
Figure 5.26: Comparison of current and voltage limit for 1 OPF with 2N and healthy at rated current	87
Figure 5.27: 2 OPFs (case 2b) for S6-2N: (a) rated phase currents; (b) modulating signals (c) line voltages	88
Figure 5.28: Line-to-line voltage vector representation of symmetrical six-phase induction machine in healthy (named without hat) and post-fault (named with hat) for case 2c with 1N at rated ω_s and rated $\omega_{slip} = 10$ rad/s.....	89
Figure 5.29: Line-to-line voltage vector representation of symmetrical six-phase induction machine in healthy (named without hat) and post-fault (named with hat) for case 2c with 1N at rated ω_s and rated $\omega_{slip} = 30$ rad/s.....	90

LIST OF TABLES

Table 2.1: Independent fault scenarios for S6-IM under 1N and 2N.....	15
Table 3.1: 6 possibilities of open-phase fault when one phase missing.....	27
Table 3.2: 15 possibilities of open-phase fault when two phases missing.....	30
Table 3.3: 20 possibilities of open-phase fault when three phases missing.....	32
Table 3.4: Reconfiguration of x - y and θ_+ - θ_- reference currents in post-fault situation (MT) for all independent scenarios in S6 (a) 1N and (b) 2N.....	36
Table 3.5: Reconfiguration of x - y and θ_+ - θ_- reference currents in post-fault situation (ML) for all independent scenarios in S6 (a) 1N and (b) 2N.....	36
Table 3.6: Reconfiguration of x - y and θ_+ - θ_- reference currents in post-fault situation (MT) for all independent scenarios in A6 and D3 with (a) 1N (b) 2N	46
Table 4.1: Estimated parameters for S6-IM.....	64
Table 5.1: Line-to-line voltages for healthy operation.....	72
Table 5.2: Line-to-line voltages for symmetrical six-phase machine based on neutral connections 1N and 2N for post-fault operation	73
Table 5.3: Maximum slip frequency ω_{slip} based on neutral connections 1N and 2N for different post-fault scenarios and derating factor, a	75
Table 5.4: Maximum line-to-line voltages in case 2c with 1N under different ω_{slip}	88
Table 5.5: Maximum line-to-line voltages comparison between $\omega_{slip}=10$ rad/s and $\omega_{slip}=30$ rad/s in case 2c with 1N.....	90

LIST OF SYMBOLS AND ABBREVIATIONS

Symbols

a	:	Derating factor
d	:	d -component after rotational transformation
f	:	Frequency
i_r	:	Rotor current (A)
i_s	:	Stator current (A)
K	:	Coefficient
L_{lm}	:	Mutual leakage inductance (H)
L_{lr}	:	Rotor leakage inductance (H)
L_{ls}	:	Stator leakage inductance (H)
L_m	:	Magnetizing inductance (H)
L_r	:	Rotor inductance (H)
L_s	:	Stator inductance (H)
K_{inv}	:	Gain of inverter
p	:	Number of pole pair
P	:	Active power (W)
q	:	q -component after rotational transformation
r	:	Rotor variable
R	:	Resistance (Ω)
R_r	:	Rotor resistance (Ω)
R_s	:	Stator resistance (Ω)
s	:	Stator variable
T	:	Torque (Nm)
$[T]$:	Decoupling (stationary) transformation matrix

V_{dc}	:	DC-link voltage (V)
V_{dis}	:	Disturbance voltage (V)
v_r	:	Rotor voltage (V)
v_s	:	Stator voltage (V)
V_{ZSI}	:	Zero-sequence signal voltage
γ	:	Arbitrary angle
\wedge	:	Theoretical quantities
$0+$:	Positive zero sequence components
$0-$:	Negative zero sequence components
α	:	α -component after decoupling transformation
β	:	β -component after decoupling transformation
δ	:	Angle between the largest two phases within the same winding
ψ	:	Flux (Wb)
ψ_r	:	Rotor flux (Wb)
ψ_s	:	Stator flux (Wb)
τ_r	:	Rotor time constant (s)
ω_m	:	Rotor mechanical speed (rad ^s)
ω_r	:	Rotor electrical speed (rad ^s)
ω_s	:	Synchronous frequency (rad ^s)
ω_{slip}	:	Slip frequency (rad ^s)
x	:	x -component after decoupling transformation
y	:	y -component after decoupling transformation

Abbreviations

1N	:	Single isolated neutral
2N	:	Two isolated neutrals

A6	:	Asymmetrical six-phase
CMV	:	Common-mode voltage
D3	:	Dual three-phase
DTC	:	Direct torque control
FOC	:	Flux oriented control
FOT	:	Full-order transformation
FRML	:	Full-range minimum loss
FT	:	Fault-tolerant
IGBT	:	Insulated-gate bipolar transistor
IM	:	Induction machine
ML	:	Minimum loss
MMF	:	Magneto-motive force
MPC	:	Model-based predictive control
MT	:	Maximum torque
OCF	:	Open-circuit fault
OPF	:	Open-phase fault
PI	:	Proportional integral (controller)
PR	:	Proportional resonant (controller)
PWM	:	Pulse-width modulation
ROT	:	Reduced-order transformation
S6	:	Symmetrical six-phase
V/F	:	Volt/Frequency
VSC	:	Voltage source converter
VSD	:	Vector space decomposition

LIST OF APPENDICES

Appendix A: Matlab/Simulink and dSPACE	106
Appendix B: Test Rig	117
Appendix C: Zero-Sequence Transformations and Min-Max Injection	122
Appendix D: Table of Coefficients for S6 and D3 Machines	135

University of Malaya

CHAPTER 1: INTRODUCTION

1.1 Background of Study

Since the invention of electrical machines in the 19th century, single- and three-phase machines have been the major type of electric machines due to the fact that existing power supplies are mainly single- or three-phase. However, the advancements in power electronics technology these days have enabled the utilization of electric drives with phase numbers higher than three. Over the years, it is known that multiphase drives give some benefits over three-phase drives such as reducing the current per phase without increasing the voltage per phase, lowering DC harmonics and high reliability (Levi, 2008). In particular, the higher fault tolerance has motivated the use of multiphase machines in applications such as electrical or hybrid vehicles (Diallo, Benbouzid, & Makouf, 2004; Parsa & Toliyat, 2007; Simões & Vieira, 2002), “more electric” ships (Sulligoi & Tassarolo, 2009, 2013) and aircraft (Bennett, Mecrow, Atkinson, & Atkinson, 2011; Cao, Mecrow, Atkinson, Bennett, & Atkinson, 2012), offshore wind farms generators (Andresen & Birk, 2007; Gjerde & Undeland, 2012), high-speed elevators (Jung, Yoo, Sul, Choi, & Choi, 2012), where robustness of the drive system is of paramount importance.

Even though the use of five-phase (Guzman et al., 2016; Guzman, Barrero, & Duran, 2015; Guzman, Duran, Barrero, Bogado, & Toral, 2014), seven-phase (Tani, Mengoni, Zarri, Serra, & Casadei, 2012) and eleven-phase (Ashoush, Gadoue, Abdel-Khalik, & Mohamadein, 2011) drives has drawn attention within the scientific community, the development of multiphase demonstrations and industrial products has been mainly restricted to machines with multiple sets of three-phase windings (Cao et al., 2012; Jung et al., 2012). This is fundamentally due to the fact that $3k$ -phase machines inherit the well-established three-phase technology and this reduces, to some extent, the uncertainty in

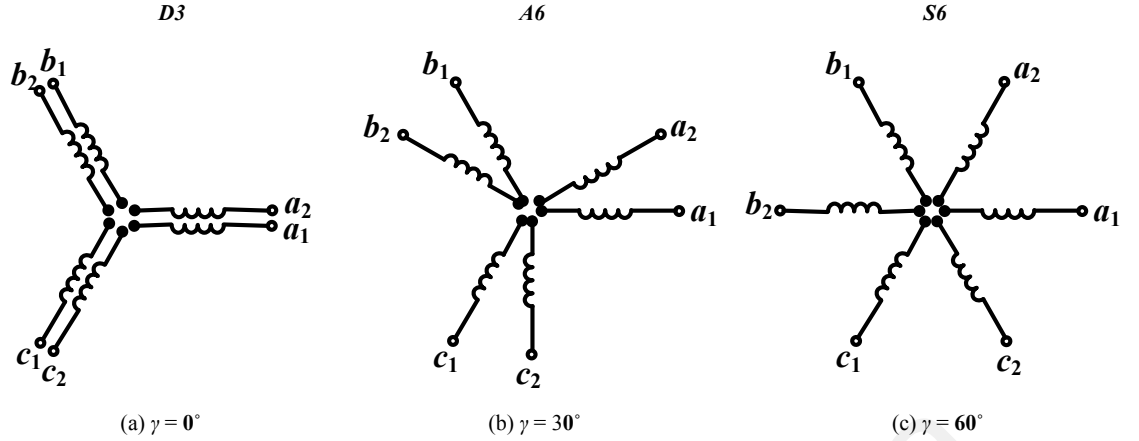


Figure 1.1: Three mainstream six-phase machines: (a) D3: Dual three-phase machine ($\gamma = 0^\circ$) (b) A6: Asymmetrical six-phase machine ($\gamma = 30^\circ$) and (c) S6: Symmetrical six-phase machine ($\gamma = 60^\circ$)

new developments. Among different multiphase machines, six-phase machines have received the most attention from the research community.

There are three mainstream six-phase machines which differ in terms of the phase angle between the two three-phase windings namely asymmetrical (A6), symmetrical (S6), and dual three-phase (D3) as shown in Figure 1.1. For all S6, A6, and D3, the stator windings can be configured with two three-phase windings. By connecting all six-phases together as $a1-b1-c1-a2-b2-c2$ in one winding or connecting two separated three-phase windings as $a1-b1-c1$ and $a2-b2-c2$, it can be configured as single isolated neutral point (1N) or two isolated neutral points (2N) respectively. 1N improves fault tolerance as it gives an additional degree of freedom. However, it allows zero sequence currents to flow which cause distortion to the phase currents and result in losses. On the other hand, 2N eliminates the 1N problem in terms of zero sequence current.

The main advantage of a six-phase machine is its ability to continuously operate after fault, particularly open-circuit fault between the inverter and the machine, which is also known as open-phase fault (OPF). Over the years, various research works have been dedicated to the study of fault-tolerant six-phase drives (Ayman S. Abdel-Khalik, Hamdy, Massoud, & Ahmed, 2018; Bermudez et al., 2017; Hang Seng Che, Duran, et al., 2014; Gonzalez-Prieto, Duran, & Barrero, 2017). Even though it has been demonstrated that the six-phase machine can continue to operate smoothly after OPFs, the machine has to be derated to satisfy current limits. The study of post-fault machine derating has been done for five-phase (A. S. Abdel-Khalik, Masoud, Ahmed, & Massoud, 2014) and A6 (Hang Seng Che, Levi, Jones, Hew, & Rahim, 2014) machines concerning mainly the current limit. More recently, it was pointed out that apart from current limits, the voltage limits should also be considered when determining the fault-tolerant capability of multiphase machines (Ayman S Abdel-Khalik, Massoud, & Ahmed, 2018).

In this thesis, the fault-tolerant capability of star-connected S6-IM with 1N and 2N is evaluated by taking into consideration both current and voltage limits under different OPFs. Determining voltage limits for S6-IM requires accurate knowledge of the machine parameter. Hence machine parameters estimation using closed-loop control waveforms curve fitting are used to further analyze the voltage limits of S6-IM. Three areas have been identified as the focus of this thesis: current limit, machine parameter estimation and voltage limit.

1.2 Problem Statements

The main problem statements of this thesis are as follows:

- i. Till date, the post-fault current limits for asymmetrical six-phase and symmetrical six-phase machines have been explored, but with a limited number of open-phase faults. There is a lack of understanding on the complete post-fault current limits under all possible open-phase fault scenarios.
- ii. Apart from current limits, voltage limits are also an important factor that will determine the performance of a machine, particularly in terms of the maximum achievable speed, and hence, power. However, there is a lack of discussion on the voltage limits of the symmetrical six-phase machine under open-phase faults.
- iii. Unlike current limits, the voltage limits of an induction machine depend on the machine parameters. An effective method for machine parameters estimation is required to allow accurate determination of the post-fault voltage limits.

1.3 Research Objectives

The main objectives of this research are as follows:

- i. To identify the post-fault current limits of a symmetrical six-phase induction machine considering all possible combinations of open-phase faults.
- ii. To propose machine parameters estimation technique to be used in voltage equations for evaluating post-fault voltage limits of a symmetrical six-phase induction machine.
- iii. To identify the post-fault voltage limits of a symmetrical six-phase induction machine considering all possible combinations of open-phase faults.

1.4 Scope of Study

The scope of this study is mainly focused on S6-IM with 1N and 2N configurations. In this thesis, both current and voltage limits of S6-IM are investigated to provide additional contributions to the control of the machine.

For this project, a dSPACE1103 rapid prototyping platform is used to perform the control using a two-level voltage source inverter. 0.55 kW three-phase induction machine is used for experimental verifications. OPFs are created by physically disconnecting the inverter from the motor phases using relays.

1.5 Thesis Novelty and Originality

The novel contribution provided by this thesis are as follows:

- i. Identification of the post-fault current limits for symmetrical six-phase induction machine configured with single and two isolated neutrals under different OPF are presented in Chapter 3.
- ii. Development of machine parameters estimation technique using closed-loop control signals curve fitting method as reported in Chapter 4.
- iii. Identification of the post-fault voltage limits for symmetrical six-phase induction machine, considering the effect of slip frequency, ω_{slip} and synchronous frequency, ω_s as highlighted in Chapter 5.

1.6 Thesis Structure

This thesis is structured as follows: Chapter 2 gives a detailed literature review in the areas associated with the topics covered in the thesis highlighting the recent work related to symmetrical six-phase. Chapters 3, 4 and 5 provide the main contributions of this thesis: Chapter 3 investigates post-fault current limits for S6-IM configured with two neutral points and single neutral point under different OPF conditions.

Chapter 4 discusses the machine parameters estimation technique using closed-loop control signals curve fitting. By using the measured currents and the machine voltage equations, the theoretical voltages for the machine can be calculated using some initial values for the machine parameters. The machine parameters are optimized by minimizing the theoretical voltage and the actual control voltages, accurate machine parameters can be obtained. It is shown that the estimated machine parameters are accurate enough to predict the control voltage references under varying operating conditions.

Chapter 5 investigates the voltage limits of post-fault S6-IM under different operating conditions. It is demonstrated that the maximum line-to-line voltage is heavily influenced by ω_{slip} and ω_s , which in turn decide the post-fault voltage limits for S6 under different OPFs. Using the estimated machine parameters, the maximum line-to-line voltage under different OPFs can be identified through machine equations, which are confirmed using experimental results. It is shown that the voltage limit is not significant for the S6 machine studied in this project, and the current limit is the main limiting factor for the post-fault performance of the machine.

Finally, Chapter 6 gives a summary of the work done and proposes some potential topics for future work.

In addition, some materials useful for understanding the project have been included in appendices. Appendix A shows the developed simulation model of S6-IM using Matlab/Simulink software. The experimental setup used for testing the S6-IM is described in Appendix B. Appendix C shows the effect of zero-sequence transformations and min-max injection on the fault-tolerant symmetrical six-phase drive with single isolated neutral. Lastly, Appendix D gives the post-fault current coefficients for maximum torque and minimum loss operation of S6 and D3 machines under different fault scenarios and neutral connections.

CHAPTER 2: LITERATURE REVIEW

2.1 Introduction

Since beginning of the 20th century, the use of multiphase (more than three-phase) machines have been explored (Levi, Barrero, & Duran, 2015) for their various advantages over conventional three-phase machines, such as reducing the current per phase without increasing the voltage per phase, lowering DC harmonics and increasing reliability (Levi, Bojoi, Profumo, Toliyat, & Williamson, 2007). Even though the multiphase grid does not exist by default, advanced applications of power electronics these days have enabled the use of multiphase electric drives with literally no restriction on the number of phases. This has opened the possibility for the utilization of multiphase machines on applications such as electric vehicles (Subotic, Bodo, Levi, & Jones, 2015), “more electric” ships and aircraft (Cao et al., 2012), offshore wind farm generators (Hang Seng Che, Levi, Jones, Duran, et al., 2014), high-speed elevators (Jung et al., 2012) and etc.

One particular important feature of the multiphase machine is its inherent fault tolerance which makes it favorable in safety critical applications. Hence, various research works have been devoted to the development and study of fault-tolerant multiphase machines and drives, particularly in terms of fault-tolerant machine design (Ayman S. Abdel-Khalik, Elgenedy, Ahmed, & Massoud, 2016; Cavagnino, Li, Tenconi, & Vaschetto, 2013; Huang, Goodman, Gerada, Fang, & Lu, 2012; Xue et al., 2013; Zhang, Hua, Cheng, & Liao, 2016), modelling (Pantea et al., 2016; Shao, Hua, Dai, & Shao, 2016) and control (Hang Seng Che, Levi, Jones, Hew, et al., 2014; Hang Seng Che, Duran, et al., 2014; Gonzalez-Prieto et al., 2016).

Based on the literature reviewed, discussions on the operations of healthy and post-fault multiphase drives are presented in subsequent sections of this chapter, with focus on the following three areas:

- i. Control based on vector space decomposition approach
- ii. Current limits
- iii. Voltage limits

2.2 Operation of Healthy Multiphase Machine

The six-phase drive consists of a six-phase induction motor with two sets of three-phase windings ($a_1b_1c_1$ and $a_2b_2c_2$) independently supplied by two IGBT-based two-level voltage source converters (VSC₁ and VSC₂). Three-phase windings 1 and 2 are star-connected as shown in Figure 2.1(a) and neutrals n_1 and n_2 can be either isolated, resulting in a two neutrals configuration (2N), or connected in the single neutral arrangement (1N).

Generally, the three-phase windings 1 and 2 are considered to be spatially shifted an arbitrary angle γ as illustrated in Figure 2.1(b) i.e. for S6. Following are the three mainstream six-phase machines:

- D3: Dual three-phase machine ($\gamma = 0^\circ$)
- A6: Asymmetrical six-phase machine ($\gamma = 30^\circ$)
- S6: Symmetrical six-phase machine ($\gamma = 60^\circ$)

The six-phase machine is fed with phase currents $i_{a1}, i_{b1}, i_{c1}, i_{a2}, i_{b2}, i_{c2}$.

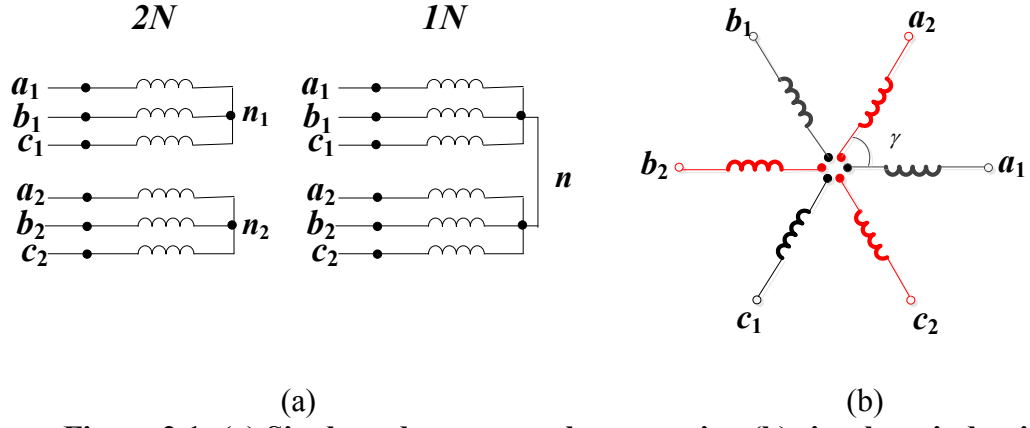


Figure 2.1: (a) Single and two neutrals connection (b) six-phase induction motor with a generic spatial shifting γ between three-phase windings

2.2.1 Control of S6 Machine based on Vector Space Decomposition Approach

The phase currents can be mapped into $\alpha, \beta, x, y, 0_+$ and 0_- components using the vector space decomposition (VSD) approach and the generalized Clarke transformation matrix which is given by

$$[\alpha \quad \beta \quad x \quad y \quad 0_+ \quad 0_-]^T = [T6] \cdot [a_1 \quad b_1 \quad c_1 \quad a_2 \quad b_2 \quad c_2]^T \quad (2.1)$$

In the literature, there are two six-phase decoupling transformation matrices that are commonly considered for S6 machine, given as follows

$$[T6] = [T_{ind}] = \frac{1}{\sqrt{3}} \cdot \begin{bmatrix} 1 & \cos(\theta) & \cos(2\theta) & \cos(\gamma) & \cos(\theta + \gamma) & \cos(2\theta + \gamma) \\ 0 & \sin(\theta) & \sin(2\theta) & \sin(\gamma) & \sin(\theta + \gamma) & \sin(2\theta + \gamma) \\ 1 & \cos(2\theta) & \cos(\theta) & -\cos(\gamma) & -\cos(\theta + \gamma) & -\cos(2\theta + \gamma) \\ 0 & \sin(2\theta) & \sin(\theta) & \sin(\gamma) & \sin(\theta + \gamma) & \sin(2\theta + \gamma) \\ 1 & 1 & 1 & 0 & 0 & 0 \\ 0 & 0 & 0 & 1 & 1 & 1 \end{bmatrix} \quad (2.2)$$

$$[T_6] = [T_{comb}] = \frac{1}{\sqrt{3}} \cdot$$

$$\begin{bmatrix} 1 & \cos(\theta) & \cos(2\theta) & \cos(\gamma) & \cos(\theta + \gamma) & \cos(2\theta + \gamma) \\ 0 & \sin(\theta) & \sin(2\theta) & \sin(\gamma) & \sin(\theta + \gamma) & \sin(2\theta + \gamma) \\ 1 & \cos(2\theta) & \cos(\theta) & -\cos(\gamma) & -\cos(\theta + \gamma) & -\cos(2\theta + \gamma) \\ 0 & \sin(2\theta) & \sin(\theta) & \sin(\gamma) & \sin(\theta + \gamma) & \sin(2\theta + \gamma) \\ 1/\sqrt{2} & 1/\sqrt{2} & 1/\sqrt{2} & 1/\sqrt{2} & 1/\sqrt{2} & 1/\sqrt{2} \\ 1/\sqrt{2} & 1/\sqrt{2} & 1/\sqrt{2} & -1/\sqrt{2} & -1/\sqrt{2} & -1/\sqrt{2} \end{bmatrix} \quad (2.3)$$

where $\theta = 2\pi/3$ and $\gamma = \pi/3$.

The main difference between the two decoupling matrices $[T_{comb}]$ and $[T_{ind}]$ lies on the transformation for the θ_+ and θ_- components which are the last two rows of the matrices. The α - β currents are solely responsible for the flux and torque production in distributed-winding machines, while the x - y currents are theoretically not involved in the energy conversion process. Zero sequence currents θ_+ and θ_- can flow in 1N but they are zero in 2N.

In healthy operation, the steady-state six-phase currents form a balanced set with equal amplitudes. In healthy operation, the x - y currents are null and the α - β current phasor describes a circle translating into a rotating MMF that smoothly drives the machine with constant torque where

$$|I_{\alpha peak}| = |I_{\beta peak}|. \quad (2.4)$$

If the six-phase windings are treated as two separate sets of three-phase windings, i.e. $a_1b_1c_1$ and $a_2b_2c_2$, the zero-sequence currents for each respective winding set can be defined as

$$\begin{aligned} i_{01} &= i_{a1} + i_{b1} + i_{c1} \\ i_{02} &= i_{a2} + i_{b2} + i_{c2}. \end{aligned} \quad (2.5)$$

For S6-2N, the zero-sequence current cannot flow, therefore the θ_+ and θ_- currents can be neglected regardless of the choice of the transformation matrix. However, for the S6-

1N, the zero-sequence currents can flow, depending on the choice of the transformation matrix.

For $[T_{ind}]$, both 0_+ and 0_- currents can flow. As a matter of fact, the two currents are not independent but have equal magnitude and opposite signs, such that

$$i_{0+} + i_{0-} = 0. \quad (2.6)$$

For $[T_{comb}]$, 0_+ current will sum to zero while the 0_- current theoretically would be zero only in healthy operation. The $[T_{comb}]$ is selected in this thesis hereafter.

2.2.2 Current Limits

The current limit for a healthy drive is determined based on the rated phase current i.e. when the machine running at rated synchronous frequency, ω_s and rated slip frequency, ω_{slip} . For normal operation, the machine is controlled by regulating the α - β current components while keeping the x - y and zero sequence components to zero.

2.2.3 Voltage Limits

Unlike current limits, the voltage limits of the multiphase machine depend on the machine parameters. To allow accurate determination of the voltage limits, an effective method for estimating machine parameters is needed (Ayman S Abdel-Khalik et al., 2018).

In addition, the maximum utilization of DC-bus voltage under the linear modulation region for healthy operation is defined when the peak value of the line voltage is equal to the DC-bus voltage (Levi, Dujic, Jones, & Grandi, 2008). The voltage limit of a star-connected six-phase machine can be varied based on the neutral connections either using 1N or 2N.

2.3 Operation of Post-fault Multiphase Machine

Nowadays, the scope of research mainly concentrates on short-circuit and open-circuit faults albeit the fault in machine and drives can happen in many other forms, such as driving circuit fault, power electronics failures, broken rotor bar, machine insulation failure, magnet demagnetization, and etc. The research publications of fault-tolerant drives can be generally categorized into three aspects based on their areas of contributions namely fault-tolerant machine design, fault detection and post-fault control.

Majority of the researchers focus on designing of the machines that are inherently tolerant to faults (Alberti & Bianchi, 2012; M. Barcaro, Bianchi, & Magnussen, 2009; Massimo Barcaro, Bianchi, & Magnussen, 2010; Bianchi, Bolognani, & Pr , 2008; Semail, Locment, Ensam, & Xiv, 2008) such that the machine itself would be designed tolerant to the fault current level in order to eliminate the short-circuit fault. Contrarily, limited attention is on fault detection as the open-circuit fault and short-circuit fault can be detected using current measurement. (Zarri et al., 2013) and (Mengoni et al., 2014) proposed a method for detecting high resistance connections to be investigated into the typical drives. As of today, the majority of studies on fault-tolerant multiphase drives aiming at the control aspect of the machine after the occurrence of the fault, i.e. fault-tolerant control.

Regardless of the motivation to use a $3k$ -phase machine (Gonzalez-Prieto, Duran, & Barrero, 2017), the existence of multiple (redundant) windings opens the possibility to withstand open-circuit faults (OCFs) with no extra hardware and smooth post-fault operation. The post-fault capability is however dependent on the arrangement of the supplying voltage source converters (VSCs). If the DC-links are cascaded, the fault tolerance is lost unless one uses parallel converters (Hang Seng Che, Levi, Jones, Duran, et al., 2014; Gjerde, Olsen, Lj kels y, & Undeland, 2014) and if the DC-links are

independent then the OCFs imply the disconnection of the whole three-phase VSC (Ditmanson, Hein, Kolb, Mölck, & Bernet, 2014). The fault tolerance can, however, be improved by using a single DC-link because the power oscillations of the faulted VSC can be compensated by the healthy ones obtaining a constant DC-link power (Hang Seng Che, Duran, et al., 2014; M. Duran et al., 2016).

It is noted that the OCFs can occur as either open IGBT fault or open-phase fault (OPF). The former case refers to the condition where one or more IGBT(s) in a converter leg is open-circuited, due to either IGBT gating failure (Guzman et al., 2015) or fault remedial control (e.g. for the one-transistor trigger suppression control in (Ginart, Kalgren, Roemer, Brown, & Abbas, 2010)), such that the freewheeling diode(s) is still functional.

On the other hand, OPF refers to the case where one or more phase connection(s) between the converter and machine is completely open-circuited, due to poor connection issues (Tani et al., 2012) or fault remedial actions that disconnect the phase using protection devices such as circuit breakers or fuses (Ryu, Kim, & Sul, 2006). While the two cases represent significantly different OPFs, it has been demonstrated in (Guzman et al., 2015) that standard post-fault strategy based on OPF gives satisfactory performance even during open IGBT faults (if the two switches in the same leg are kept open but the freewheeling diodes are operational). Furthermore, an open IGBT fault can be converted into an OPF using additional protection devices, which can help to reduce deterioration of the drive during post-fault operation (Guzman et al., 2015). Hence in this thesis, the OCF considered is referring to the OPF.

In addition, the post-fault performances of six-phase induction motor drives considering up to three simultaneous open-circuit faults are investigated. Although the faults are schematically indicated in the figure as open-phases (Barrero & Duran, 2016),

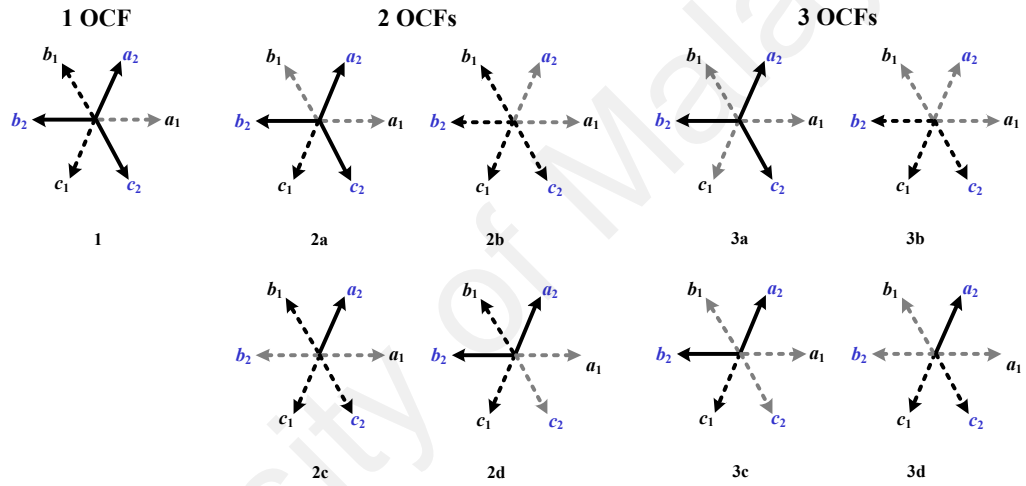
(Guzman et al., 2016, 2015, 2014), (H. S. Che et al., 2013; M. Duran et al., 2016; Ginart et al., 2010; Ryu et al., 2006; Tani et al., 2012), (Ayman S. Abdel-Khalik et al., 2016; Pantea et al., 2016; Xue et al., 2013), (Gonzalez-Prieto et al., 2016), they correspond in general to machine faults, poor connection between the machine and the converter or IGBT faults that are subsequently converted into open-phase faults (OPFs) by proper isolation after the fault detection.

In principle, there are 41 different fault scenarios for arbitrary values of γ , but only a maximum of seven independent fault scenarios remain for S6 machine, respectively if configured with single isolated neutral. Moreover, maximum of three independent fault scenarios remain for the S6 under two isolated neutrals. These independent scenarios are shown as shaded boxes in Table 2.1. The winding configurations under various fault scenarios are further illustrated in Figure 2.2 for the S6 machine.

The reductions in the number of independent fault scenarios are due to two distinctively different reasons: structural symmetry and single-phase operation. In the “structural symmetry” cases, the post-fault machines in two or more fault scenarios have similar post-fault structure. This gives rise to the same post-fault current waveforms (but different phase order), same derating factor are hence considered redundant. For example, case 2d for S6 is a redundant scenario for case 2b, as indicated in Table 2.1. Apart from structural symmetry, there are scenarios where α and/or β currents are no longer controllable, making condition (2.4) impossible. In such scenarios, the machine is reduced to be equivalent to a single-phase machine, and post-fault operation is not possible. Such single-phase operation scenarios are indicated as “-” in Table 2.1.

Table 2.1: Independent fault scenarios for S6-IM under 1N and 2N

<i>No.OPF</i>	<i>Scenario</i>	<i>Faulty ph.</i>	<i>1N</i>	<i>2N</i>
			<i>S6</i>	<i>S6</i>
<i>1 OPF</i>	<i>1</i>	<i>a₁</i>		
<i>2 OPFs</i>	<i>2a</i>	<i>a₁-b₁</i>		<i>(3a)</i>
	<i>2b</i>	<i>a₁-a₂</i>		
	<i>2c</i>	<i>a₁-b₂</i>		-
	<i>2d</i>	<i>a₁-c₂</i>	<i>(2b)</i>	<i>(2b)</i>
<i>3 OPFs</i>	<i>3a</i>	<i>a₁-b₁-c₁</i>		
	<i>3b</i>	<i>a₁-b₁-a₂</i>		-
	<i>3c</i>	<i>a₁-b₁-c₂</i>		-
	<i>3d</i>	<i>a₁-b₁-b₂</i>	<i>(3c)</i>	-

**Figure 2.2: Vector representation of S6 under different fault scenarios. Note: Dotted line indicates open-circuited phase windings**

2.3.1 Fault-tolerant Control based on Vector Space Decomposition Approach

Over the years, several fault-tolerant control strategies have been proposed for multiphase machines (Ayman S. Abdel-Khalik, Ahmed, Elserougi, & Massoud, 2015; Ayman S. Abdel-Khalik et al., 2016; Guzman et al., 2016, 2014), including six-phase machines (Baudart et al., 2012; M. Duran et al., 2016; Gonzalez-Prieto et al., 2016; Kianinezhad, Nahid-Mobarakeh, Baghli, Betin, & Capolino, 2008; Pantea et al., 2016; Shamsi-Nejad, Nahid-Mobarakeh, Pierfederici, & Meibody-Tabar, 2008). Some other controllers have also been introduced for OPF operation using scalar V/F (Ayman S.

Abdel-Khalik et al., 2015, 2018; Sayed-Ahmed & Demerdash, 2012), direct torque control (DTC) (Bermudez et al., 2016; Y. Zhou, Lin, & Cheng, 2016) and model-based predictive control (MPC) (Guzman et al., 2016, 2015). Despite the differences, majority of the methods are based on field-oriented control (FOC) (Hang Seng Che, Levi, Jones, Hew, et al., 2014; M. J. Duran, Gonzalez-Prieto, Rios-Garcia, & Barrero, 2018; M. Duran et al., 2016), where the machine phase variables are transformed into stationary or rotating reference frame variables using suitable transformation matrix before being controlled using controllers such as PI-controller, PR-controller, predictive controller, etc.

The control strategies hence rely on the choice of decoupling transformation (or extended Clarke transformation) matrix $[T]$ which can be broadly classified into two categories: control using reduced-order transformation (ROT) (Kianinezhad et al., 2008; Pantea et al., 2016; Ryu et al., 2006; Zhao & Lipo, 1996a, 1996b; H. Zhou, Zhao, Liu, Cheng, & Xie, 2017) and control using full-order transformation (FOT) (Baudart et al., 2012; Hang Seng Che, Levi, Jones, Hew, et al., 2014; Hang Seng Che, Duran, et al., 2014; Locment, Semail, & Kestelyn, 2008; Tani et al., 2012). Between the two, the FOT approach provides a simpler control that uses the same transformation matrices and same machine parameters, with minimal changes to the control structure as the machine transit from healthy into post-fault operation.

Different methods have been proposed for current reference determination. Authors in (Guzman et al., 2014; Kianinezhad et al., 2008; Ryu et al., 2006; Zhao & Lipo, 1996a, 1996b) proposed a reduced-order decoupling transformation, as a medium for representing the machine during post-fault operation. Based on this reduced-order decoupling transformation, the current references are then derived in order to achieve the desired post-fault operation.

However, the machine parameters need to be taken into account as the execution of this approach is not direct. (Baudart et al., 2012) on the other hand introduced a more complex approach, where a fault identification matrix is required in completing the control scheme. Authors (Baudart et al., 2012; Hang Seng Che, Duran, et al., 2014; Locment et al., 2008; Tani et al., 2012) focus on fault-tolerant control scheme that has least changes when transiting from pre-fault to post-fault operation where the authors maintained the same decoupling transformation and only changed the current references during post-fault operations.

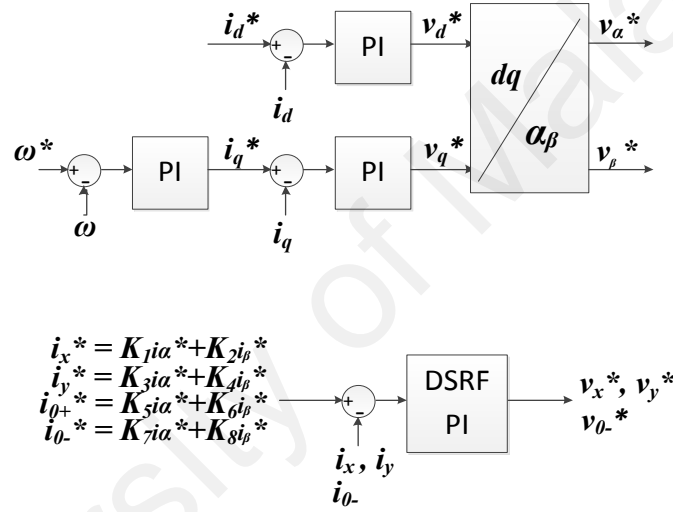


Figure 2.3: Dual-PI controllers

The implementation of fault-tolerant control is essentially divided into two stages. The first stage associates with deciding the post-fault current references where the second stage will control the currents to follow their designated references.

Following the VSD optimization approach described in Section 2.2.1, it is possible to determine the relationship between x - y - 0 - 0_+ and α - β currents for the S6 machine in all possible scenarios and neutral arrangements (see Table 2.1). It is, however, necessary to include this information into a suitable fault-tolerant control scheme in order to smoothly drive the six-phase machine after the fault occurrence. The standard indirect rotor-flux field-oriented control (IRFOC) (Levi et al., 2007) can be applied in the post-fault situation

to generate the $\alpha\beta$ reference voltages, but the regulation of the x - y plane requires to main changes: *i)* it is necessary to switch for null pre-fault values to those shown in Table 2.1 and *ii)* it is necessary to use proportional-resonant (PR) controllers, or equivalent dual-PI regulators in synchronous and anti-synchronous references frames as shown in Figure 2.3. The use of PR controllers allows tracking ac x - y reference currents with good performance (H. S. Che et al., 2013; M. Duran et al., 2016; Guzman et al., 2016).

The modified x - y current loop provides x - y reference voltages that, together with the $\alpha\beta$ reference voltages from the IRFOC are transformed into phase values for the modulation stage that finally provides the switching signals to the VSCs. Apart from the number of dual PI regulators (i.e. one less in 2N case), the control scheme remains the same regardless of the six-phase machine and neutral connection.

2.3.2 Current Limits

The derating factor (a) is used to examine the performance of the machines after fault. It is per unit value of the post-fault $\alpha\beta$ current phasor modulus, with a limitation that the maximum post-fault phase current does not exceed the rated phase current (Hang Seng Che, Duran, et al., 2014) is given by

$$a = \frac{|I_{\alpha\beta}|_{Post-fault}}{|I_{\alpha\beta}|_{Rated}} \quad (2.7)$$

Derating factor can be used to evaluate the post-fault torque available for a given faulted machine without violating the nominal current limit. A higher derating factor indicates a higher maximum torque can be obtained for a given current limit.

The key issue in the system reconfiguration is thus to define new current references that comply with restrictions (2.4)-(2.6), but the solution is not unique. Since the number of unknowns is higher than the number of restrictions the problem is undetermined, and

consequently, there is room to optimize the post-fault currents. In order to do that, new optimized post-fault current references need to be defined, based on the minimum loss (ML) and maximum torque (MT) optimization objectives commonly used in literature.

One of the most acclaimed features of the multiphase machine is its ability to tolerate open-circuit faults in its phase windings. To do this, a suitable set of new (post-fault) current references is necessary to avoid negative sequence components in the fundamental magneto-motive force (MMF) of the machine, which will otherwise manifest as undesirable torque and speed oscillations. Over the years, many works have been devoted to the optimization of such post-fault current references for different multiphase machines, based on different optimization targets.

Open-circuit faults for dedicated phase such as five-phase machine has been reported by (Ryu et al., 2006) highlighting both minimum loss and maximum torque while (Ayman S. Abdel-Khalik et al., 2015) has proposed the calculation of derating factor to avoid overheating of the machine after fault occurrence and maximum torque in order to maintain equal phase currents. On the other hand, a different approach using the Lagrange multiplier method has been investigated in (Baudart et al., 2012) for six-phase machine focusing on minimum loss only and in (Tani et al., 2012) for seven-phase machine solving minimum loss and maximum torque in transient and steady-state operating conditions. Nevertheless, the overall comparison of post-fault performance for faulted n -phase indicating minimum loss, maximum torque as well as derating factor still not been stated yet in literature.

To obtain a better overall view of the post-fault performance for machines with different phase numbers, some researchers have performed analysis on a range of multiphase machines. (Fu & Lipo, 1994) presented post-fault current analysis for three- to seven-phase induction machines with the aim of equalizing amplitude of all remaining

currents after fault whereas in (Zheng, Fletcher, & Williams, 2006) uses the symmetrical component transformation based on Fortescue to analyze the stator copper loss minimization and the inverter peak current minimization for three- to nine-phase machines in steady-state operating conditions. In addition, (Baudart et al., 2012) addressed the minimum loss of three- to eight-phase machines operating under open-phase conditions. However, the derating factor which is the restriction of the maximum post-fault current does not exceed the rated phase current to maintain the reliability of the system has not been considered in (Baudart et al., 2012).

Based on the literature reviewed, three optimizations objectives are found to be common: equalizing current amplitudes after fault, minimizing copper losses and maximizing torque/power under a given current limit. Among these, minimum loss (ML) and maximum torque (MT) are of particular importance. Full-range minimum loss (FRML) post-fault strategy for dual-three phase machine has been proposed by (Baneira, Doval-Gandoy, Yepes, Lopez, & Perez-Estevez, 2017) as a hybrid strategy to have the best combination features of MT and ML. Similar concept of FRML has been adopted by (Ayman Samy Abdel-Khalik, Hamad, Massoud, & Ahmed, 2017) for nine-phase six-terminal induction machine.

2.3.2.1 Operation with Minimum Loss (ML)

When the phase a_l current, i_{al} is restricted to zero, the objective of ML is to minimize the stator copper losses defined by the cost function J_{ML}

$$J_{ML} = \min\{\sqrt{(i_\alpha^2 + i_\beta^2 + i_x^2 + i_y^2 + i_{0+}^2 + i_{0-}^2)}\} \quad (2.8)$$

However, ML will results in unequal phase currents i.e.: S6 results in two sets of equal phase currents and one phase current with different amplitude. This mode also leads to the reduction of maximum achievable torque.

2.3.2.2 Operation with Maximum Torque (MT)

Since the inverter is usually designed to operate with current limited to the nominal value, this current limit should be obeyed even during fault to avoid damaging the drive. Hence, in the MT post-fault operation, the aim is to minimize the maximum phase current of the remaining healthy phases. This is equivalent to the inverter peak current minimization used in (Zheng et al., 2006). In this case, the cost function J_{MT} targets to maximize the torque, which in turn indicates maximizing the amplitude of the α - β phasor

$$J_{MT} = \max(|I_{\alpha\beta}|) \quad (2.9)$$

Subject to:

- $I_{fault} = 0 \in \{\text{Faulted phases}\}$
 - $i_{0+} = 0$
 - min the maximum phase current $\in \{\text{Healthy phases}\}$.
- (2.10)

2.3.2.3 Optimization of Post-Fault Currents

There are various ways to optimize the post-fault currents, and the approach in (Hang Seng Che, Duran, et al., 2014), i.e. based on decoupled variables, has been adopted here. Coefficients “ K ” are used to relate the non-energy-converting currents with the α - β references. For S6, only x - y currents and zero sequence 0 current need to be optimized, as shown in Equation (2.11). Zero sequence 0_+ is set to be zero.

$$i_x^* = K_1 \cdot i_\alpha^* + K_2 \cdot i_\beta^*$$

$$i_y^* = K_3 \cdot i_\alpha^* + K_4 \cdot i_\beta^*$$

$$i_{0+}^* = K_5 \cdot i_\alpha^* + K_6 \cdot i_\beta^*$$

$$i_{0-}^* = K_7 \cdot i_\alpha^* + K_8 \cdot i_\beta^* \quad (2.11)$$

A non-linear optimization method, i.e. the generalized reduced gradient (GRG) approach, provided by “Solver”, an add-on in MS Office Excel is used to optimize the post-fault currents. The optimization objectives for ML and MT modes are based on (2.8) and (2.9) respectively and are subject to (2.10). The coefficients will be varied at each iteration and the subsequent phase currents amplitudes are obtained by applying inverse decoupling transformation matrix $[T]^{-1}$ onto the VSD currents.

2.3.3 Voltage Limits

Apart from current limits, the capability of a machine should also be evaluated in terms of voltage limits. The performance of fault-tolerant control for three-phase induction motor drives considering current and voltage limit have been recently investigated by (Tousizadeh, Che, Abd Rahim, Selvaraj, & Ooi, 2018).

For fault-tolerant of multiphase machines, the DC-link voltage limitations for some open phases to obtain optimum currents in the remaining healthy phases have been investigated (A. S. Abdel-Khalik et al., 2014; Ayman S Abdel-Khalik et al., 2018; Eldeeb, Abdel-Khalik, & Hackl, 2019).

In some cases, the DC-link is assumed to be sufficiently high for the controller to operate in post-fault operation without going into the overmodulation region. If the stator voltage exceeds 1 p.u. and alpha-beta trajectory goes into the overmodulation region, there is a need to utilize the available DC-link voltage without exceeding the machine voltage and current rating (Levi et al., 2008).

In order to evaluate the voltage limit of the multiphase machine, the accuracy of machine parameters (Hang Seng Che, Abdel-Khalik, Dordevic, & Levi, 2017) is essential to calculate the voltage equations in terms of α - β , x - y and $0+0$ - subspaces. The effect of DC-link limitation together with machine parameters identification using steady-state

circuit that combines all sub-spaces in a single circuit has been proposed by (Abdel-Khalik et al. 2018). Based on the literature reviewed, it was found that the maximum line voltage is a function of rated line voltage and machine parameters (Abdel-Khalik et al. 2018). Here, the existing literature is reviewed based on fault tolerance point of view which will incorporate both machine parameters and determination of maximum line voltage.

2.4 Conclusion

Relevant studies have been reviewed for the healthy and faulty operation of the multiphase machine. The existing control of the six-phase machine based on VSD methods have been reported from the view of current and voltage limits. The available fault-tolerant control strategies in literature are then analyzed to identify a suitable approach for S6-IM. From the survey literature, there is no comparative analysis of the fault-tolerant capability of star-connected S6-IM considering both current and voltage limits. A unified analysis is still missing considering different neutral connections, modes of operation and fault scenarios. Hence, this research aims to fill this gap and provide a complete picture of the fault-tolerant capability of star-connected S6-IM with 1N and 2N taking into account both current and voltage limits.

CHAPTER 3: POST-FAULT CURRENT LIMITS OF SYMMETRICAL SIX-PHASE INDUCTION MACHINE

3.1 Introduction

Traditionally, the asymmetrical six-phase machine has been favored over the other six-phase machines for its low torque ripples (Nelson & Krause, 1974). However, with the modern high-frequency pulse-width modulation (PWM) method, it has been shown that symmetrical six-phase machines can have similar torque performance as asymmetrical six-phase machines (Dujic et al., 2007). Thus, symmetrical six-phase machine can be considered as a promising alternative to the asymmetrical six-phase machine (Hang Seng Che & Hew, 2016). Application of symmetrical six-phase machine can be seen in electric vehicles (EVs) (Diab, Elserougi, Abdel-Khalik, Massoud, & Ahmed, 2016).

The fault tolerance of electric drives is highly appreciated at the industry for security and economic reasons, and the inherent redundancy of six-phase machines provides the desired fault-tolerant capability with no extra hardware. For this reason, some recent research focus has been placed mainly on the fault-tolerant design (Ayman S. Abdel-Khalik et al., 2016; Cavagnino et al., 2013; Huang et al., 2012; Xue et al., 2013; Zhang et al., 2016), modelling (Pantea et al., 2016; Shao et al., 2016) and control aspects [(Guzman et al., 2016, 2015, 2014), (Bojoi, Cavagnino, Tenconi, & Vaschetto, 2016; Gonzalez-Prieto, Duran, Barrero, Bermudez, & Guzman, 2017; Gonzalez-Prieto et al., 2016).

In order to preserve the integrity of the system, a mandatory derating of the system needs to be set after the fault occurrence (A. S. Abdel-Khalik et al., 2014). The asymmetrical six-phase machine achieved a maximum current production of 69.4% in 1N and 57.5% in 2N (Hang Seng Che, Duran, et al., 2014). However, the post-fault current/torque capability of the symmetrical six-phase machine has not been stated yet.

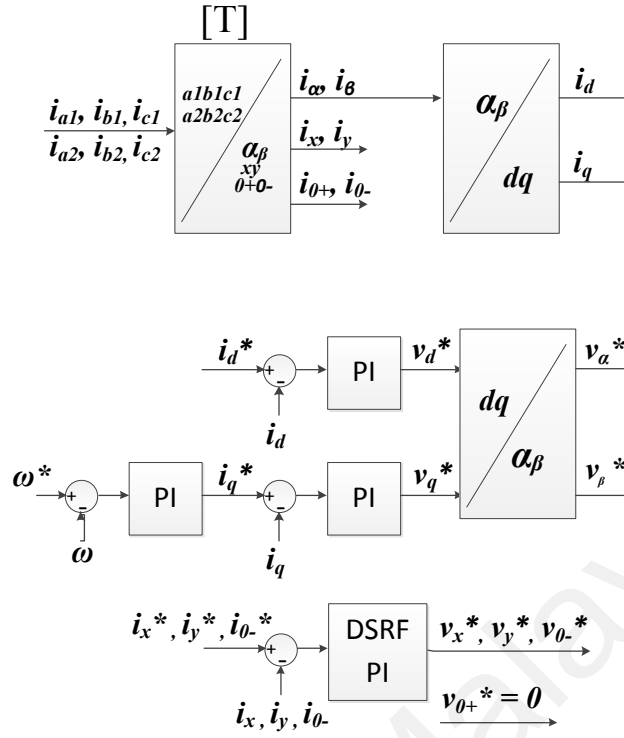


Figure 3.1: Fault-tolerant control scheme with DSRF (dual PI) controllers in the x-y current loop

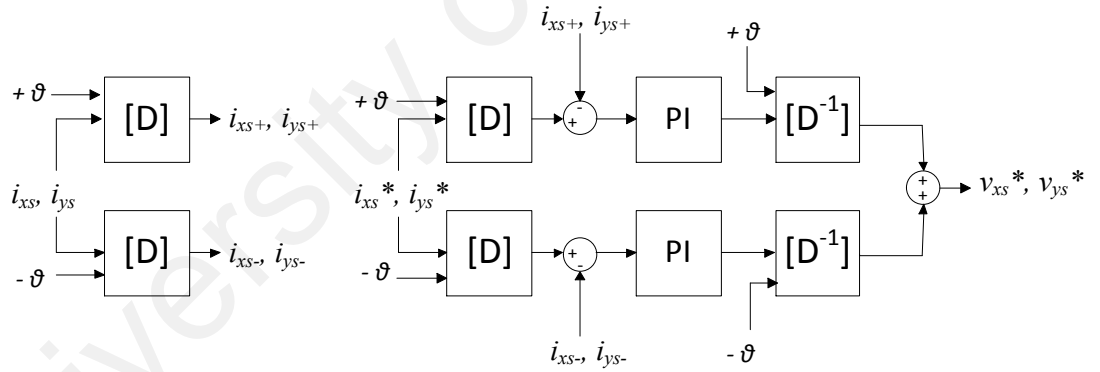


Figure 3.2: Dual PI current control of x-y currents

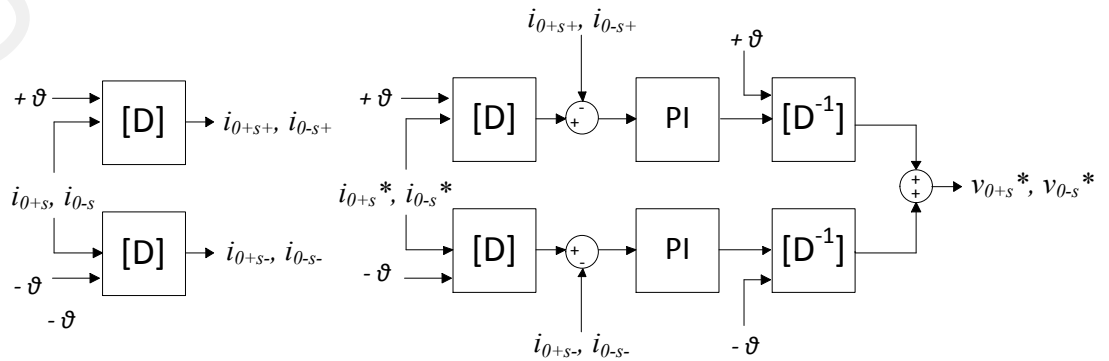


Figure 3.3: Dual PI current control of 0+0- currents

Nevertheless, a unified and conclusive analysis of the post-fault capability of symmetrical six-phase compared to other types of six-phase machine is still missing. This work provides a full picture of the post-fault derating and subsequently the post-fault current limits of the symmetrical six-phase machine.

Indirect rotor-flux field-oriented control (IRFOC) method based on SRF-PI and DSRF-PI controllers (Hang Seng Che, Duran, et al., 2014), as shown in Figure 3.1, is used to control the machine stator currents to follow the designated post-fault current references. The controller generates reference voltages in stationary reference frame (α , β , x , y , θ_+ and θ) which are then transformed into phase reference voltages, V_{a1}^* , V_{b1}^* , V_{c1}^* , V_{a2}^* , V_{b2}^* , V_{c2}^* using the inverse decoupling transformation $[T]^{-1}$.

Meanwhile, Figure 3.2 and Figure 3.3 show the dual PI use to control x - y currents and θ_+ - θ - currents respectively. However, only one DSRF-PI controller is need for θ - current control and $V_{\theta+}^*$ can be set to zero to further simplify the controller. A rotational transformation to transform the α - β variables into a synchronously rotating reference frame (d - q) can be also applied to x - y currents and θ - currents which given by

$$[D] = \begin{bmatrix} \cos \theta & \sin \theta \\ -\sin \theta & \cos \theta \end{bmatrix} \quad (3.1)$$

Experimental results confirm the theoretical post-fault current limits and allow concluding which is the best performance in terms of fault scenario and neutral arrangement for the symmetrical six-phase machine.

The chapter is structured as follows. Section 3.2 describes the type of open-circuit fault(s) and machine equations with single isolated neutral and two isolated neutrals. Section 3.3 provides the simulation results for 1 OPF to 3 OPFs. Section 3.4 compares the theoretical and experimental parts for S6-IM. In addition, a performance comparison

in terms of current limits with the other two mainstream machines (D3 and A6) for 1N and 2N in all possible scenarios are also investigated. Finally, the conclusion of this chapter is highlighted in Section 3.5.

3.2 Types of Open-Phase Fault and Machine Equations

Tables 3.1, 3.2 and 3.3 illustrate the stator winding arrangement from one up to three phases missing based on several cases. When phase $a1$ is open-circuited, i_{a1} is zero. While β and y currents are unaffected by this fault, the equations for α , x , $0+$, $0-$ currents become:

Table 3.1: 6 possibilities of open-phase fault when one phase missing

One phase missing	Faulted Stator Winding Arrangement
Case 1a: Phase- $a1$ or phase- $b2$	
Case 1b: Phase- $a2$ or phase- $c1$	
Case 1c: Phase- $b1$ or phase- $c2$	

$$\begin{aligned}
i_{as} &= \frac{1}{\sqrt{3}} \left(-\frac{1}{2}i_{b1} - \frac{1}{2}i_{c1} + \frac{1}{2}i_{a2} - i_{b2} + \frac{1}{2}i_{c2} \right) \\
i_{\beta s} &= \frac{1}{\sqrt{3}} \left(\frac{\sqrt{3}}{2}i_{b1} - \frac{\sqrt{3}}{2}i_{c1} + \frac{\sqrt{3}}{2}i_{a2} - \frac{\sqrt{3}}{2}i_{c2} \right) \\
i_{xs} &= \frac{1}{\sqrt{3}} \left(-\frac{1}{2}i_{b1} - \frac{1}{2}i_{c1} - \frac{1}{2}i_{a2} + i_{b2} - \frac{1}{2}i_{c2} \right) \\
i_{ys} &= \frac{1}{\sqrt{3}} \left(-\frac{\sqrt{3}}{2}i_{b1} + \frac{\sqrt{3}}{2}i_{c1} + \frac{\sqrt{3}}{2}i_{a2} - \frac{\sqrt{3}}{2}i_{c2} \right) \\
i_{0+s} &= \frac{1}{\sqrt{3}} \left(\frac{1}{\sqrt{2}}i_{b1} + \frac{1}{\sqrt{2}}i_{c1} + \frac{1}{\sqrt{2}}i_{a2} + \frac{1}{\sqrt{2}}i_{b2} + \frac{1}{\sqrt{2}}i_{c2} \right) \\
i_{0-s} &= \frac{1}{\sqrt{3}} \left(\frac{1}{\sqrt{2}}i_{b1} + \frac{1}{\sqrt{2}}i_{c1} - \frac{1}{\sqrt{2}}i_{a2} - \frac{1}{\sqrt{2}}i_{b2} - \frac{1}{\sqrt{2}}i_{c2} \right)
\end{aligned} \tag{3.2}$$

3.2.1 S6-IM under One Phase Loss - Single Isolated Neutral (1 OPF-1N)

If the machine is configured with single isolated neutral, $i_{a1} = 0$ meaning that $i_{b1} + i_{c1} + i_{a2} + i_{b2} + i_{c2} = 0$. Therefore, $i_{b1} + i_{c1} = -i_{a2} - i_{b2} - i_{c2}$.

$$\begin{aligned}
i_{as} &= \frac{1}{\sqrt{3}} \left(-\frac{1}{2}i_{b1} - \frac{1}{2}i_{c1} + \frac{1}{2}i_{a2} - i_{b2} + \frac{1}{2}i_{c2} \right) \\
i_{\beta s} &= \frac{1}{\sqrt{3}} \left(\frac{\sqrt{3}}{2}i_{b1} - \frac{\sqrt{3}}{2}i_{c1} + \frac{\sqrt{3}}{2}i_{a2} - \frac{\sqrt{3}}{2}i_{c2} \right) \\
i_{xs} &= \frac{1}{\sqrt{3}} \left(-\frac{1}{2}i_{b1} - \frac{1}{2}i_{c1} - \frac{1}{2}i_{a2} + i_{b2} - \frac{1}{2}i_{c2} \right) \\
i_{ys} &= \frac{1}{\sqrt{3}} \left(-\frac{\sqrt{3}}{2}i_{b1} + \frac{\sqrt{3}}{2}i_{c1} + \frac{\sqrt{3}}{2}i_{a2} - \frac{\sqrt{3}}{2}i_{c2} \right) \\
i_{0+s} &= \frac{1}{\sqrt{3}} \left(\frac{1}{\sqrt{2}}i_{b1} + \frac{1}{\sqrt{2}}i_{c1} + \frac{1}{\sqrt{2}}i_{a2} + \frac{1}{\sqrt{2}}i_{b2} + \frac{1}{\sqrt{2}}i_{c2} \right) = 0 \\
i_{0-s} &= \frac{1}{\sqrt{3}} \left(\frac{1}{\sqrt{2}}i_{b1} + \frac{1}{\sqrt{2}}i_{c1} - \frac{1}{\sqrt{2}}i_{a2} - \frac{1}{\sqrt{2}}i_{b2} - \frac{1}{\sqrt{2}}i_{c2} \right) = -\sqrt{2}(i_{xs} + i_{as})
\end{aligned} \tag{3.3}$$

The currents will be constrained by the following conditions:

For $i_{0-s} = \frac{1}{\sqrt{3}} \left(\frac{1}{\sqrt{2}}i_{b1} + \frac{1}{\sqrt{2}}i_{c1} - \frac{1}{\sqrt{2}}i_{a2} - \frac{1}{\sqrt{2}}i_{b2} - \frac{1}{\sqrt{2}}i_{c2} \right)$, we know that $i_{b1} + i_{c1} = -i_{a2} - i_{b2} - i_{c2}$.

Then, the simplified equation is given by

$$\begin{aligned}
i_{0-s} &= \frac{1}{\sqrt{3}} \left(\frac{1}{\sqrt{2}} i_{b1} + \frac{1}{\sqrt{2}} i_{c1} \frac{1}{\sqrt{2}} i_{b1} + \frac{1}{\sqrt{2}} i_{c1} \right) \\
i_{0-s} &= \frac{1}{\sqrt{3}} \left(\frac{1}{\sqrt{2}} (2(i_{b1} + i_{c1})) \right) \\
i_{0-s} &= \frac{1}{\sqrt{3}} (\sqrt{2} (i_{b1} + i_{c1}))
\end{aligned} \tag{3.4}$$

When $i_{xs} + i_{as}$, the equation will becomes $i_{xs} + i_{as} = \frac{1}{\sqrt{3}} (-i_{b1} - i_{c1})$. Hence, i_{0-s} can be expressed as

$$\begin{aligned}
i_{0-s} &= -\sqrt{2} (i_{xs} + i_{as}) \\
i_{0+s} &= 0 \\
i_{a1s} &= 0
\end{aligned} \tag{3.5}$$

3.2.2 S6-IM under One Phase Loss - Two Isolated Neutrals (1 OPF-2N)

If the machine is configured with two isolated neutrals, $i_{a1} = 0$ meaning that $i_{b1} = -i_{c1}$.

$$\begin{aligned}
i_{\alpha s} &= \frac{1}{\sqrt{3}} \left(-\frac{1}{2} i_{b1} - \frac{1}{2} i_{c1} + \frac{1}{2} i_{a2} - i_{b2} + \frac{1}{2} i_{c2} \right) \\
i_{\beta s} &= \frac{1}{\sqrt{3}} \left(\frac{\sqrt{3}}{2} i_{b1} - \frac{\sqrt{3}}{2} i_{c1} + \frac{\sqrt{3}}{2} i_{a2} - \frac{\sqrt{3}}{2} i_{c2} \right) \\
i_{xs} &= \frac{1}{\sqrt{3}} \left(-\frac{1}{2} i_{b1} - \frac{1}{2} i_{c1} - \frac{1}{2} i_{a2} + i_{b2} - \frac{1}{2} i_{c2} \right) = -i_{\alpha s} \\
i_{ys} &= \frac{1}{\sqrt{3}} \left(-\frac{\sqrt{3}}{2} i_{b1} + \frac{\sqrt{3}}{2} i_{c1} + \frac{\sqrt{3}}{2} i_{a2} - \frac{\sqrt{3}}{2} i_{c2} \right) \\
i_{0+s} &= \frac{1}{\sqrt{3}} \left(\frac{1}{\sqrt{2}} i_{b1} + \frac{1}{\sqrt{2}} i_{c1} + \frac{1}{\sqrt{2}} i_{a2} + \frac{1}{\sqrt{2}} i_{b2} + \frac{1}{\sqrt{2}} i_{c2} \right) = 0 \\
i_{0-s} &= \frac{1}{\sqrt{3}} \left(\frac{1}{\sqrt{2}} i_{b1} + \frac{1}{\sqrt{2}} i_{c1} - \frac{1}{\sqrt{2}} i_{a2} - \frac{1}{\sqrt{2}} i_{b2} - \frac{1}{\sqrt{2}} i_{c2} \right) = 0
\end{aligned} \tag{3.6}$$

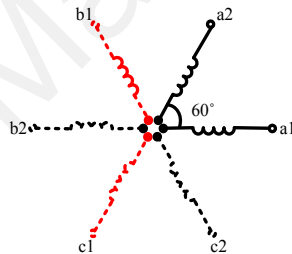
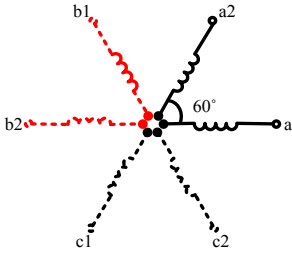
The currents will be constrained by the following conditions:

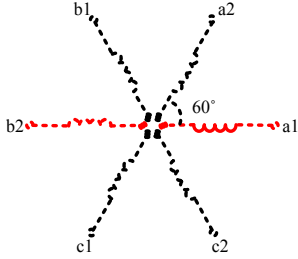
$$i_{xs} = -i_{as}$$

$$i_{0+s} = i_{0-s} = 0 \quad (3.7)$$

$$i_{a1s} = 0$$

Table 3.2:15 possibilities of open-phase fault when two phases missing

Two phases missing	Faulted Stator Winding Arrangement
Case 2a: Phase- <i>b1</i> and phase- <i>c1</i> Phase- <i>b2</i> and phase- <i>c2</i> Phase- <i>c1</i> and phase- <i>a1</i> Phase- <i>c2</i> and phase- <i>a2</i> Phase- <i>a1</i> and phase- <i>b1</i> Phase- <i>a2</i> and phase- <i>b2</i>	
Case 2b: Phase- <i>b1</i> and phase- <i>b2</i> Phase- <i>b2</i> and phase- <i>c1</i> Phase- <i>c1</i> and phase- <i>c2</i> Phase- <i>c2</i> and phase- <i>a1</i> Phase- <i>a1</i> and phase- <i>a2</i> Phase- <i>a2</i> and phase- <i>b1</i>	

<p>Case 2c:</p> <p>Phase-<i>a1</i> and phase-<i>b2</i></p> <p>Phase-<i>a2</i> and phase-<i>c1</i></p> <p>Phase-<i>b1</i> and phase-<i>c2</i></p>	
---	--

3.2.3 S6-IM under Two Phases Loss - Single Isolated Neutral (2 OPFs-1N)

For case 2b, if the machine is configured with single isolated neutral, i_{a1} and $i_{b1} = 0$ meaning that $i_{c1} + i_{a2} + i_{b2} + i_{c2} = 0$.

$$\begin{aligned}
i_{\alpha s} &= \frac{1}{\sqrt{3}} \left(-\frac{1}{2} i_{c1} + \frac{1}{2} i_{a2} - i_{b2} + \frac{1}{2} i_{c2} \right) \\
i_{\beta s} &= \frac{1}{\sqrt{3}} \left(-\frac{\sqrt{3}}{2} i_{c1} + \frac{\sqrt{3}}{2} i_{a2} - \frac{\sqrt{3}}{2} i_{c2} \right) \\
i_{xs} &= \frac{1}{\sqrt{3}} \left(-\frac{1}{2} i_{c1} - \frac{1}{2} i_{a2} + i_{b2} - \frac{1}{2} i_{c2} \right) \\
i_{ys} &= \frac{1}{\sqrt{3}} \left(\frac{\sqrt{3}}{2} i_{c1} + \frac{\sqrt{3}}{2} i_{a2} - \frac{\sqrt{3}}{2} i_{c2} \right) = i_{\beta s} - \sqrt{3} (i_{xs} + i_{\alpha s}) \\
i_{0+s} &= \frac{1}{\sqrt{3}} \left(\frac{1}{\sqrt{2}} i_{c1} + \frac{1}{\sqrt{2}} i_{a2} + \frac{1}{\sqrt{2}} i_{b2} + \frac{1}{\sqrt{2}} i_{c2} \right) = 0 \\
i_{0-s} &= \frac{1}{\sqrt{3}} \left(\frac{1}{\sqrt{2}} i_{c1} - \frac{1}{\sqrt{2}} i_{a2} - \frac{1}{\sqrt{2}} i_{b2} - \frac{1}{\sqrt{2}} i_{c2} \right) = -\sqrt{2} (i_{xs} + i_{\alpha s})
\end{aligned} \tag{3.8}$$

The currents will be constrained by the following conditions:

$$i_{0+s} = 0$$

$$i_{0-s} = -\sqrt{2} (i_{xs} + i_{\alpha s}) \tag{3.9}$$

$$i_{a1s} \text{ and } i_{b1s} = 0$$

$$i_{ys} = i_{\beta s} - \sqrt{3} (i_{xs} + i_{\alpha s})$$

3.2.4 S6-IM under Two Phases Loss -Two Isolated Neutrals (2 OPFs-2N)

For case 2b, if the machine is configured with two isolated neutrals, i_{a1} and $i_{b1} = 0$ meaning that $i_{c1} = 0$.

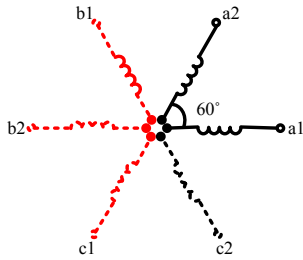
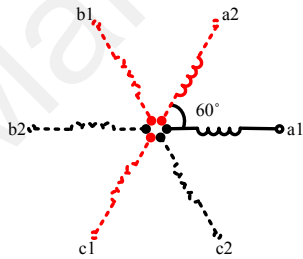
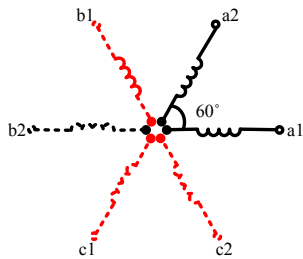
$$\begin{aligned}
 i_{\alpha s} &= \frac{1}{\sqrt{3}} \left(-\frac{1}{2} i_{c1} + \frac{1}{2} i_{a2} - i_{b2} + \frac{1}{2} i_{c2} \right) \\
 i_{\beta s} &= \frac{1}{\sqrt{3}} \left(-\frac{\sqrt{3}}{2} i_{c1} + \frac{\sqrt{3}}{2} i_{a2} - \frac{\sqrt{3}}{2} i_{c2} \right) \\
 i_{xs} &= \frac{1}{\sqrt{3}} \left(-\frac{1}{2} i_{c1} - \frac{1}{2} i_{a2} + i_{b2} - \frac{1}{2} i_{c2} \right) = -i_{\alpha s} \\
 i_{ys} &= \frac{1}{\sqrt{3}} \left(\frac{\sqrt{3}}{2} i_{c1} + \frac{\sqrt{3}}{2} i_{a2} - \frac{\sqrt{3}}{2} i_{c2} \right) = i_{\beta s} \\
 i_{0+s} &= \frac{1}{\sqrt{3}} \left(\frac{1}{\sqrt{2}} i_{c1} + \frac{1}{\sqrt{2}} i_{a2} + \frac{1}{\sqrt{2}} i_{b2} + \frac{1}{\sqrt{2}} i_{c2} \right) = 0 \\
 i_{0-s} &= \frac{1}{\sqrt{3}} \left(\frac{1}{\sqrt{2}} i_{c1} - \frac{1}{\sqrt{2}} i_{a2} - \frac{1}{\sqrt{2}} i_{b2} - \frac{1}{\sqrt{2}} i_{c2} \right) = 0
 \end{aligned} \tag{3.10}$$

The currents will be constrained by the following conditions:

$$\begin{aligned}
 i_{0+s} &= i_{0-s} = 0 \\
 i_{a1s} \text{ and } i_{b1s} &= 0 \\
 i_{xs} &= -i_{\alpha s} \\
 i_{ys} &= i_{\beta s}
 \end{aligned} \tag{3.11}$$

Table 3.3: 20 possibilities of open-phase fault when three phases missing

Three phases missing	Faulted Stator Winding Arrangement
Case 3a: Phase-a2, phase-b2, and phase-c2 Phase-a1, phase-b1, and phase-c1	

<p>Case 3b:</p> <p>Phase-<i>b1</i>, phase-<i>b2</i>, and phase-<i>c1</i></p> <p>Phase-<i>b2</i>, phase-<i>c1</i>, and phase-<i>c2</i></p> <p>Phase-<i>c1</i>, phase-<i>c2</i>, and phase-<i>a1</i></p> <p>Phase-<i>c2</i>, phase-<i>a1</i>, and phase-<i>a2</i></p> <p>Phase-<i>a1</i>, phase-<i>a2</i>, and phase-<i>b1</i></p> <p>Phase-<i>a2</i>, phase-<i>b1</i>, and phase-<i>b2</i></p>	
<p>Case 3c:</p> <p>Phase-<i>a2</i>, phase-<i>b1</i>, and phase-<i>c1</i></p> <p>Phase-<i>b1</i>, phase-<i>b2</i>, and phase-<i>c2</i></p> <p>Phase-<i>b2</i>, phase-<i>c1</i>, and phase-<i>a1</i></p> <p>Phase-<i>c1</i>, phase-<i>c2</i>, and phase-<i>a2</i></p> <p>Phase-<i>c2</i>, phase-<i>a1</i>, and phase-<i>b1</i></p> <p>Phase-<i>a1</i>, phase-<i>a2</i>, and phase-<i>b2</i></p>	
<p>Case 3d:</p> <p>Phase-<i>c2</i>, phase-<i>b1</i>, and phase-<i>c1</i></p> <p>Phase-<i>a1</i>, phase-<i>b2</i>, and phase-<i>c2</i></p> <p>Phase-<i>a2</i>, phase-<i>c1</i>, and phase-<i>a1</i></p> <p>Phase-<i>b1</i>, phase-<i>c2</i>, and phase-<i>a2</i></p> <p>Phase-<i>b2</i>, phase-<i>a1</i>, and phase-<i>b1</i></p> <p>Phase-<i>c1</i>, phase-<i>a2</i>, and phase-<i>b2</i></p>	

3.2.5 S6-IM under Three Phases Loss - Single Isolated Neutral (3 OPFs-1N)

For case 3a, if the machine is configured with single isolated neutral, i_{a1} , i_{b1} and $i_{c1} = 0$ meaning that $i_{a2} + i_{b2} + i_{c2} = 0$.

$$\begin{aligned}
 i_{\alpha s} &= \frac{1}{\sqrt{3}} \left(\frac{1}{2} i_{a2} - i_{b2} + \frac{1}{2} i_{c2} \right) \\
 i_{\beta s} &= \frac{1}{\sqrt{3}} \left(\frac{\sqrt{3}}{2} i_{a2} - \frac{\sqrt{3}}{2} i_{c2} \right) \\
 i_{xs} &= \frac{1}{\sqrt{3}} \left(-\frac{1}{2} i_{a2} + i_{b2} - \frac{1}{2} i_{c1} \right) = -i_{\alpha s} \\
 i_{ys} &= \frac{1}{\sqrt{3}} \left(\frac{\sqrt{3}}{2} i_{a2} - \frac{\sqrt{3}}{2} i_{c2} \right) = i_{\beta s} \\
 i_{0+s} &= \frac{1}{\sqrt{3}} \left(\frac{1}{\sqrt{2}} i_{a2} + \frac{1}{\sqrt{2}} i_{b2} + \frac{1}{\sqrt{2}} i_{c2} \right) = 0 \\
 i_{0-s} &= \frac{1}{\sqrt{3}} \left(-\frac{1}{\sqrt{2}} i_{a2} - \frac{1}{\sqrt{2}} i_{b2} - \frac{1}{\sqrt{2}} i_{c2} \right) = 0
 \end{aligned} \tag{3.12}$$

The currents will be constrained by the following conditions:

$$\begin{aligned}
 i_{0+s} &= i_{0-s} = 0 \\
 i_{xs} &= -i_{\alpha s} \\
 i_{a1s}, i_{b1s} \text{ and } i_{c1s} &= 0 \\
 i_{ys} &= i_{\beta s}
 \end{aligned} \tag{3.13}$$

3.2.6 S6-IM under Three Phases Loss - Two Isolated Neutrals (3 OPFs-2N)

For case 3a, if the machine is configured with two isolated neutrals, i_{a1} , i_{b1} and $i_{c1} = 0$ meaning that $i_{a2} + i_{b2} + i_{c2} = 0$.

$$\begin{aligned}
 i_{\alpha s} &= \frac{1}{\sqrt{3}} \left(\frac{1}{2} i_{a2} - i_{b2} + \frac{1}{2} i_{c2} \right) \\
 i_{\beta s} &= \frac{1}{\sqrt{3}} \left(\frac{\sqrt{3}}{2} i_{a2} - \frac{\sqrt{3}}{2} i_{c2} \right) \\
 i_{xs} &= \frac{1}{\sqrt{3}} \left(-\frac{1}{2} i_{a2} + i_{b2} - \frac{1}{2} i_{c1} \right) = -i_{\alpha s} \\
 i_{ys} &= \frac{1}{\sqrt{3}} \left(\frac{\sqrt{3}}{2} i_{a2} - \frac{\sqrt{3}}{2} i_{c2} \right) = i_{\beta s} \\
 i_{0+s} &= \frac{1}{\sqrt{3}} \left(\frac{1}{\sqrt{2}} i_{a2} + \frac{1}{\sqrt{2}} i_{b2} + \frac{1}{\sqrt{2}} i_{c2} \right) = 0 \\
 i_{0-s} &= \frac{1}{\sqrt{3}} \left(-\frac{1}{\sqrt{2}} i_{a2} - \frac{1}{\sqrt{2}} i_{b2} - \frac{1}{\sqrt{2}} i_{c2} \right) = 0
 \end{aligned} \tag{3.14}$$

The currents will be constrained by the following conditions:

$$\begin{aligned}
 i_{0+s} &= i_{0-s} = 0 \\
 i_{xs} &= -i_{\alpha s} \\
 i_{a1s}, i_{b1s} \text{ and } i_{c1s} &= 0 \\
 i_{ys} &= i_{\beta s}
 \end{aligned} \tag{3.15}$$

The independent scenarios based on maximum torque (MT) with single isolated neutral (1N) and two isolated neutrals (2N) are tabulated in Table 3.4(a) and Table 3.4(b) respectively. In addition, the minimum loss (ML) with single isolated neutral (1N) and two isolated neutrals (2N) are tabulated in Table 3.5(a) and Table 3.5(b) respectively. By optimizing the coefficients, $K1, K2, \dots, K8$, based on different optimization objective (ML or MT) the x - y and $0+$ - $0-$ currents references as given in (2.11) for the

Table 3.4: Reconfiguration of x - y and θ_+ - θ_- reference currents in post-fault situation (MT) for all independent scenarios in S6 (a) 1N and (b) 2N

<i>Fault</i>	<i>1N</i>								
	K_1	K_2	K_3	K_4	K_5	K_6	K_7	K_8	a
	<i>S6</i>								
<i>1</i>	-0.648	0	0	-0.368	0	0	-0.497	0	0.771
<i>2a</i>	-0.750	0.433	-0.433	0.250	0	0	-0.354	-0.612	0.577
<i>2b</i>	-1	0	-1.155	-1	0	0	0	0	0.500
<i>2c</i>	0	0	0	0	0	0	-1.414	0	0.577
<i>2d</i>	-1	0	1.155	-1	0	0	0	0	0.500
<i>3a</i>	-1	0	0	1	0	0	0	0	0.500
<i>3b</i>	0	1.732	-1.732	-2	0	0	-1.414	-2.449	0.167
<i>3c</i>	-1.500	0.866	0.866	-0.500	0	0	0.707	-1.225	0.289
<i>3d</i>	0	0	-1.732	1	0	0	-1.414	0	0.289

(a)

<i>Fault</i>	<i>2N</i>				
	K_1	K_2	K_3	K_4	a
	<i>S6</i>				
<i>1</i>	-1	0	0	-0.333	0.500
<i>2a</i>	-1	0	0	1	0.500
<i>2b</i>	-1	0	-1.155	-1	0.500
<i>2d</i>	-1	0	1.155	-1	0.500
<i>3a</i>	-1	0	0	1	0.500

(b)

Table 3.5: Reconfiguration of x - y and θ_+ - θ_- reference currents in post-fault situation (ML) for all independent scenarios in S6 (a) 1N and (b) 2N

<i>Fault</i>	<i>1N</i>								
	K_1	K_2	K_3	K_4	K_5	K_6	K_7	K_8	a
	<i>S6</i>								
<i>1</i>	-0.667	0	0	0	0	0	-0.471	0	0.688
<i>2a</i>	-0.833	0.289	-0.289	0.500	0	0	-0.236	-0.408	0.567
<i>2b</i>	-0.900	-0.173	-1.212	-0.900	0	0	-0.141	0.245	0.475
<i>2c</i>	0	0	0	0	0	0	-1.414	0	0.577
<i>2d</i>	-0.900	0.173	1.212	-0.900	0	0	-0.141	-0.245	0.475
<i>3a</i>	-1	0	0	1	0	0	0	0	0.500
<i>3b</i>	0	1.732	-1.732	-2	0	0	-1.414	-2.449	0.167
<i>3c</i>	-1.500	0.866	0.866	-0.500	0	0	0.707	-1.225	0.289
<i>3d</i>	0	0	-1.732	1	0	0	-1.414	0	0.289

(a)

<i>Fault</i>	$2N$				
	K_1	K_2	K_3	K_4	a
	$S6$				
1	-1	0	0	0	0.500
$2a$	-1	0	0	1	0.500
$2b$	-1	0	-1.155	-1	0.500
$2d$	-1	0	1.155	-1	0.500
$3a$	-1	0	0	1	0.500

(b)

corresponding post-fault modes can be attained. In terms of derating factor, a , i.e S6-1N, the post-fault modulus $\alpha-\beta$ is 1.888751 while the rated modulus $\alpha-\beta$ is 2.4495. Therefore, the derating factor as in (2.7) gives 0.771. As expected, the ML criterion significantly reduces the maximum achievable torque compared to MT.

3.3 Simulation Results for the S6-IM under 1 OPF to 3 OPFs

The phase currents for the S6-IM under pre- and post-fault have been plotted using the information tabulated in Table 3.4 and Table 3.5. Figure 3.4 to Figure 3.17 show the phase currents in healthy operation ($t < 0.02s$), ML ($0.02s < t < 0.04s$), and MT ($0.04s < t < 0.06s$) under different OPF scenarios for 1N and 2N respectively.

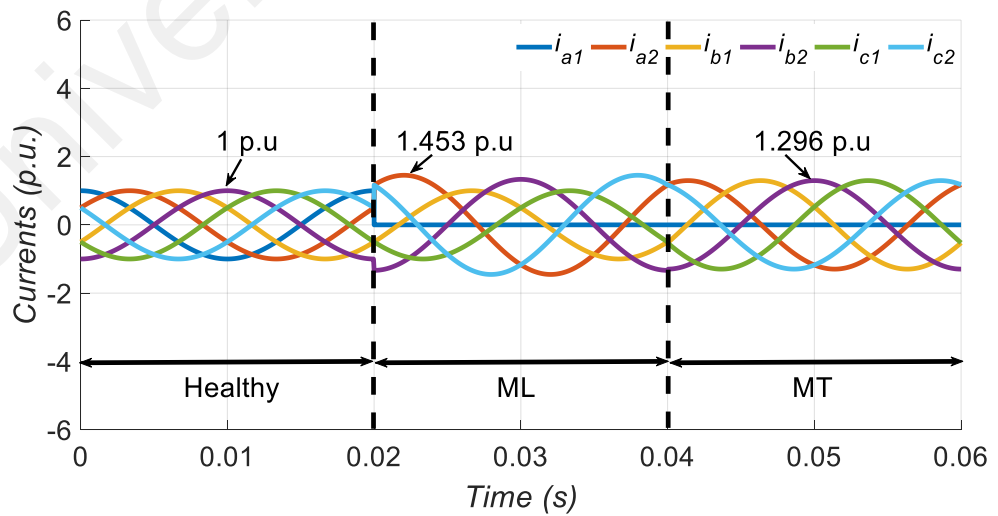


Figure 3.4: Stator phase currents in 1 OPF with 1N

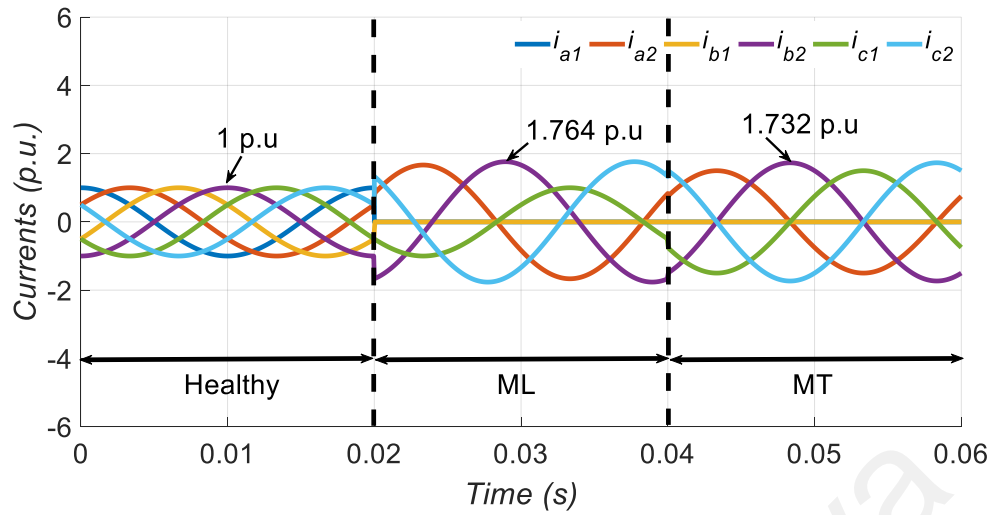


Figure 3.5: Stator phase currents in 2 OPFs (case 2a) with 1N

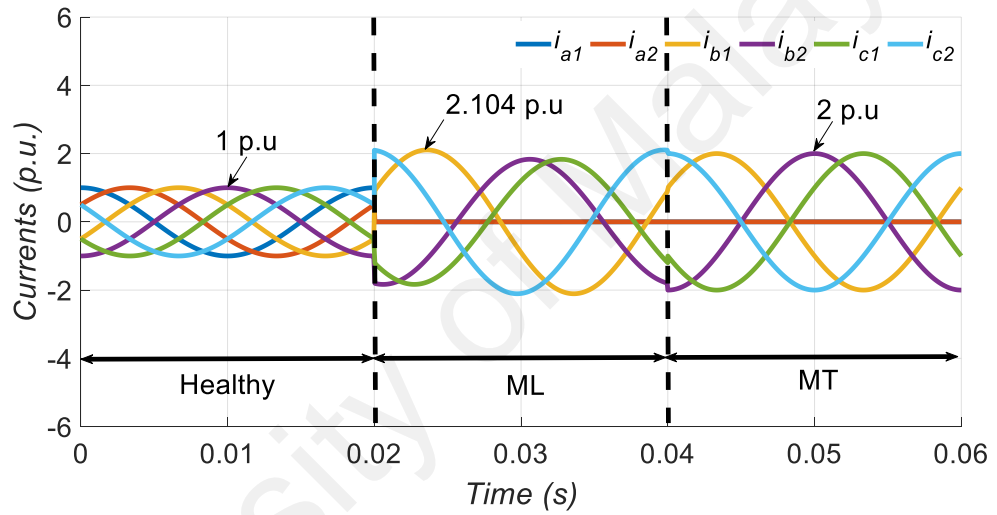


Figure 3.6: Stator phase currents in 2 OPFs (case 2b) with 1N

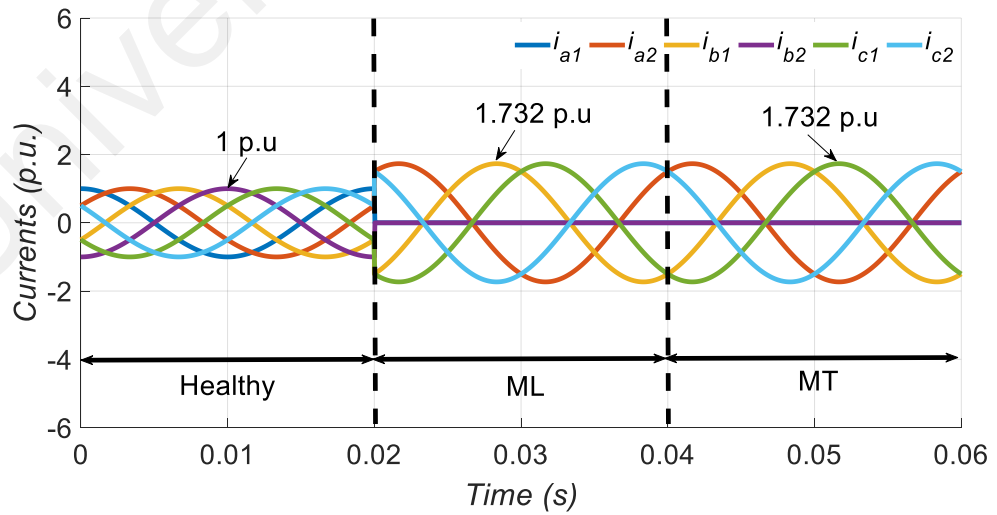


Figure 3.7: Stator phase currents in 2 OPFs (case 2c) with 1N

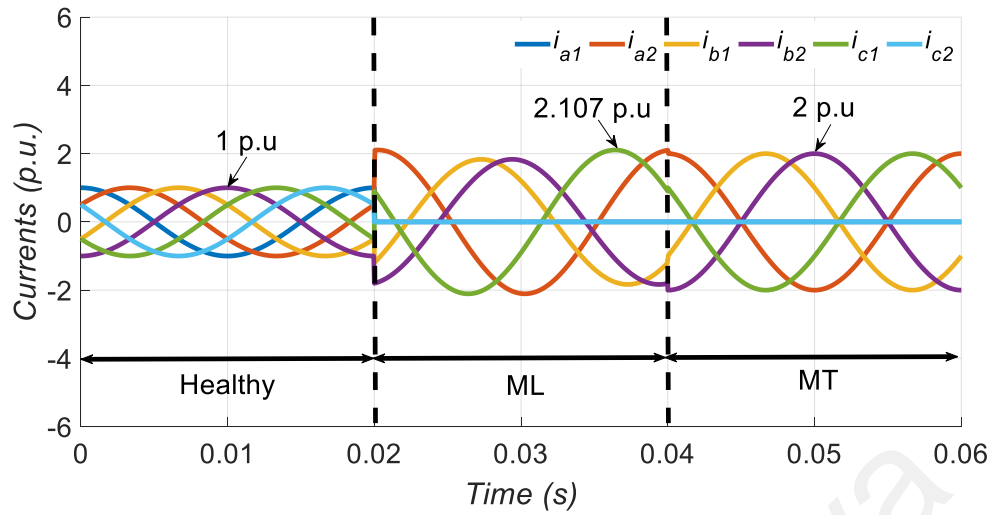


Figure 3.8: Stator phase currents in 2 OPFs (case 2d) with 1N

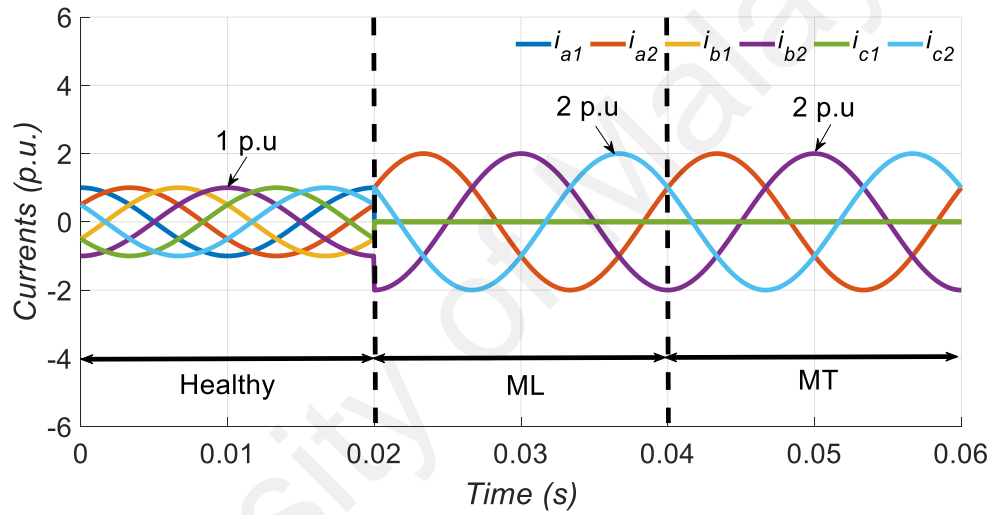


Figure 3.9: Stator phase currents in 3 OPFs (case 3a) with 1N

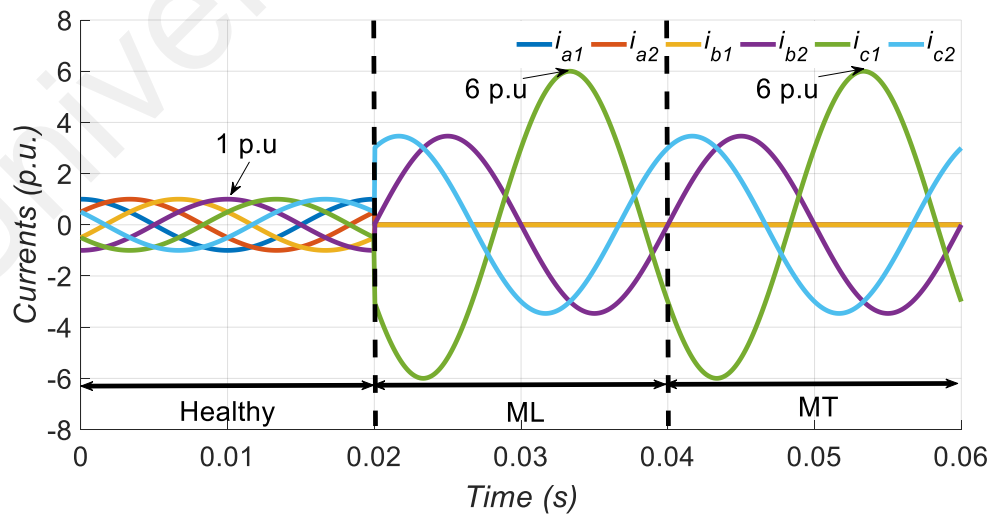


Figure 3.10: Stator phase currents in 3 OPFs (case 3b) with 1N

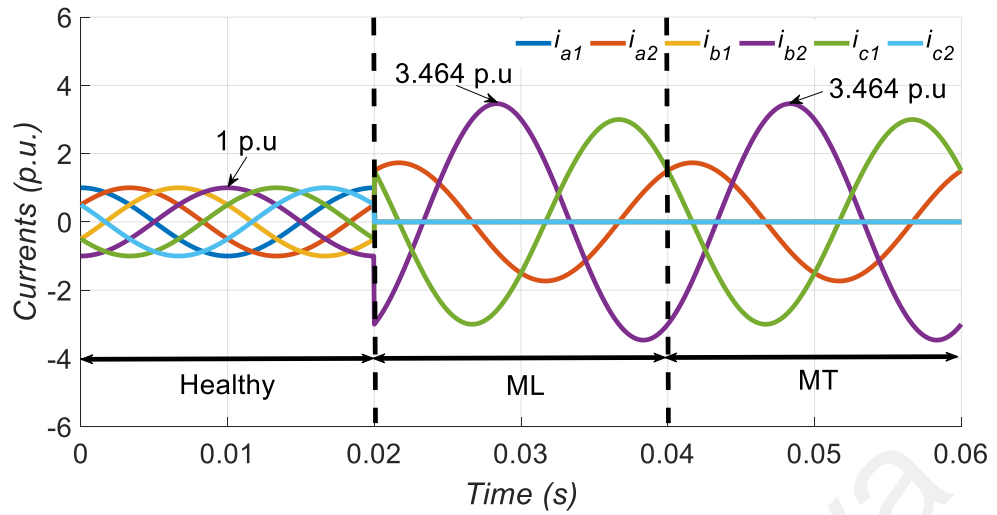


Figure 3.11: Stator phase currents in 3 OPFs (case 3c) with 1N

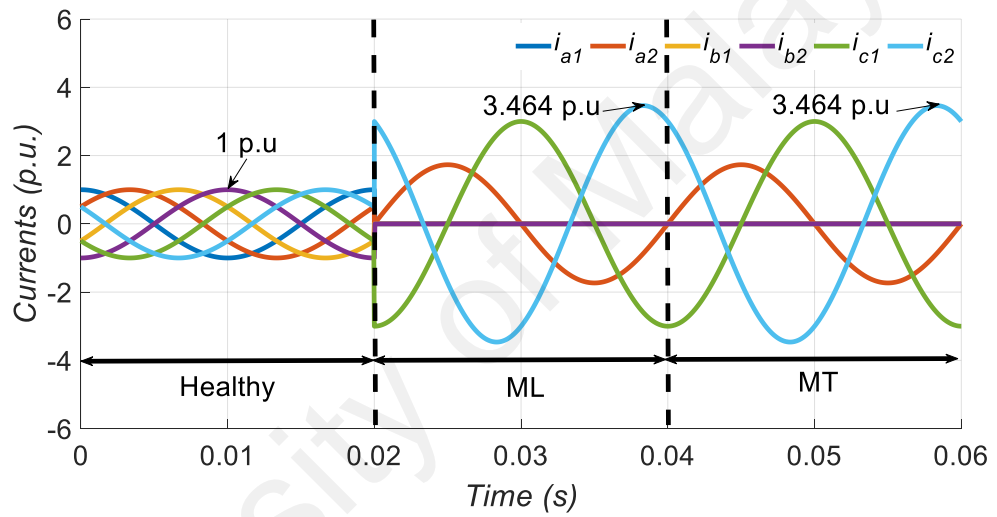


Figure 3.12: Stator phase currents in 3 OPFs (case 3d) with 1N

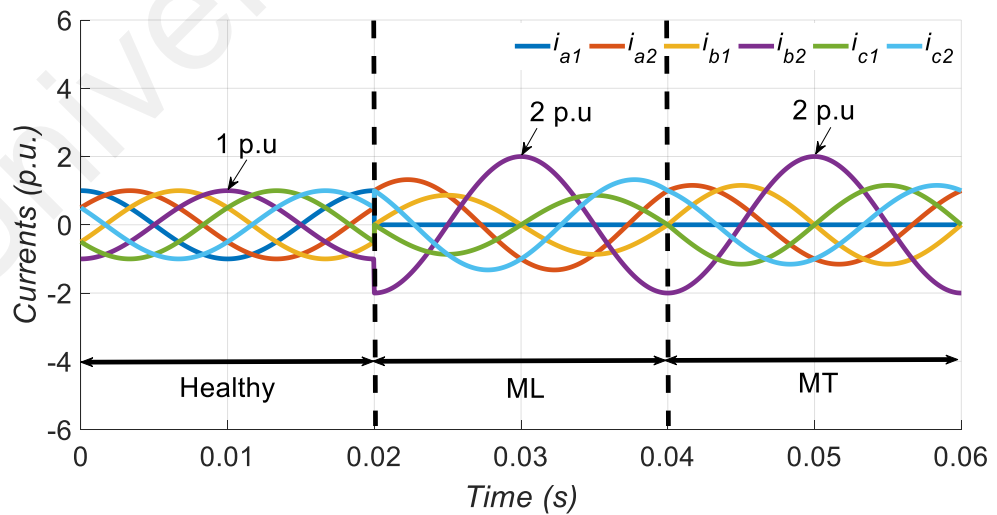


Figure 3.13: Stator phase currents in 1 OPF with 2N

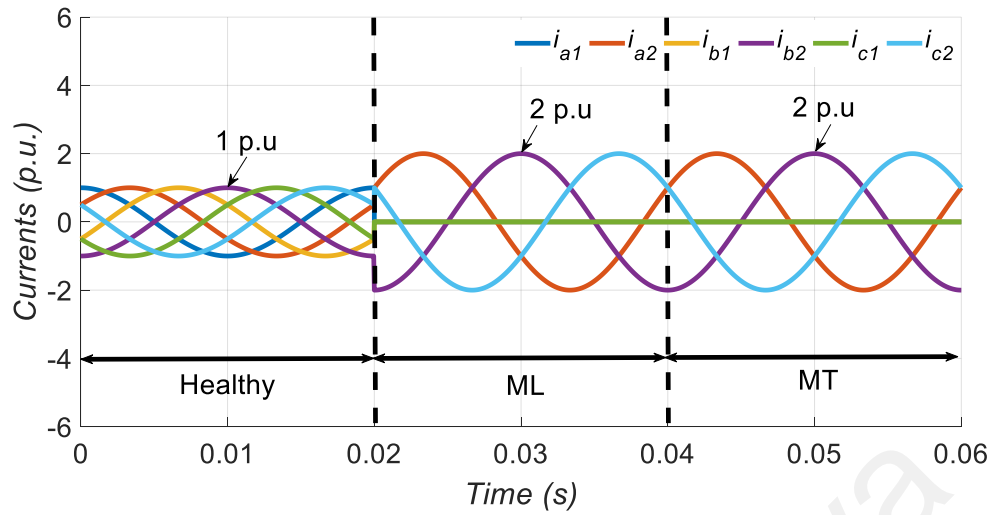


Figure 3.14: Stator phase currents in 2 OPFs (case 2a) with 2N

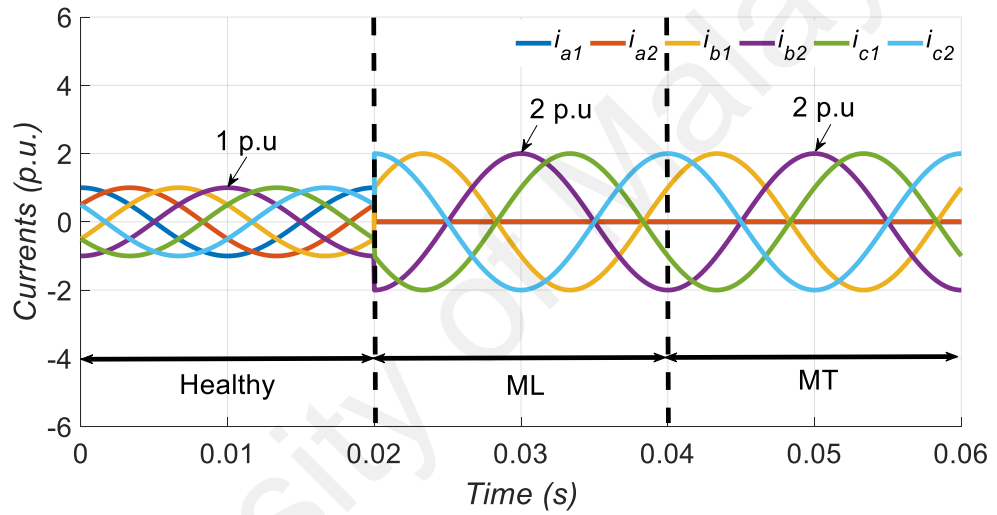


Figure 3.15: Stator phase currents in 2 OPFs (case 2b) with 2N

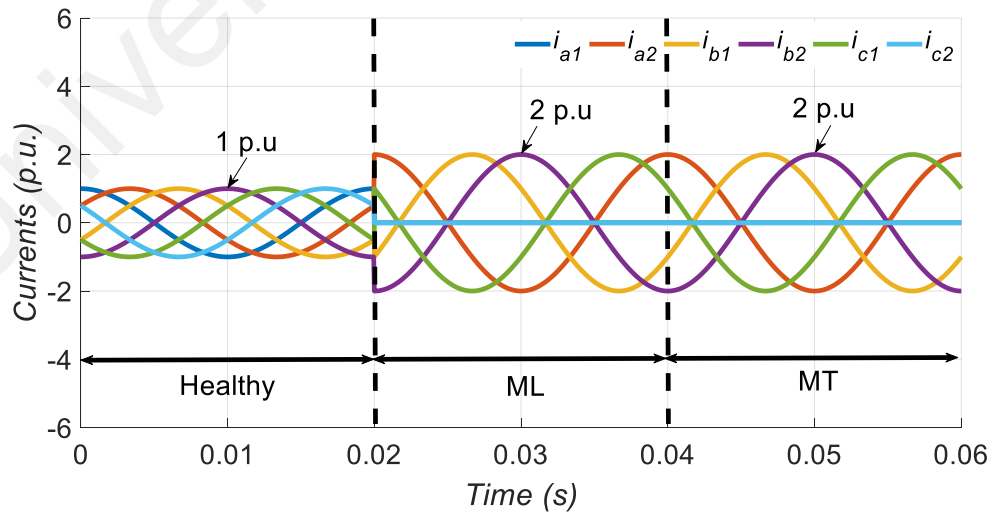


Figure 3.16: Stator phase currents in 2 OPFs (case 2d) with 2N

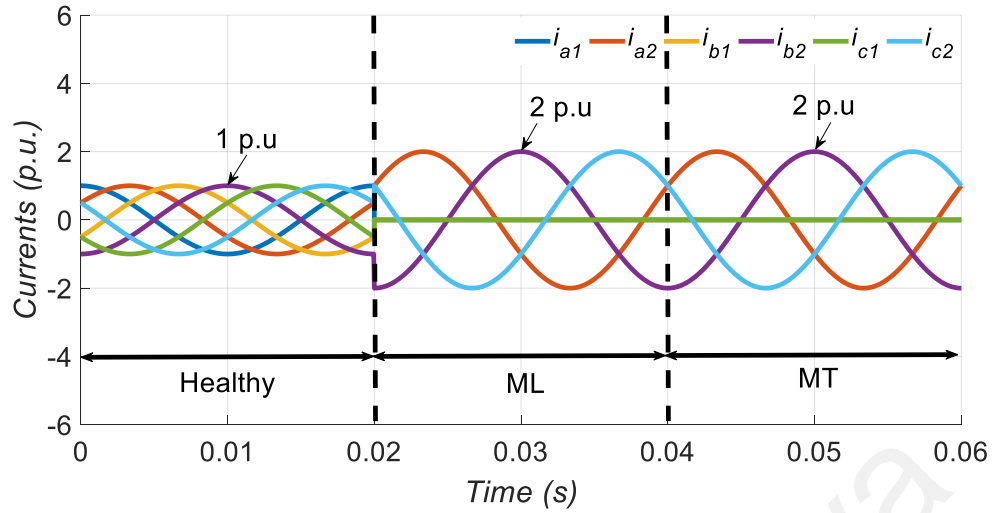


Figure 3.17: Stator phase currents in 3 OPFs (case 3a) with 2N

3.4 Experimental Results and Discussion

The experimental results are obtained using a test rig for the S6 machine. The S6 machine is obtained by rewinding a 0.55 kW three-phase induction machine. The general layout for the test rig is shown in Appendix B.9. In the test rig, the S6-IM is driven by two three-phase two-level voltage source converters based on Semikron SKM75GB12T4 modules that correspond to VSC₁ and VSC₂ in Appendix B.2. The converters are connected to a DC power supply system and the control is implemented dSPACE DS1103 rapid prototyping system. Current and speed measurements are taken with LEM LTSR-15-NP hall-effect sensors and E60H20-5000-3-N-5 digital encoder, respectively. The load torque is provided by a permanent magnet generator connected to a variable resistive-inductive load. OPFs are created by physically disconnecting the inverter from between the motor phases using relays.

3.4.1 Verification of Current Limits

Since the aim of this section is to explore the limits of torque capability in fault-tolerant six-phase drives, the subsequent results will focus exclusively on MT criterion. The number of independent tests to cover all possible scenarios and neutral arrangements is high, the following subset is selected as representative of the post-fault performance in

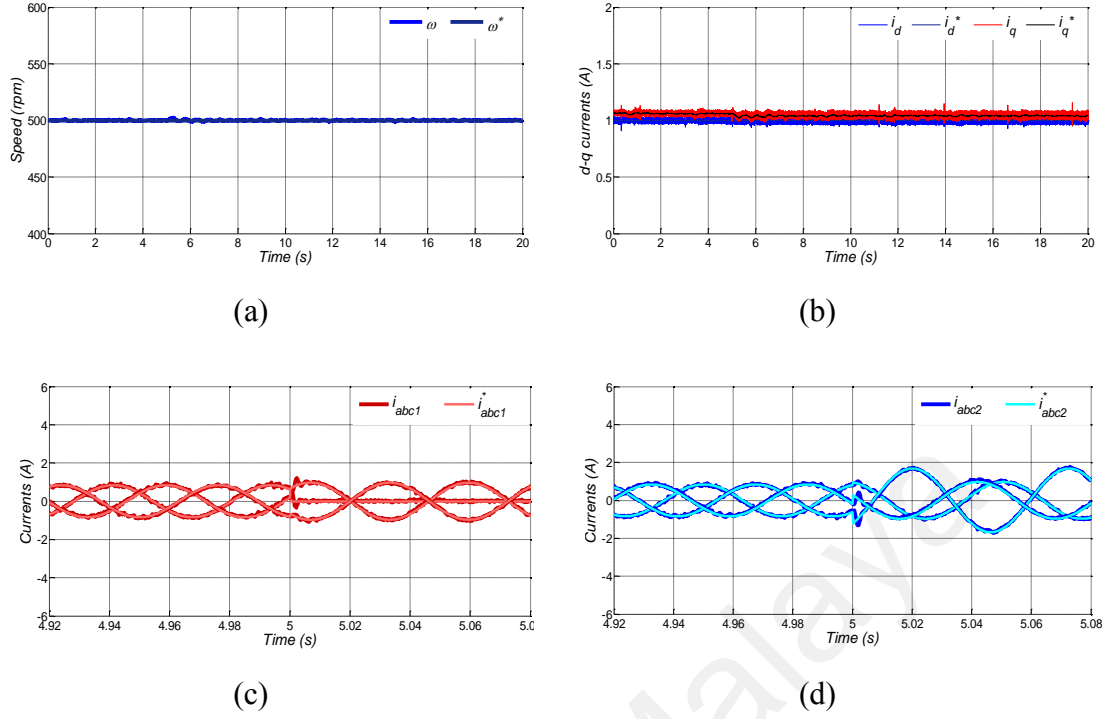


Figure 3.18: Test 1 (scenario 1) for S6-2N. From top to bottom: (a) Motor speed; (b) d - q currents; (c) phase currents of winding 1 and (d) phase currents of winding 2.

the event of 1, 2 or 3 OPFs: test 1 covers scenario 1 for 2N, test 2 covers scenario 2a for 1N and test 3 covers scenario 3a for 1N.

Results from test 1, test 2 and test 3 are shown in Figure 3.18, Figure 3.19 and Figure 3.20 respectively. In all cases, the speed (subplot (a) in Figures 3.18 – 3.20) is maintained in pre- ($t < 5s$) and post- ($t > 5s$) fault situations. This is achieved because the d - q currents maintain the same value before and after the fault (subplot (b) in Figures 3.18 – 3.20). On the contrary, x - y and θ_+ - θ_- current references need to be changed from zero (pre-fault) to the values shown in Table 3.4 (post-fault). The dual PI controller shown in Figure 3.1 is in charge of tracking these non-zero components.

The injection of the secondary currents, in turn, modifies the phase currents according to the MT criterion. Subplots (c) and (d) show the measured phase currents for windings 1 (dark red trace) and 2 (dark blue trace) together with the optimal currents for windings

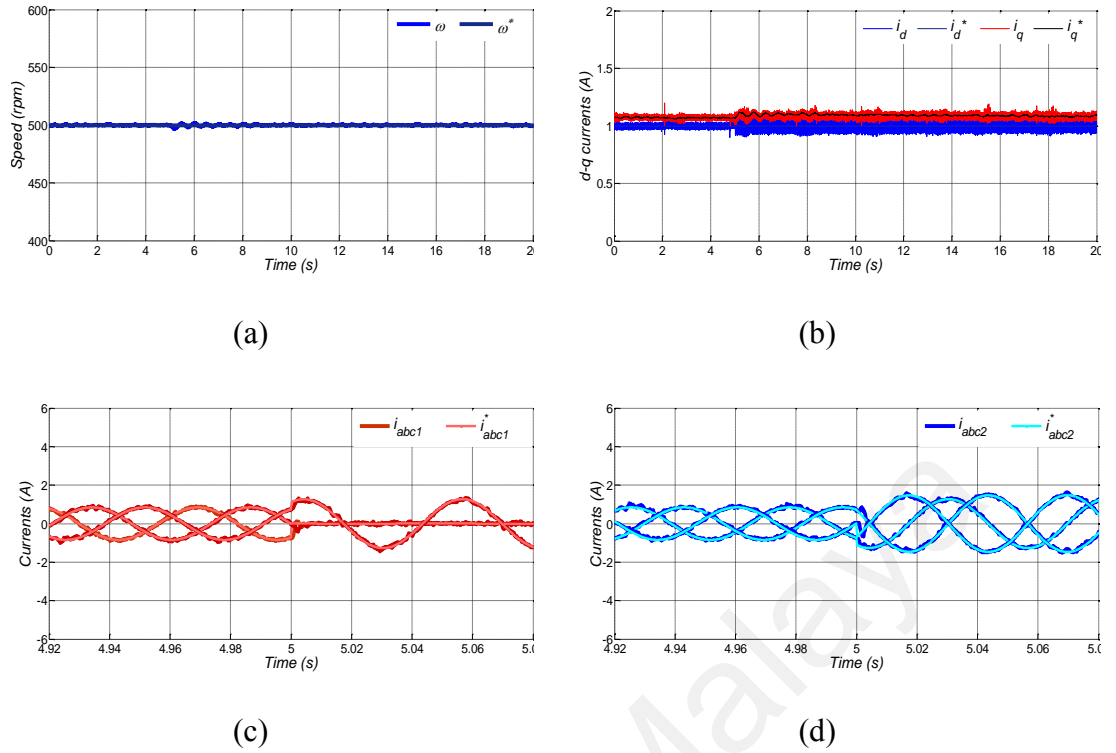


Figure 3.19: Test 2 (scenario 2a) for S6-1N. From top to bottom: (a) Motor speed; (b) d - q currents; (c) phase currents of winding 1 and (d) phase currents of winding 2.

1 (light red trace) and 2 (light blue trace) calculated with software (General Algebraic Modeling System (GAMS) and Excel Solver) according to the optimization procedure as explained in Section 2.3.2.3. Generally, the current tracking is satisfactory both in pre- and post-fault situations for all cases.

For test 1, the speed and d - q currents are essentially the same before and after fault, confirming the validity of the post-fault control. As expected, the max phase current amplitude increased to 2.0A, which is 2 times higher than the healthy case. This implies a derating factor of 0.5 as tabulated in Table 3.4.

The results for tests 2 and test 3 for S6 are shown next in Figures 3.19 and 3.20. As in test 1, the speed is maintained and consequently, d - q currents are also maintained before and after the fault occurrence (subplot (b) in Figures 3.19 and 3.20). Again a good match

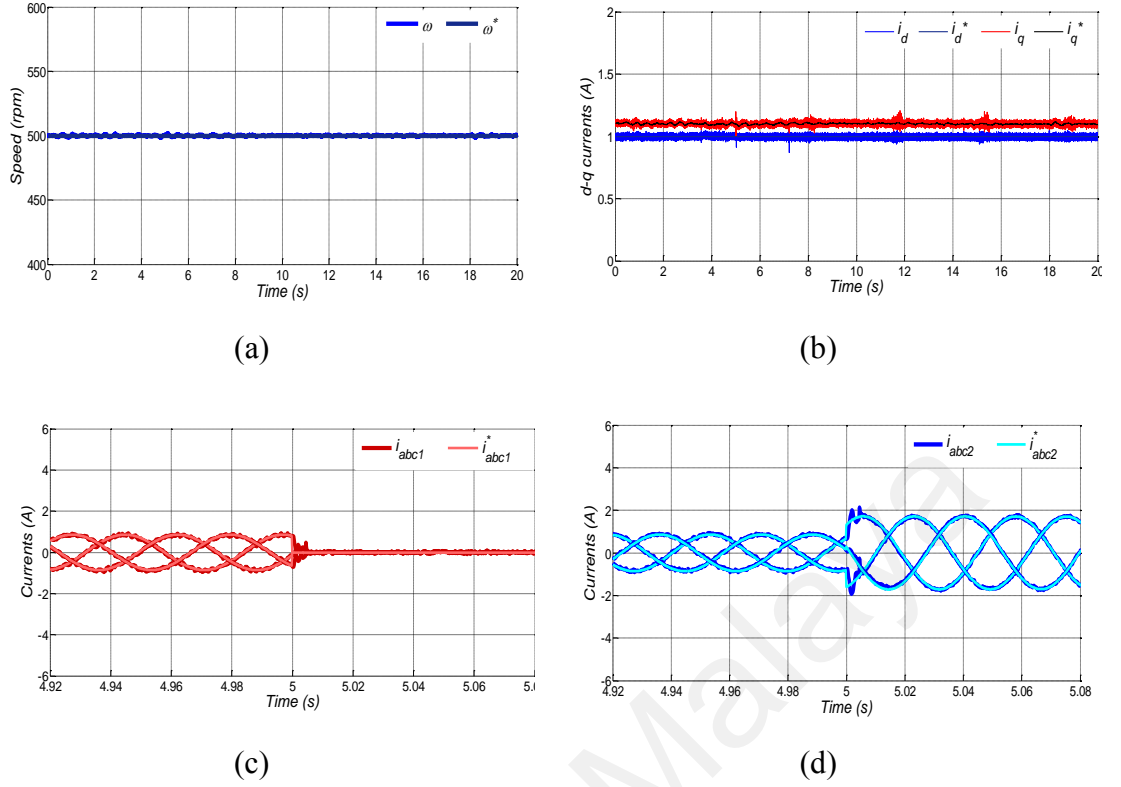


Figure 3.20: Test 3 (scenario 3a) for S6-1N. From top to bottom: (a) Motor speed; (b) d - q currents; (c) phase currents of winding 1 and (d) phase currents of winding 2.

between the reference currents (based on Table 3.4) and actual post-fault currents was obtained. It is worth noting that the x - y and 0_+-0_- current references are obtained from Table 3.4 and the dual PI controller shown in Figure 3.1 allows a satisfactory tracking of the secondary components.

3.4.2 Fault-tolerant Performance Comparison with A6 and D3

In order to extract global conclusions, a performance comparison in terms of current limits with the other two mainstream machines (D3 and A6) for 1N and 2N in all possible scenarios are investigated. Since the motivation of this chapter is to explore the current limits and efficiency is not the main concern in fault-tolerant six-phase drives, Table 3.6 will focus exclusively on MT criterion for A6 and D3.

Table 3.6: Reconfiguration of x - y and θ - θ reference currents in post-fault situation (MT) for all independent scenarios in A6 and D3 with (a) 1N (b) 2N

<i>Fault</i>	<i>1N</i>								
	K_1	K_2	K_3	K_4	K_5	K_6	K_7	K_8	a
	<i>A6</i>								
<i>1</i>	-0.641	-0.209	-0.754	-0.296	0	0	-0.507	0.296	0.694
<i>2a</i>	-0.536	0.268	-0.804	0.536	0	0	-0.656	-0.379	0.558
<i>2b</i>	-1	0	-3.464	-1	0	0	0	0	0.289
<i>2c</i>	0	-0.268	-0.268	0	0	0	-1.414	0.379	0.558
<i>2d</i>	-1	0	0	-1	0	0	0	0	0.577
<i>3a</i>	-1	0	0	1	0	0	0	0	0.500
<i>3b</i>	1.366	1.366	-4.097	-1.366	0	0	-3.345	-1.932	0.122
<i>3c</i>	-1	0.732	0	-0.268	0	0	0	-1.035	0.408
<i>3d</i>	0.732	-1	-3	2.732	0	0	-2.449	1.414	0.149
<i>D3</i>									
<i>1</i>	-0.667	0.577	1.732	0	0	0	-0.471	-0.817	0.500
<i>2a</i>	-0.333	0	-1.155	1	0	0	-0.943	0	0.500
<i>2c</i>	0	-0.577	-0.577	0	0	0	-1.414	0.817	0.500
<i>2d</i>	0	0.577	0.577	0	0	0	-1.414	-0.817	0.500
<i>3a</i>	-1	0	0	1	0	0	0	0	0.500
<i>3c</i>	-0.667	0.577	-0.577	0	0	0	-0.471	-0.817	0.500

(a)

<i>Fault</i>	<i>2N</i>				
	K_1	K_2	K_3	K_4	a
	<i>A6</i>				
<i>1</i>	-1	0	0	-1	0.577
<i>2a</i>	-1	0	0	1	0.500
<i>2b</i>	-1	0	-3.464	-1	0.289
<i>2c</i>	-1	0	3.464	-1	0.289
<i>2d</i>	-1	0	0	-1	0.577
<i>3a</i>	-1	0	0	1	0.500
<i>D3</i>					
<i>1</i>	-1	0	0	-0.3334	0.500
<i>2a</i>	-1	0	0	1	0.500
<i>2c</i>	-1	0	-1.155	-1	0.500
<i>2d</i>	-1	0	1.155	-1	0.500
<i>3a</i>	-1	0	0	1	0.500

(b)

Based on Tables 3.4 and 3.6, it can be concluded that the S6 is the best six-phase machine when in 1N whereas A6 is the best choice in 2N. Meanwhile, D3 is the worst option from the fault tolerance point of view in single OPF. It can also be inferred that the 1N provides better performance in two aspects: *i*) it can withstand a wider range of

faults and still obtain some fault tolerance, and *ii)* it provides the highest post-fault current/torque for S6 in scenario 1, which is the most likely to occur in practice.

As general rules for the selection of a six-phase machine, the following situations would benefit the selection of D3, A6, and S6:

- i. D3-2N can be selected if the fault tolerance is not a relevant issue and other features (simplicity, DC-bus utilization, no excitation x - y currents) are promoted instead. D3-1N is not a good option in any case.
- ii. A6-2N can be selected to improve the fault-tolerant capability of D3 and still maintain simplicity and better DC-bus utilization. It also has the best fault tolerance if up to 2 OPFs are anticipated.
- iii. S6-1N is the best choice if fault tolerance is a main concern.

3.5 Conclusion

In this chapter, the fault-tolerant performance of symmetrical six-phase (S6) induction machine in terms of current limits considering up to three simultaneous open-phase faults have been investigated. The post-fault equations for S6 machine with 1N and 2N under 1OPF to 3 OPFs have been derived from the Clarke transformation giving the post-fault relationship.

Several concluding remarks can be inferred in terms of performance of S6 machine:

- i. As far as scenario 1 is concerned, the use of 1N highly promotes the post-fault torque production. S6 is the best choice in 1N, and the maximum torque production using MT is 77.1%.
- ii. Some additional conclusions can be extracted from the analysis of the scenarios with 2 OPFs. The performance improvement obtained with the connection of the neutrals is low, 1N is only clearly better than 2N in one out of four

scenarios. In 2N the fault-tolerant performance of the S6 machine is similar, with maximum torque production is 50%. In 1N the performance of S6 is globally the best.

- iii. The derating under 3 OPFs is finally examined in Table 3.4. It must be noted that in the post-fault operation in 2N is only feasible for scenario 3a, where the 3 OPFs occur in the VSC_1 and the solution is consequently trivial and equal to the 'single VSC' mode of operation that provides 50% of the current production. The additional degree of freedom added in 1N makes it possible to operate in scenarios 3b, 3c and, 3d, but with a low fault-tolerant capability for S6. S6 have some fault tolerance in all scenarios with 3 OPFs, but obtaining low torque/power. Generally, the fault-tolerant capability with 3 OPFs is mostly inexistent for 2N and low for 1N.

CHAPTER 4: MACHINE PARAMETERS ESTIMATION USING CLOSED- LOOP CONTROL SIGNALS CURVE FITTING

4.1 Introduction

Apart from the current limits, the voltage limits will also affect the achievable performance of a motor drive. In (Tousizadeh, Che, Abd Rahim, et al., 2018), it was demonstrated that the voltage limits for a fault-tolerant three-phase drive will decide the maximum operating speed of the three-phase machine, hence the attainable output power. Some studies on the voltage limits for the multiphase machine have also been presented in the past, such that the case for five-phase (Ayman S. Abdel-Khalik et al., 2015) and asymmetrical six-phase machine (Ayman S Abdel-Khalik et al., 2018). Unlike current limits, the voltage limits of the fault-tolerant drive depend on the machine parameters (Ayman S Abdel-Khalik et al., 2018; Tousizadeh, Che, Abd Rahim, et al., 2018). Hence, an accurate machine parameter needs to be obtained to estimate the voltage variations under different fault scenarios.

4.2 Existing Machine Parameter Estimation Methods for Multiphase Machines

Several works on machine parameter estimation for multiphase machines have been reported in the literature. Machine parameter estimation based on a standard test for five and six-phase machines has been reported in (Jacobina, Azevedo, Silva, Lima, & Silva, 2002; Riveros et al., 2012; Yepes, Riveros, Jones, & Levi, 2012), where the authors assumed that the stator leakage inductances, L_{ls} in the x - y and θ_+ - θ_- voltage are equivalent with the α - β subspace. Later, (Hang Seng Che et al., 2017) proposed an improved parameter estimation technique based on modified standard no-load and locked-rotor tests for asymmetrical six-phase, where the leakage inductance for different subspaces is considered to be different.

Moreover, the proposed method considered the effect of mutual stator leakage inductance and the impact of rotor coupling in the zero-sequence plane. Another parameter identification technique of asymmetrical six-phase induction machine has been proposed by (Ayman S Abdel-Khalik et al., 2018) using a modified blocked-rotor test under open phase. The proposed method eliminated the need for winding reconfiguration as in (Hang Seng Che et al., 2017) by combining the effect of all subspaces in a single circuit.

While the previous parameter estimation methods have been demonstrated to achieve good performance, they are mainly offline parameter estimation techniques that suffer from two main drawbacks:

- i. The machine needs to be disconnected and reconfigured for parameter testing. For the case of no-load and locked rotor tests, the machine needs to be decoupled from the load and locked from rotation respectively, which can be difficult to achieve in certain applications.
- ii. The parameter estimations methods do not consider the effects of parasitic impedance such as switching dead-time and forward voltage drop of switches. These parasitic parameters will affect the effective machine parameters "seen" by the controller, which is slightly different from the machine parameters determined through the offline approach (Tousizadeh, Che, Selvaraj, Abd Rahim, & Ooi, 2018).

In this chapter, a parameter estimation technique for an S6-IM is proposed to overcome the aforementioned problems. Based on the machine equations, it is known that the machine voltages can be calculated from the operating currents, slip frequency, synchronous frequency, and machine parameters. Since the machine currents, slip frequency, and synchronous frequency information are readily available in field-oriented

control, the theoretical machine voltages can be calculated using the machine equations while making assumptions on the values of machine parameters.

These parameters are then adjusted through optimization tool such that the theoretical machine voltages match the voltages generated by the controller. The final machine parameters will be the “effective machine parameters” seen by the controller, which inherently considers the parasitic parameters. Furthermore, the proposed method uses the control and measurement variables that are readily available in the drive, such that there is no need to reconfigure the machine connection. In the subsequent part of this chapter, the detailed concept of the parameter estimation technique is explained and experimental results using an S6-IM are shown to validate the proposed method.

4.3 Proposed Machine Parameters Estimation Method

Figure 4.1 shows the controller structure for a typical induction motor drive based on voltage source inverter with the RFOC method. Under this control scheme, the controller generates control voltages (v_k^* , where $k = \{a_1, b_1, c_1, a_2, b_2, c_2\}$) which are realized and applied onto the machine using PWM and VSC. The machine current is the result of these control voltages and the machine impedance. From the controller’s perspective, an ideal inverter with PWM operating in the linear modulation region can be considered as a unity gain, such that the machine’s terminal voltages are controlled directly by the control voltages (as seen in Figure 4.1). For a balanced n-phase machine with star-connected winding, these control voltages will be equal to the machine phase voltages, $v_k^* = v_k$. Hence, as illustrated in Figure 4.2, the machine currents can be considered as a function of the machine impedance and the control voltages, i.e.

$$i_k = \frac{v_k}{z_k} = \frac{v_k^*}{z_k} \quad (4.1)$$

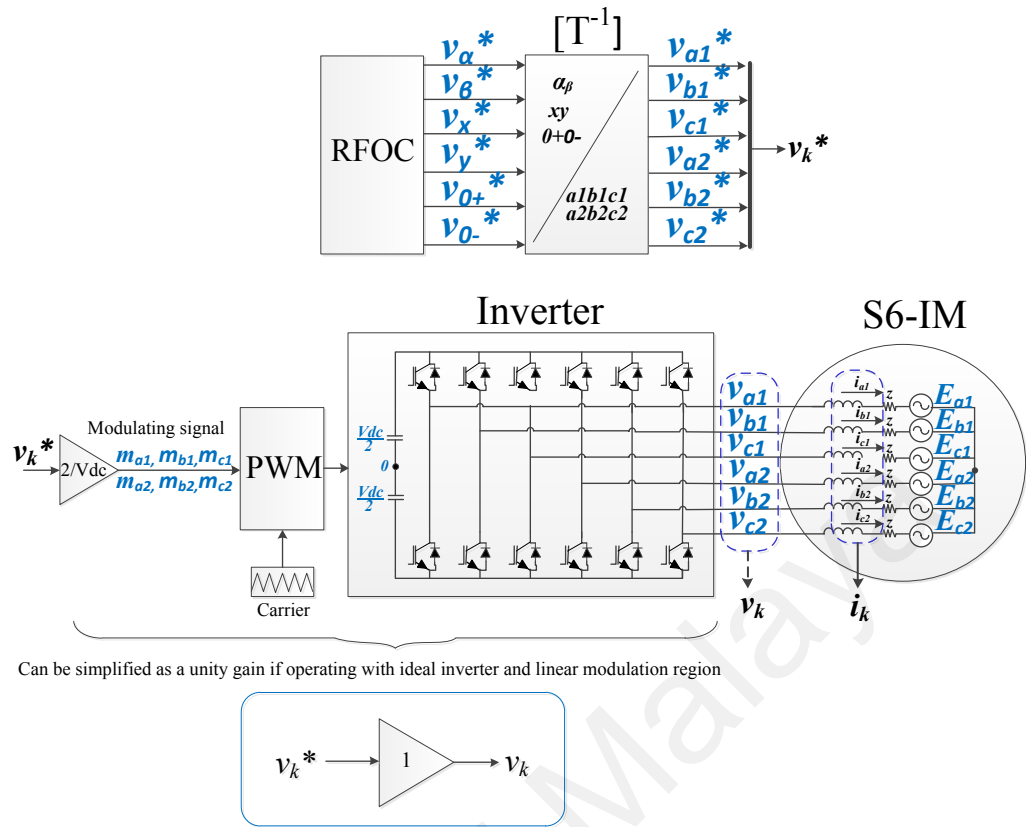


Figure 4.1: Typical six-phase machine

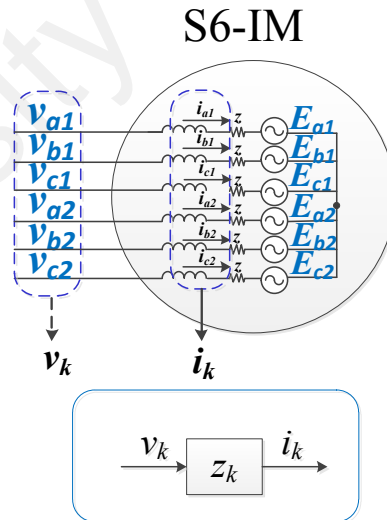


Figure 4.2: Ideal six-phase induction machine

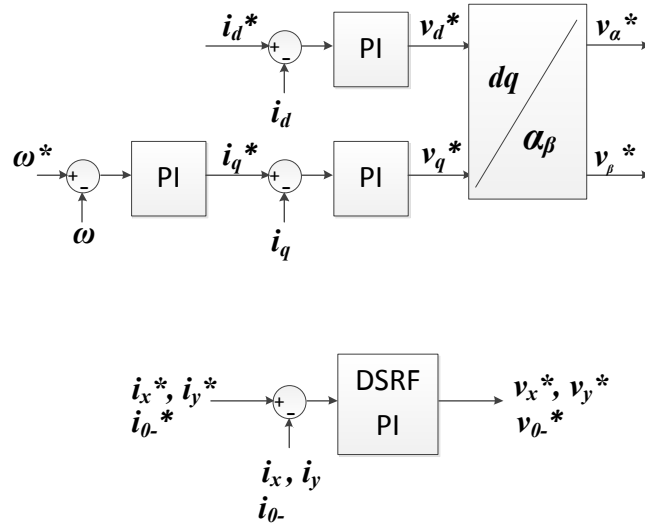


Figure 4.3: Fault-tolerant control scheme with DSRF (dual PI) controllers in the x - y current loop

Since the control voltages and the phase currents are known in RFOC, machine impedance can be easily deduced. This forms the basis of the parameter estimation technique presented here in this chapter. Using some initial guesses on the machine parameters, the theoretical machine voltage equation can be obtained as a function of the machine current and operation point (flux, torque, and speed), the machine parameters can be estimated by adjusting the machine parameters to curve fit the theoretical machine voltage with the known control voltage.

There are, however, some additional considerations required for the implementation of this parameter estimation techniques, namely:

- i) Effect of inverter non-ideality and parasitic impedance
- ii) Selection of machine equation reference frame

4.3.1 Effect of Inverter Non-idealities and Parasitic Impedance

It is known that in practice, the actual inverter leg voltage will deviate from the control voltages due to the inverter dead time and switch forward voltage drop. In (Tousizadeh, Che, Selvaraj, et al., 2018), it was demonstrated that these inverter non-idealities can be

approximated as a fundamental frequency voltage component that is in phase with the phase current polarity. The magnitude of this voltage depends on the dead time, switching frequency as well as the forward voltage drop of the switch selected (Tousizadeh, Che, Selvaraj, et al., 2018).

In addition, the connection between the inverter and the machine will create additional parasitic impedance to the machine impedance. The effects of inverter non-ideality and parasitic impedance will appear as disturbance voltage and additional impedance between the controller and the machine. Nevertheless, these effects can be collectively lumped together to form the effective machine parameters seen by the controller, as illustrated in Figure 4.4.

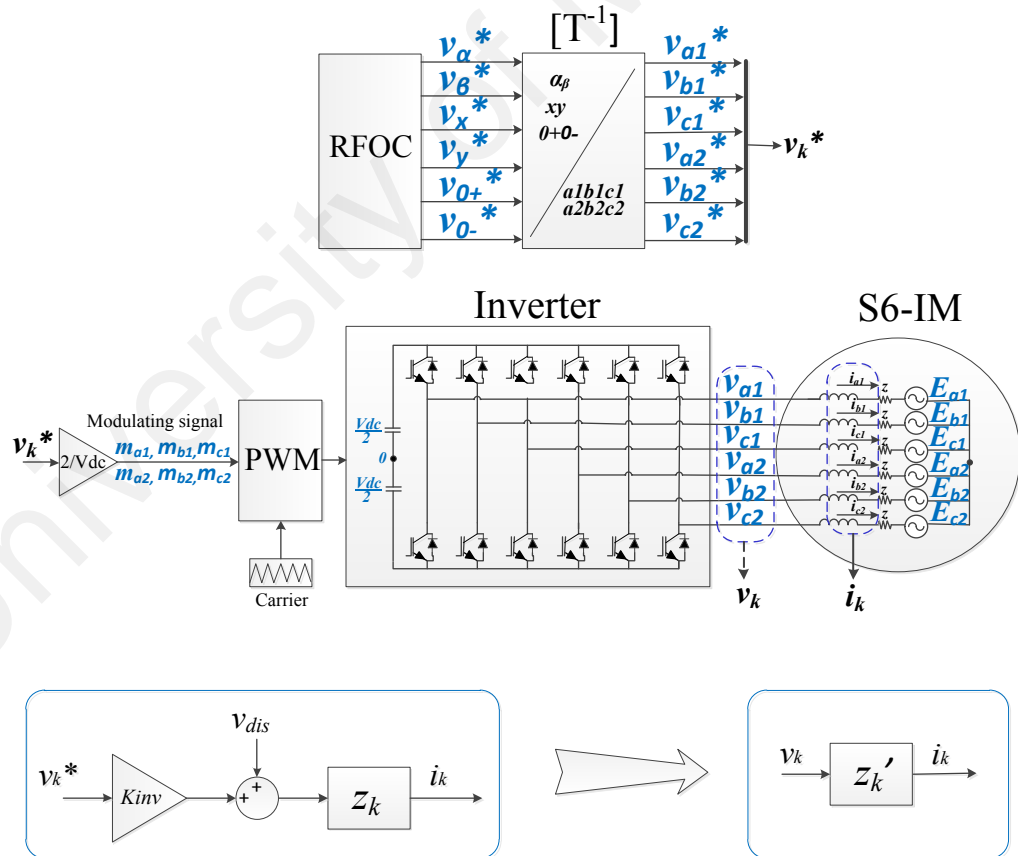


Figure 4.4: Disturbance added with additional impedance becomes an effective impedance

These effective machine parameters are more important than the actual machine parameters since these are the machine parameters seen by the controller and affect the operation of the inverter.

4.3.2 Selection of Machine Equation Reference Frame

To estimate the effective machine parameter through curve fitting the theoretical voltage with the control voltage, it is necessary to select the suitable frame of reference in which the theoretical voltage equations will be derived. For RFOC, the voltage and currents are available in three reference frames:

- a. Phase reference frame, i.e. a_1, b_1, c_1, a_2, b_2 and c_2
- b. Stationary decoupled reference frame, i.e. $\alpha, \beta, x, y, \theta_+$ and θ_- .
- c. Synchronous rotating (rotor flux) reference frame, i.e. d, q, x, y, θ_+ and θ_- .

Among the three, the synchronous rotating (rotor flux) reference frame cannot be utilized because the machine equation in this reference frame requires the d -axis to be aligned to the rotor flux which is not possible without accurate knowledge of the rotor parameters. Between the remaining two reference frames, the stationary decoupled reference frame has been chosen because of the decoupled vector space approach that allows more insights to the parameters in different subspaces.

4.4 Theoretical Voltage Equations for S6 Induction Machine

In this section, the equivalent circuits of a S6-IM are derived based on the stationary decoupled reference frame, specifically in the $\alpha\text{-}\beta, x\text{-}y$ and $\theta_+\theta_-$ subspaces. For healthy induction motor drive under two isolated neutrals 2N, only voltage in $\alpha\text{-}\beta$ and $x\text{-}y$ are considered. Meanwhile, for single isolated neutral 1N, all the $\alpha\text{-}\beta, x\text{-}y$ and $\theta_+\theta_-$ subspaces need to be considered. It is worth noting for the decoupling transformation matrix selected, θ_+ current will be zero while the θ_- current can flow.

4.4.1 Voltage Equations in α - β Subspace

Using the well-established VSD concept, the voltage equations in the α - β subspace can be written as functions of the machine parameters, stator, and rotor flux as well as stator and rotor currents.

$$\begin{aligned}
 \hat{v}_{\alpha s} &= R_s \cdot i_{\alpha s} + \frac{d}{dt} \hat{\psi}_{\alpha s} \\
 \hat{v}_{\beta s} &= R_s \cdot i_{\beta s} + \frac{d}{dt} \hat{\psi}_{\beta s} \\
 0 &= R_r \cdot i_{\alpha r} + \frac{d}{dt} \hat{\psi}_{\alpha r} + \omega_r \hat{\psi}_{\beta r} \\
 0 &= R_r \cdot i_{\beta r} + \frac{d}{dt} \hat{\psi}_{\beta r} - \omega_r \hat{\psi}_{\alpha r}
 \end{aligned} \tag{4.2}$$

where

$$\begin{aligned}
 \hat{\psi}_{\alpha s} &= L_s \cdot i_{\alpha s} + L_m \cdot i_{\alpha r} \\
 \hat{\psi}_{\beta s} &= L_s \cdot i_{\beta s} + L_m \cdot i_{\beta r} \\
 \hat{\psi}_{\alpha r} &= L_s \cdot i_{\alpha r} + L_m \cdot i_{\alpha s} \\
 \hat{\psi}_{\beta r} &= L_s \cdot i_{\beta r} + L_m \cdot i_{\beta s}
 \end{aligned} \tag{4.3}$$

Here, machine parameters R_s , R_r , L_m , L_s , L_r , ω_{sl} are the stator resistance, rotor resistance, magnetizing inductance, stator inductance, rotor inductance, and slip frequency respectively, while the symbol $\hat{}$ denotes the theoretical voltages and flux.

Since in the RFOC, the rotor quantities cannot be directly measured but need to be estimated using the machine parameters, they must be eliminated from the voltage equations. By using (4.2) and (4.3), the α - β voltages for the induction machine can be expressed as functions of the stator currents, machine parameters and operating points which given in (4.4) and (4.5).

$$\hat{v}_{\alpha s} = \left(R_s + \frac{L_m^2 \cdot \omega_s \cdot \omega_{slip}}{R_r \left(1 + \frac{L_r^2 \cdot \omega_{slip}^2}{R_r^2} \right)} \right) \cdot i_{\alpha s} - \left(\sigma \cdot L_s \cdot \omega_s + \frac{L_m^2 \cdot \omega_s}{L_r \left(1 + \frac{L_r^2 \cdot \omega_{slip}^2}{R_r^2} \right)} \right) \cdot i_{\beta s} \quad (4.4)$$

$$\hat{v}_{\beta s} = \left(\sigma \cdot L_s \cdot \omega_s + \frac{L_m^2 \cdot \omega_s}{L_r \left(1 + \frac{L_r^2 \cdot \omega_{slip}^2}{R_r^2} \right)} \right) \cdot i_{\alpha s} + \left(R_s + \frac{L_m^2 \cdot \omega_s \cdot \omega_{slip}}{R_r \left(1 + \frac{L_r^2 \cdot \omega_{slip}^2}{R_r^2} \right)} \right) \cdot i_{\beta s} \quad (4.5)$$

The variables σ and ω_{sl} can be defined as:

$$\sigma = 1 - \frac{L_m^2}{L_s L_r} \quad (4.6)$$

$$\omega_{sl} = \omega_s - \omega_r \quad (4.7)$$

4.4.2 Parameter Estimation in x - y and θ - Subspaces

Similarly, the theoretical voltages in the x - y and θ - subspaces can be calculated from machine parameters and machine currents. Compared to the α - β subspace, the x - y and θ -voltage equations are much simpler since they do not contain any rotor components, as shown below:

$$\begin{aligned} \hat{v}_{xs} &= R_s \cdot i_{xs} + L_{lsxy} \cdot \frac{d}{dt} i_{xs} \\ \hat{v}_{ys} &= R_s \cdot i_{ys} + L_{lsxy} \cdot \frac{d}{dt} i_{ys} \\ \hat{v}_{0-s} &= R_s \cdot i_{0-s} + L_{ls0-} \cdot \frac{d}{dt} i_{0-} \end{aligned} \quad (4.8)$$

Based on (4.8), the machine parameters L_{lsxy} , L_{ls0-} , ω_s are the stator leakage inductance for x - y , stator leakage inductance for θ - and synchronous frequency respectively. As explained in Chapter 3, the x - y and θ - currents during post-fault operation can be expressed as functions of α - β currents using coefficients $K1$ - $K8$.

Substituting coefficients into (4.8) give the simplified x - y and 0 - voltage equations based on α - β currents for the induction motor

$$\hat{v}_{xs} = A \cdot i_{\alpha s} + B \cdot i_{\beta s} \quad (4.9)$$

$$\hat{v}_{ys} = C \cdot i_{\alpha s} + D \cdot i_{\beta s} \quad (4.10)$$

$$\hat{v}_{0-s} = E \cdot i_{\alpha s} + F \cdot i_{\beta s} \quad (4.11)$$

where

$$\begin{aligned} A &= R_s \cdot K_1 + \omega_s \cdot L_{lsxy} \cdot K_2 \\ B &= R_s \cdot K_2 - \omega_s \cdot L_{lsxy} \cdot K_1 \\ C &= R_s \cdot K_3 + \omega_s \cdot L_{lsxy} \cdot K_4 \\ D &= R_s \cdot K_4 - \omega_s \cdot L_{lsxy} \cdot K_3 \\ E &= R_s \cdot K_7 + \omega_s \cdot L_{ls0} \cdot K_8 \\ F &= R_s \cdot K_8 - \omega_s \cdot L_{ls0} \cdot K_7 \end{aligned} \quad (4.12)$$

4.5 Parameter Estimation Process

Figure 4.5 illustrates the overall machine parameter estimation method used in this chapter. The proposed machine parameters estimation method starts with x - y subspaces, then 0 - subspace parameter estimation for S6-1N, and finally α - β subspaces parameter estimation.

For the x - y and 0 - subspace parameter estimation, the machine is operated under a pseudo-open phase fault (pseudo-OPF) mode instead of physically open-circuiting the inverter to machine connection. This is because once the connection is physically open-circuited, the machine phase voltages are not fully reflected by the control voltages and this renders equation (4.1) invalid. By keeping all connections intact, but just setting the x - y and 0 - current references according to the post-fault current references, the machine will operate in a pseudo-OPF mode where the corresponding phase current will fall to zero.

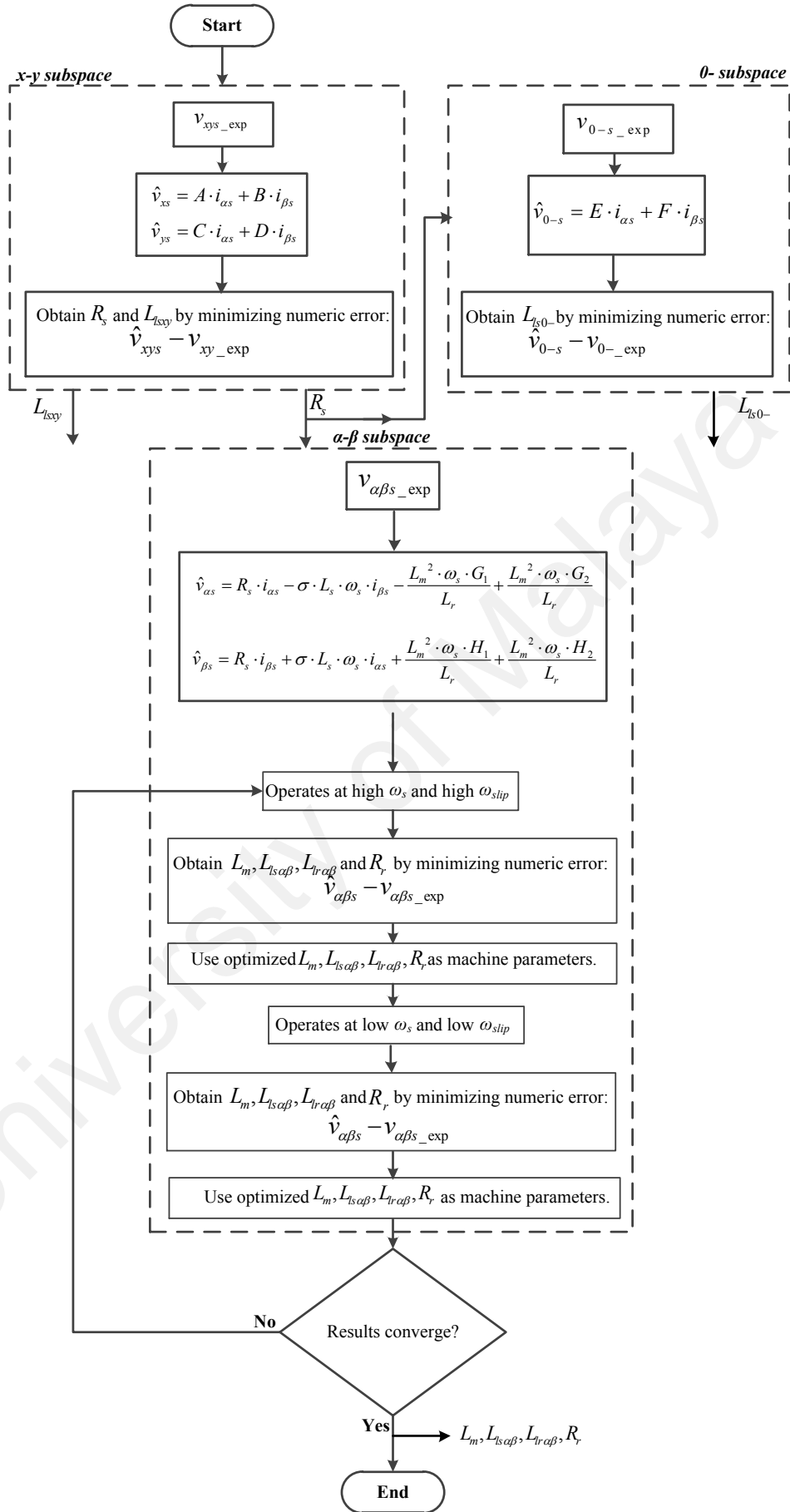


Figure 4.5: Flowchart showing the overall parameter estimation process

Firstly, the machine is operated at pseudo-OPF mode with a rated control voltage, slip frequency, and synchronous frequency of 1400 rpm. With the rated flux current set to be 1.3 A, the load is slowly increased until the maximum phase current is equal to the rated phase current. The control voltages, measured currents, and synchronous frequency are recorded for at least one fundamental cycle. These data are exported into Excel where Excel Solver, a nonlinear optimization algorithm in MS Office Excel, is used to optimize the x - y and θ - subspace parameters. The optimum values of R_s , $L_{ls\ x-y}$, and $L_{ls\ \theta}$ are obtained by minimizing the errors between the recorded x - y and θ - control voltages and the theoretical voltages calculated based on (4.8) – (4.12), i.e. $\hat{v}_{xys} - v_{xy_exp}$ and $\hat{v}_{\theta-s} - v_{\theta_exp}$.

Then, the remaining machine parameters in the α - β plane, namely R_r , L_m , $L_{lr\ \alpha-\beta}$, $L_{ls\ \alpha-\beta}$, are estimated. To reduce the number of parameters to estimate, the stator resistance here is assumed to be the same as R_s obtained from the x - y plane. The theoretical α - β voltages are first calculated using (4.4) – (4.5) based on the initial guesses of the machine parameters. Then, Excel Solver is used to optimizing the machine parameters by minimizing the error between theoretical and controller's α - β voltages similar to the case for x - y and θ - subspace parameter estimation.

However, unlike the x - y and θ - plane, the parameters in the α - β plane is affected by the operating condition of the machine, more specifically, the slip frequency and synchronous frequency. At high ω_s and ω_{slip} , the magnetizing branch of the α - β impedance will be more dominant than the rotor branch; at low ω_s and ω_{slip} , however, the rotor branch parameter will have a more pronounced effect on the overall α - β plane impedance.

To cater for this, the optimization for the α - β plane parameter is repeated for two operating conditions:

- a) High ω_s and high ω_{slip} (machine operating at 1400 rpm with rated i_q of 3.3 A)
- b) Low ω_s and low ω_{slip} (machine operating at 350 rpm with no-load i_q of 0.5A)

These are akin to the no-load and locked rotor tests in the standard tests.

Using the estimated machine parameters in all three sub-spaces, the theoretical VSD voltages can be calculated for the different operating conditions, where speed and load are varied. The accuracy of the estimated machine parameters is determined by comparing the theoretical line-to-line voltages (the differences between theoretical phase voltages obtained through inverse-Clarke transformation) with the experimental line-to-line voltages based on the control voltages.

4.6 Results and Discussions

4.6.1 Experimental Validation of the Proposed Method

The experimental verification of the proposed machine parameter verification method is conducted on the S6 machine (obtained by rewinding a 0.55 kW three-phase induction machine) with a V_{dc} voltage of 280V. The general layout for the test rig is shown as in Appendix B. Preliminary machine parameters have been previously obtained using the standard no-load and lock rotor tests, with the assumption that the stator leakage inductance is the same in all planes. As highlighted in Section 4.2, the standard tests do not provide a very accurate parameter but will provide a good starting point for the proposed method to verify the exact machine parameters. In the experiment, the flux current i_d is maintained at its rated value of 1.3 A and the machine is operated under different load torques and operating speeds.

Figure 4.6, Figure 4.7 and Figure 4.8 show the comparison between the theoretical voltages and experimental voltages for the x - y , θ - and α - β voltages respectively. Meanwhile, Figure 4.9 shows the optimized machine parameters for the α - β plane under

two operating conditions as described in the flowchart (see Figure 4.5). For the healthy operation of the S6 machine, the values for $L_{ls\ \alpha-\beta}$ and $L_{lr\ \alpha-\beta}$ converge after a few iterations as shown in Figure 4.9(b) and Figure 4.9(d). However, the values of L_m and R_r (as shown in Figure 4.9(a) and Figure 4.9(c)) do not converge. The value of L_m and R_r stabilize around 400 mH and 5.77 Ω at high ω_s and ω_{slip} , and around 420 mH and 6.37 Ω for low ω_s and ω_{slip} . This is likely due to the machine characteristic where L_m and R_r are influenced by the operating frequency. Based on the equivalent circuit, it is known that effective L_m will be more dominant during low frequency and R_r will be more dominant during high frequency. Hence, the values of $L_m = 420$ mH and $R_r = 5.77$ Ω are selected as the machine parameters for S6-IM.

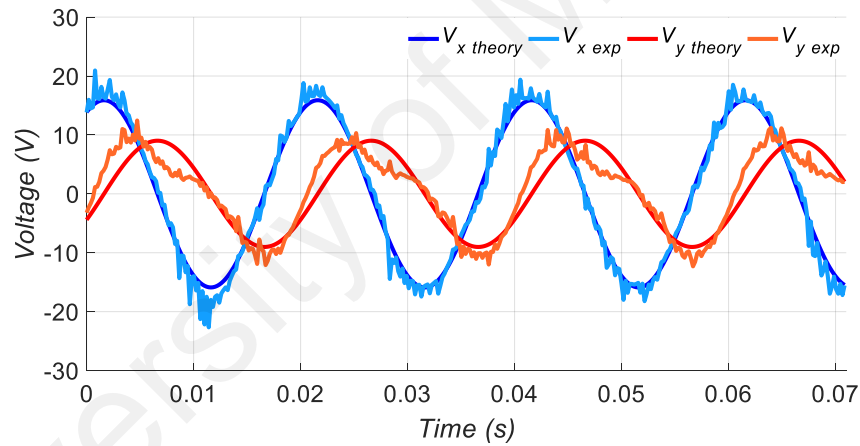


Figure 4.6: Theoretical V_{xy} and experimental V_{xy} after optimized for 1 OPF-1N

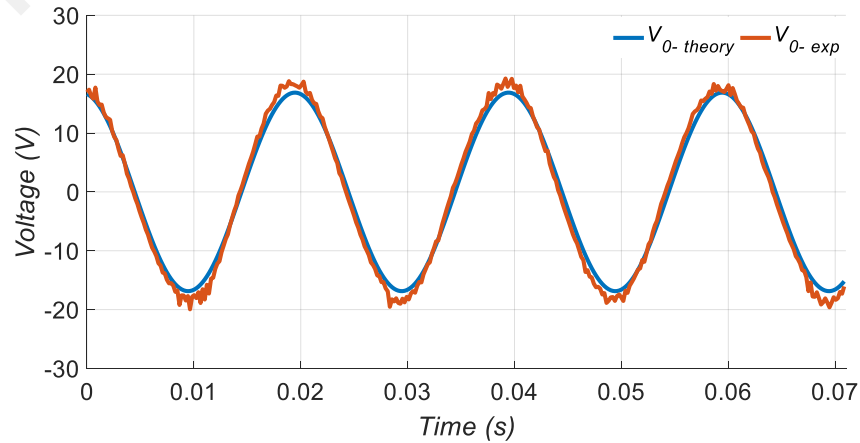


Figure 4.7: Theoretical V_{0-} and experimental V_{0-} after optimized for 1 OPF-1N

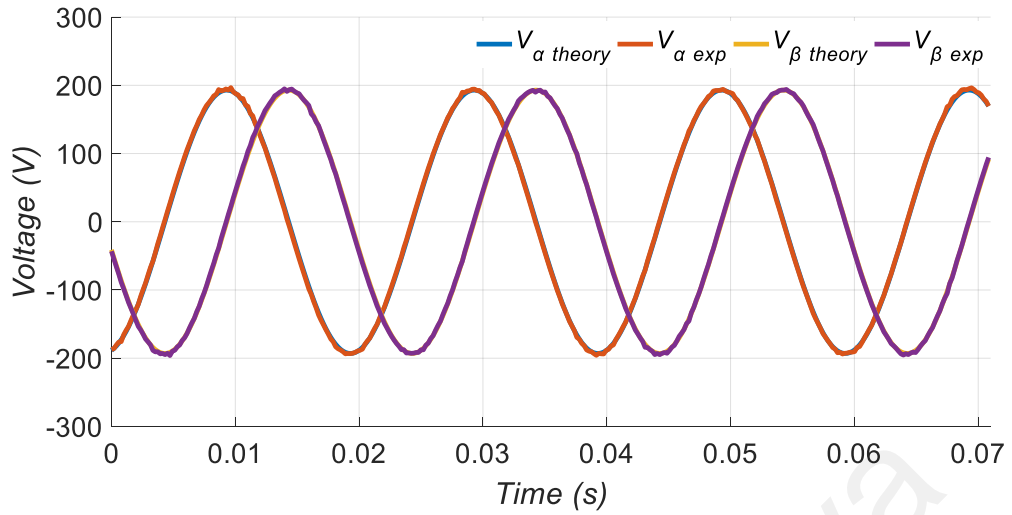


Figure 4.8: Theoretical $V_{a\beta}$ and experimental $V_{a\beta}$ after optimized for 1 OPF-1N

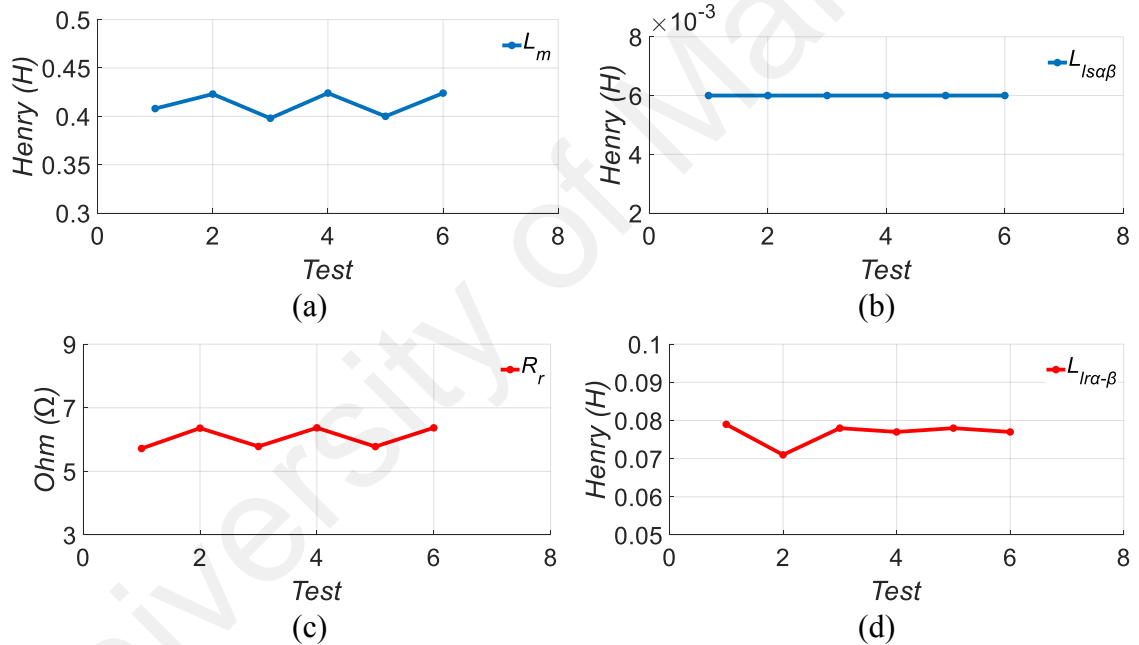


Figure 4.9: Machine parameters based on tests 1, 3, 5 (1400 rpm) and tests 2, 4, 6 (350 rpm) for healthy S6 machine. From top to bottom: (a) L_m ; (b) $L_{ls a\beta}$; (c) R_r ; (d) $L_{lr a\beta}$

Figure 4.10 demonstrates the comparison results between theoretical line voltages and experimental line voltages. The results of the proposed machine parameter estimation method are then tabulated in Table 4.1.

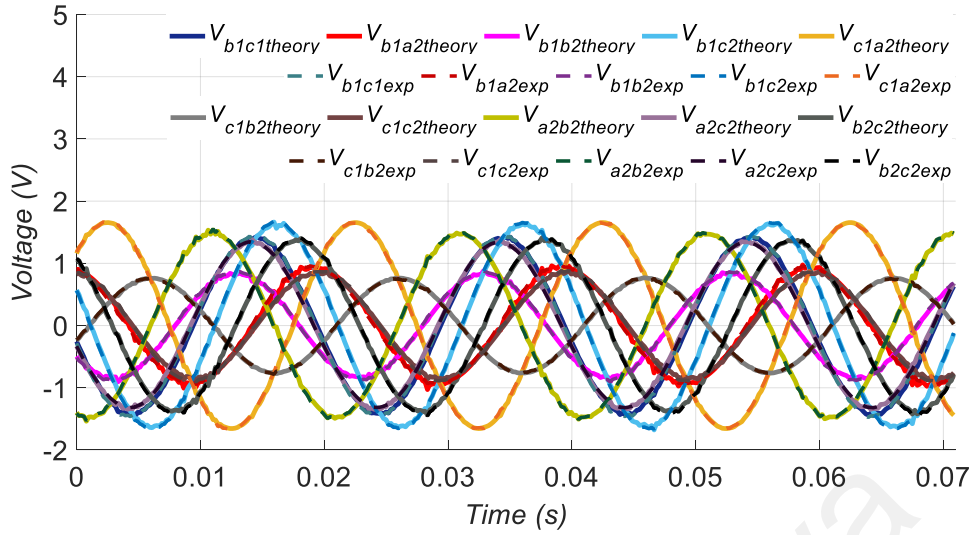


Figure 4.10: Comparison of experimental V_{line} with theoretical V_{line} calculated using estimated machine parameters under 1 OPF-1N

Table 4.1: Estimated parameters for S6-IM

Stator Resistance	$R_s = 12.532 \, \Omega$
Rotor Resistance	$R_r = 5.776 \, \Omega$
Magnetizing Inductance	$L_m = 420 \, \text{mH}$
Stator Leakage Inductance	$L_{ls} = 6 \, \text{mH}$
Rotor Leakage Inductance	$L_{lr} = 78 \, \text{mH}$
Stator Leakage Inductance (x - y)	$L_{ls \, xy} = 3.6 \, \text{mH}$
Stator Leakage Inductance (0 -)	$L_{ls \, 0-} = 38.5 \, \text{mH}$

4.6.2 Verification of Estimated Parameters under Different Operating Points

If accurate machine parameters have been obtained, the theoretical machine voltage should match with the experimental control voltages. The line-to-line voltages calculated from the theoretical voltages should match with the line-to-line voltages from the experimental voltages.

To validate the parameter estimation in the preceding subsection, several tests have been conducted under different i_{qs} and operating points namely 350 rpm, 700 rpm, 1040 rpm, and 1400 rpm to make sure that the estimated parameter can fully represent the actual machine under different operating conditions. The estimated machine parameters are used in different operating points and the results are demonstrated in Figure 4.11 and Figure 4.12.

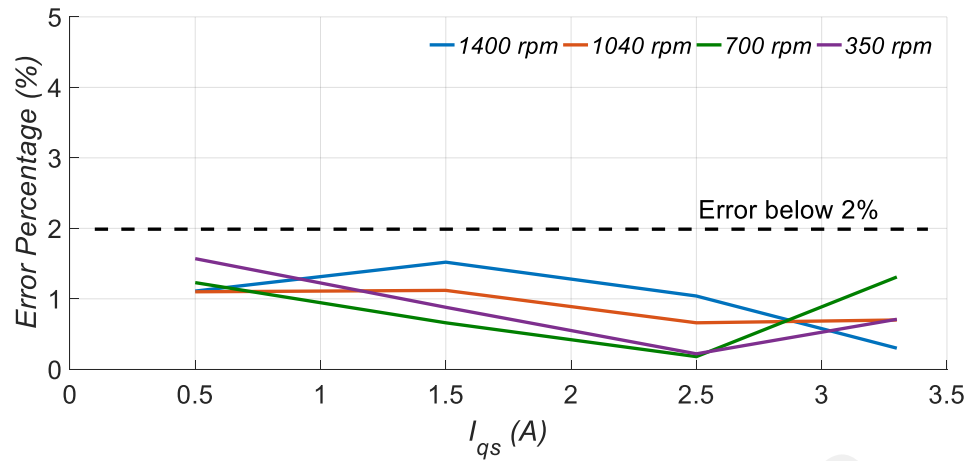


Figure 4.11: Percentage average error of estimated machine parameter under different operating points and i_{qs} in healthy operation

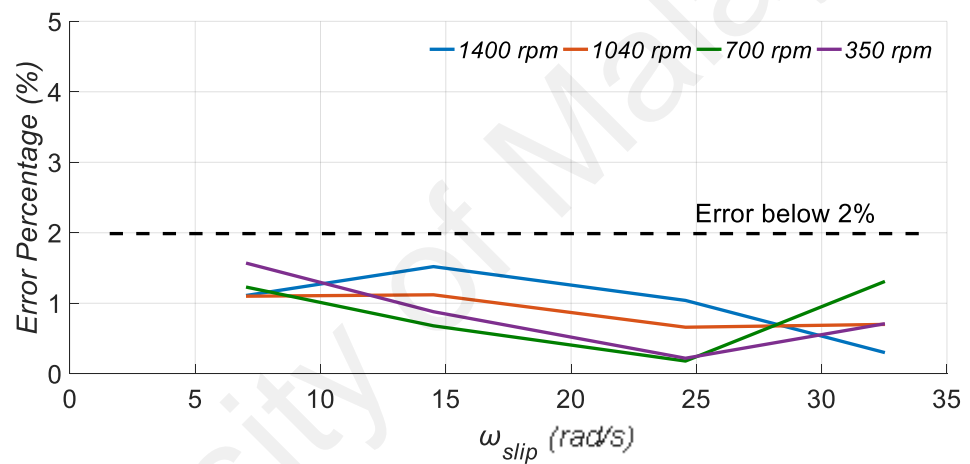


Figure 4.12: Percentage average error of estimated machine parameter under different operating points and ω_{slip} in healthy operation

Figure 4.11 shows the percentage average error based on average squared error (ASE), which is the average squared difference between the experimental values and theoretical values obtained under different speeds for i_{qs} at 0.5 A, 1.5 A, 2.5 A, and 3.3 A. It is found that the maximum percentage average error is around 1.63% with i_q value of 0.5 A recorded at 350 rpm. The most accurate machine parameters which contribute to the lowest error is 0.13% at i_{qs} value of 2.5 A when the machine runs at 700 rpm.

Figure 4.12 shows the same trend for rated speed giving the highest percentage average error at lower slip frequency and the lowest percentage average error at rated slip frequency. The results are given in Figure 4.11 and Figure 4.12 demonstrate that different

operating points will produce slightly different percentage average error but with the proposed machine parameters estimation method, the percentage average error will be less than 2%. This indicates the reliability of the estimated machine parameters.

Figure 4.13 to Figure 4.15 compare the line-to-line voltages calculated from theoretical voltage equations using estimated machine parameters (solid line) with the line-to-line voltages obtained from the experiments (dotted points). The results demonstrate that the machine parameter estimated using the proposed method can predict the experimental line-to-line voltages.

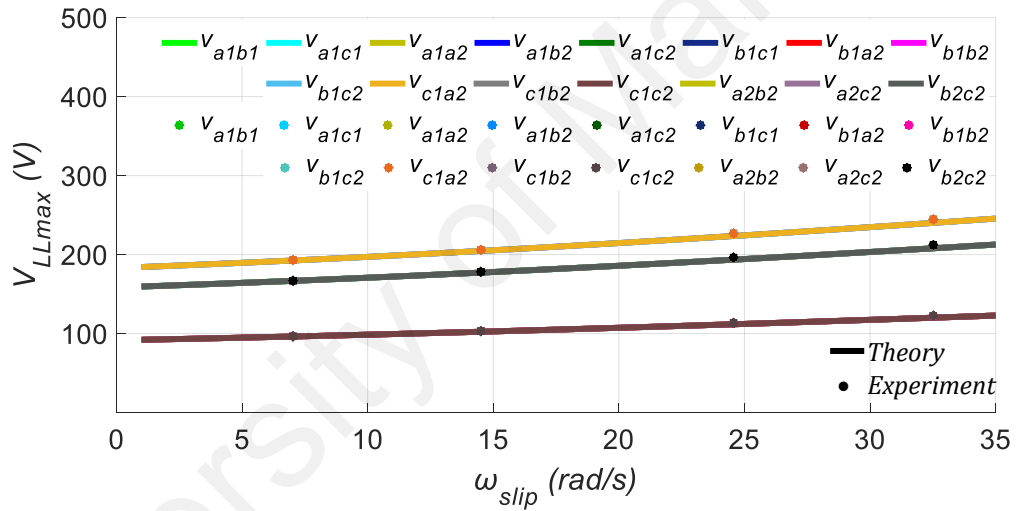


Figure 4.13: Maximum line-to-line voltages under different ω_{slip} at rated ω_s in healthy operation

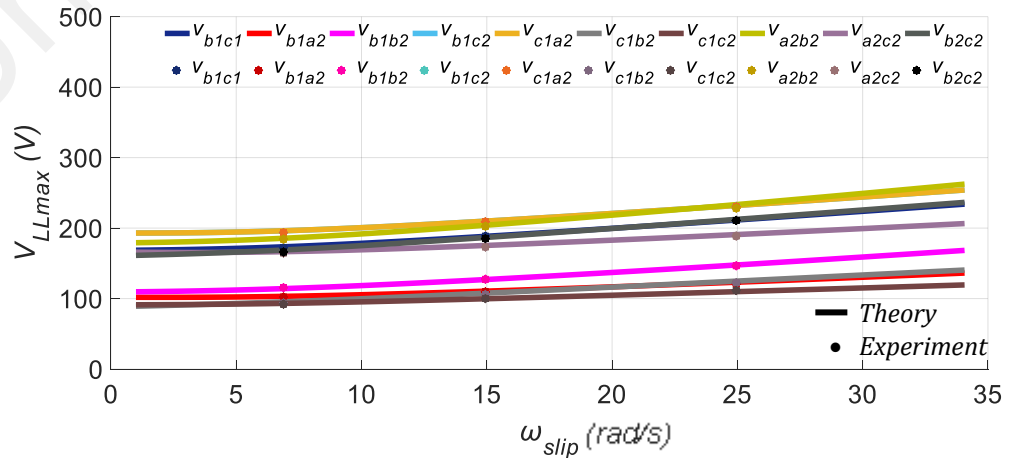


Figure 4.14: Maximum line-to-line voltages under different ω_{slip} at rated ω_s in 1OPF with 2N operation

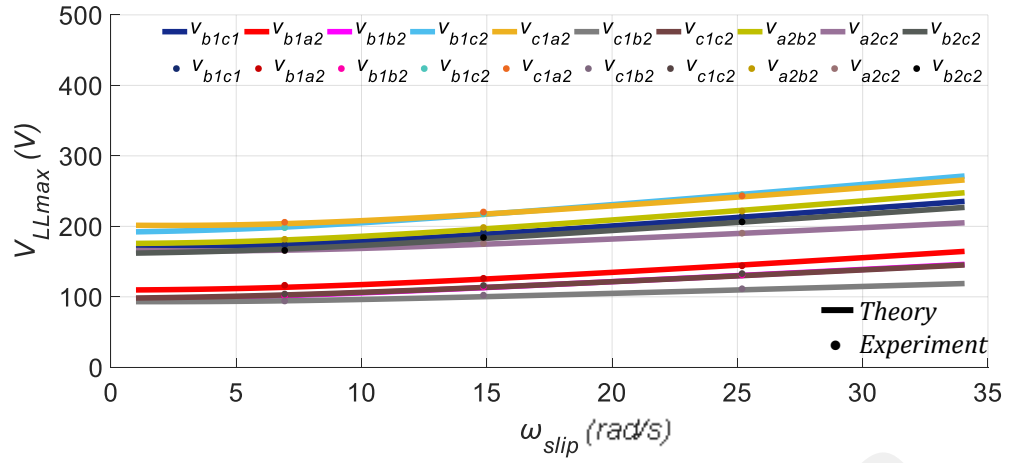


Figure 4.15: Maximum line-to-line voltages under different ω_{slip} at rated ω_s in 1OPF with 1N operation

4.7 Conclusions

In this chapter, a machine parameter estimation technique for an S6-IM has been proposed. By using a curve fitting method with nonlinear optimization algorithm, the machine parameters can be estimated and be used to accurately predict the line-to-line voltages for the S6 machine. These machine parameters are used for determining the voltage limit of the S6 machine under different OPF scenarios, which will be reported in the next chapter.

CHAPTER 5: POST-FAULT VOLTAGE LIMITS OF SYMMETRICAL SIX-PHASE INDUCTION MACHINE

5.1 Introduction

The operation of an electrical machine is not only limited by the current but also limited by the voltage. The voltage limits here refer to the ability of the inverter to provide the required voltages to the machine and depends largely on the inverter topology, machine winding configuration as well as the DC-link voltage.

For a star-connected multiphase machine with the machine neutral point(s) isolated from the inverter, the maximum voltage depends on the line-to-line voltage rather than the phase voltage (Levi et al., 2008). In order to deliver the required voltage to the machine, the DC-link voltage needs to be at least equals to the peak value of the largest line-to-line voltage of the machine. This implies that the maximum utilization of DC-bus voltage under the linear modulation region is reached when the peak value of the line voltage equal to the DC-bus voltage (Levi et al., 2008). As shown in Figure 5.1 and Figure 5.2, for a 6-phase star-connected machine driven by 6-leg VSC, the maximum line voltage for S6 with 1N connection is i.e. V_{alb2} which is the highest line voltage. In this case, the minimum DC-link voltage will be equal to the peak value of V_{alb2} .

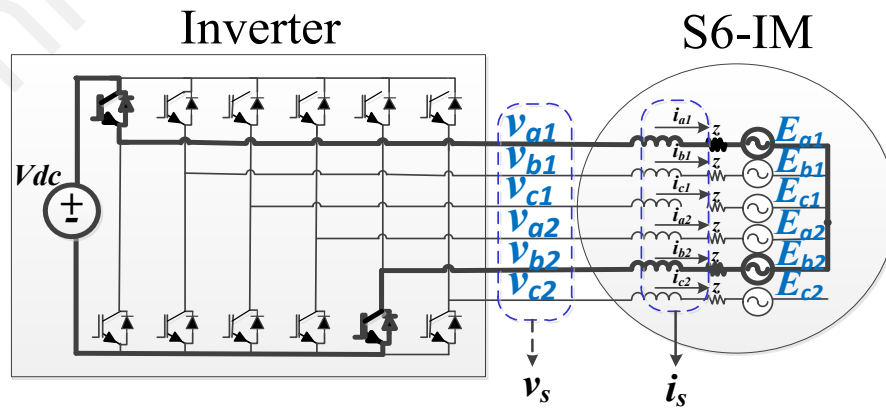


Figure 5.1: Maximum line voltage constraint for S6-1N, where $V_{dc} = V_{LLpeak}$

The largest line-to-line voltage for a star-connected multiphase machine, hence the minimum DC-link voltage required, is affected by the neutral configuration, phase number, and winding configuration. This has been demonstrated in (Levi et al., 2008) for a specific case of five-phase and seven-phase machines. For a star-connected symmetrical six-phase machine, there are two ways of connecting the neutral points, i.e. with two isolated neutrals or with single isolated neutral.

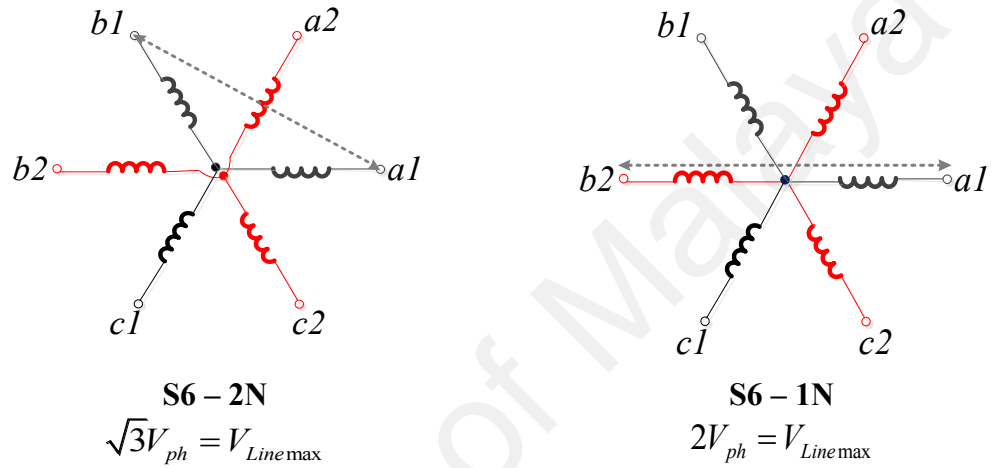


Figure 5.2: Voltage limit for S6-IM configured with 1N and 2N

As seen in Figure 5.2, the line-to-line voltage should only be considered between phases that are connected to the same neutral points, since these phases are physically connected to the VSC's DC-link during operation. From Figure 5.2, the maximum line-to-line voltage for S6-1N is $2/\sqrt{3} = 1.155$ times higher than that of the maximum line-to-line voltage for S6-2N.

For healthy multiphase, the minimum DC-link voltage is given as

$$V_{DC} \geq V_{line\ max} = 2 |\cos \delta| V_{ph} \quad (5.1)$$

where δ is the angle between the largest two phases within the same winding. However, during OPF, the machine is no longer operating in balanced mode and the voltage relation defined in (5.1) is no longer valid.

In (A. S. Abdel-Khalik et al., 2014), the authors suggested that the minimum required DC-link voltage should still equals the peak of the maximum line-to-line voltage. However, under OPF, the relation between the maximum line voltage and the phase voltage is no longer based on (5.1). It was suggested that the machine needs to be deloaded under OPF in order to operate within the voltage limit (A. S. Abdel-Khalik et al., 2014).

Comprehensive studies by taking into consideration both current and voltage limits have been performed in (Eldeeb et al., 2019; Fall et al., 2016). In (Ayman S Abdel-Khalik et al., 2018), the DC-link voltage limit studies with different optimal reference currents for post-fault of the asymmetrical six-phase induction machine are determined under one open-phase fault for both 1N and 2N. The authors using a single circuit combining effect of all subspaces and concluded that the line voltage is a function of machine parameters. However, the studies focused only on A6 with 1 OPF.

Even though the post-fault current limits for the S6 induction machine have been clearly defined in Chapter 3, it is not sure if there will be occasions where the voltage limit is reached before the current limit and become the restricting factor for the machine in post-fault operation. To have a better understanding of the post-fault capability of the S6 induction machine, both the current and voltage limits need to be considered. Hence, in this chapter, the post-fault voltage limits of S6-IM is studied.

Once the post-fault currents have been identified (as in Chapter 3), the required machine voltage to attain the post-fault currents will depend on the machine parameters.

Based on the $\alpha\text{-}\beta$ voltage equations (as in Chapter 4), it can be seen that the voltage is a function of current, machine parameters and operating points which mainly affected by the synchronous frequency, ω_s and slip frequency, ω_{slip} . To fully understand the post-fault performance of the S6 induction machine, it is necessary to determine the voltage limits in terms of different operating points.

In this chapter, the post-fault voltage limits for the S6 induction machine under different OPF scenarios are considered, including the effects of neutral connections.

Here, voltage limits using voltage equation in terms of decoupled subspaces voltages $v_{\alpha\text{-}\beta, x\text{-}y, 0+0-}$ is formulated deriving the expression for post-fault machine voltages. The maximum operating limits for different fault-tolerant drives with current limits consideration are discussed. To further illustrate the impact of voltage and current limits, the results from the experiment are used to validate the theoretical discussion.

5.2 Line-to-Line Voltages of Symmetrical Six-phase Induction Machine

Based on Table 5.1, the line-to-line voltages for healthy S6 can be divided into three groups namely large, medium and small line voltages. There are three line voltages in large group, six line voltages in both medium and small group making a total of fifteen line voltages available for a healthy machine. From Figure 5.3, it can be observed that large line-to-line voltages have the longest length in terms of magnitude which is 2 times longer than the phase voltage while the medium voltage is $\sqrt{3}$ longer than phase voltage and the small line-to-line voltages are equal in length to the phase voltage.

The magnitude and directions of the fifteen line voltages for S6-IM are shown in Figure 5.4. The dark dotted lines indicate the large line-to-line voltages, the navy dotted lines represent the medium line-to-line voltages and the red dotted line showing the small line-to-line voltages.

Table 5.1: Line-to-line voltages for healthy operation

Large	<i>Magnitude</i> $2 V_{ph}$	V_{a1b2}
		V_{b1c2}
		V_{c1a2}
Medium	$\sqrt{3} V_{ph}$	V_{a1b1}
		V_{a1c1}
		V_{b1c1}
		V_{a2b2}
		V_{a2c2}
		V_{b2c2}
Small	V_{ph}	V_{a1a2}
		V_{a1c2}
		V_{b1a2}
		V_{b1b2}
		V_{c1b2}
		V_{c1c2}

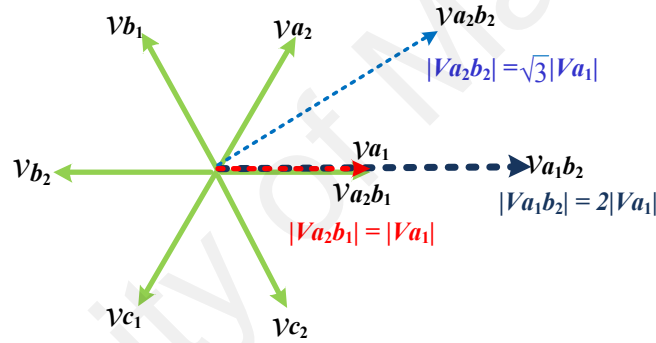


Figure 5.3: Magnitude of phase voltage and line-to-line voltage of symmetrical six-phase induction machine

During OPF, one or more of the machine phases are disconnected from the VSC. The maximum voltage that can be applied by the VSC depends only on the line-to-line voltage of the remaining phases.

For post-fault mode under 1 OPF-1N, ten line-to-line voltages need to be considered. The other available line-to-line voltages for S6-IM under different fault scenarios with 1N or 2N are tabulated in Table 5.2. For two isolated neutrals, the remaining healthy phases will be affected by the same winding only.

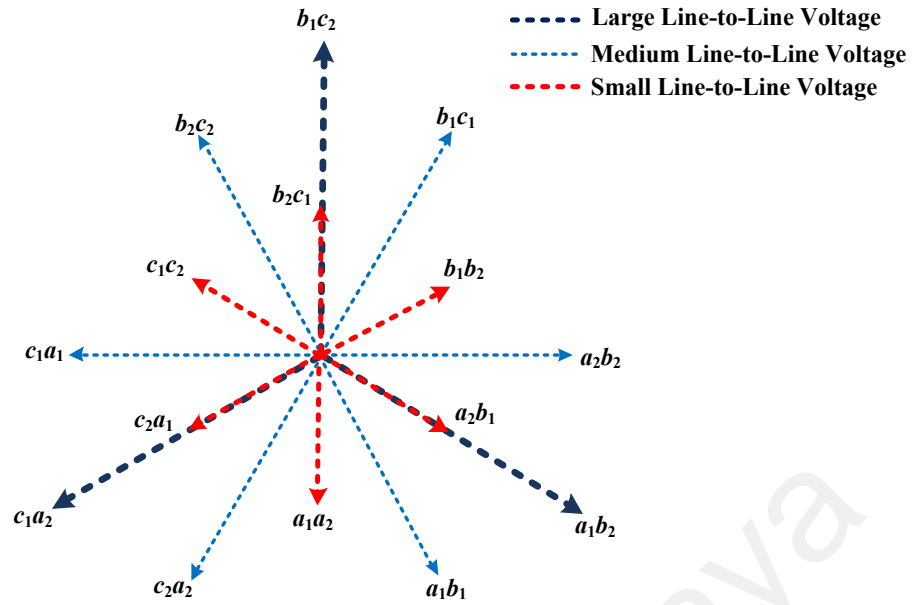


Figure 5.4: Line-to-line voltage representation of symmetrical six-phase induction machine under healthy operation

Table 5.2: Line-to-line voltages for symmetrical six-phase machine based on neutral connections 1N and 2N for post-fault operation

OPF			Line Voltages									
<i>Faulty phase (1N)</i>			V_{b1c2}	V_{c1a2}	V_{b1c1}	V_{a2b2}	V_{a2c2}	V_{b2c2}	V_{b1a2}	V_{b1b2}	V_{c1b2}	V_{c1c2}
1 OPF	1	a_1	√	√	√	√	√	√	√	√	√	√
2 OPFs	2a	$a_1 - b_1$	-	√	-	√	√	√	-	-	√	√
	2b	$a_1 - a_2$	√	-	√	-	-	√	-	√	√	√
	2c	$a_1 - b_2$	√	√	√	-	√	-	√	-	-	√
3 OPFs	3a	$a_1 - b_1 - c_1$	-	-	-	√	√	√	-	-	-	-
<i>Faulty phase (2N)</i>												
1 OPF	1	a_1	-	-	√	√	√	√	-	-	-	-
2 OPFs	2a	$a_1 - b_1$	-	-	-	√	√	√	-	-	-	-
	2b	$a_1 - a_2$	-	-	√	-	-	√	-	-	-	-
3 OPFs	3a	$a_1 - b_1 - c_1$	-	-	-	√	√	√	-	-	-	-

In such scenario, the other winding for post-fault operation is not possible. Such scenario adds together with faulted phase(s) are indicated by "-" in Table 5.2. Meanwhile, for single isolated neutral, all the line-to-line voltages that link to the same neutral connection will be available excluding the faulted phase.

5.3 Line-to-Line Voltages of Symmetrical Six-phase Induction Machine under Different Operating Points

The voltage limit is hit when the peak of the highest line-to-line voltage equal to the DC-bus voltage. In order to identify the voltage limit, it is first necessary to identify the maximum line-to-line voltage. The line-to-line voltage changing with different operating points, particularly synchronous frequency, ω_s and slip frequency, ω_{slip} . Therefore, it is necessary to understand how the line-to-line voltage changes with ω_s and ω_{slip} . The synchronous frequency represented by ω_s can be defined as

$$\omega_s = 2\pi f \quad (5.2)$$

For operation up to base speed, the maximum ω_s will be obtained when f is the rated frequency. For 50 Hz machine, the maximum $\omega_s = 314$ rad/s. On the other hand, ω_{slip} is a function of rotor time constant, i_{ds} and i_{qs} which is given by

$$\omega_{slip} = \frac{1}{\tau_r} \cdot \frac{i_{qs}}{i_{ds}} \quad (5.3)$$

where the rotor time constant is given by

$$\tau_r = L_r / R_r \quad (5.4)$$

For operation up to the rated condition, the maximum slip frequency can be defined as a function of τ_r , i_{ds} , i_{qs} and derating factor, a which is given by

$$\begin{aligned} |i'_{dqs}| &\leq a |i_{dqs}|_{rated} \\ \sqrt{i'^2_{ds} + i'^2_{qs}} &\leq a |i_{dq}|_{rated} \end{aligned} \quad (5.5)$$

where $k = a |i_{dqs}|_{rated}$

$$\begin{aligned}
& \sqrt{i_{dsrated}^2 + (\tau_r \cdot i_{dsrated} \cdot \omega_{slip})^2} \leq k \\
& \omega_{slip} \leq \sqrt{\frac{k^2 - i_{dsrated}^2}{\tau_r^2 \cdot i_{dsrated}^2}} \\
& \omega_{slipmax} = \sqrt{\frac{a^2 |i_{dqs}|_{rated}^2 - i_{dsrated}^2}{\tau_r^2 \cdot i_{dsrated}^2}} \\
& = \sqrt{\frac{a^2 (i_{dsrated}^2 + i_{qsrated}^2) - i_{dsrated}^2}{\tau_r^2 \cdot i_{dsrated}^2}} \\
& = \sqrt{\left(a \omega_{sliprated}\right)^2 - \left(\frac{1 - a^2}{\tau_r^2}\right)}
\end{aligned} \tag{5.6}$$

Table 5.3: Maximum slip frequency ω_{slip} based on neutral connections 1N and 2N for different post-fault scenarios and derating factor, a

Case			a	Max ω_{slip} (rad/s)
Healthy			1	29.4
Faulty phase (1N)				
1 OPF	1	a_1	0.771	21.43
2 OPFs	2a	$a_1 - b_1$	0.577	14.07
	2b	$a_1 - a_2$	0.500	10.73
	2c	$a_1 - b_2$	0.577	14.07
3 OPFs	3a	$a_1 - b_1 - c_1$	0.500	10.73
Faulty phase (2N)				
1 OPF	1	a_1	0.500	10.73
2 OPFs	2a	$a_1 - b_1$		
	2b	$a_1 - a_2$		
3 OPFs	3a	$a_1 - b_1 - c_1$		

5.4 Results and Discussions

Using the machine parameters and voltage equations described in Chapter 4, the machine decoupled subspaces voltages $v_{\alpha-\beta, x-y, 0+0-}$, can be calculated based on the operating point and post-fault currents. The phase voltages for the post-fault machine can then be calculated by applying inverse Clarke transformation on $v_{\alpha-\beta, x-y, 0+0-}$. Finally, the post-fault line-to-line voltages can be defined as the differences between the phase voltages, and the maximum line-to-line voltage under different OPFs can be determined.

Since the post-fault line-to-line voltages depend largely on synchronous frequency, ω_s and slip frequency, ω_{slip} , the theoretical line-to-line voltage should be evaluated over the

range of permissible ω_s and ω_{slip} discussed in Section 5.3. Two sets of line-to-line voltages are plotted: Firstly, ω_{slip} is varied while the machine runs at maximum (i.e. rated) ω_s , then secondly, ω_s is varied while the machine runs at maximum ω_{slip} (depending on the OPF, as in Table 5.3).

To validate these theoretical line-to-line voltages, experiments on S6-IM under the same OPFs and operating conditions were conducted and compared with the theoretical results. The open-circuit fault is done manually by triggering relays according to independent fault scenarios. In the post-fault control, the flux current i_{ds} is maintained at its rated value of 1.3 A, while the slip frequency, ω_{slip} is maintained at its rated value of 29.4 rad/s (see Table 5.3). The machine parameters as tabulated in Table 4.1 are used in this experiment.

5.4.1 Voltage against Synchronous Frequency, ω_s

In this chapter, Figures 5.5 to 5.14 illustrate the voltage limits in terms of line-to-line voltages under different ω_s at rated current and rated ω_{slip} . These experimental waveforms are obtained using dSPACE ControlDesk. The speed of the S6-IM is gradually increased from 500 rpm to 1360 rpm to vary ω_s while maintaining the maximum allowable ω_{slip} by decreasing the load accordingly.

To validate the theoretical discussion on voltage equations and machine parameters used, experimental results from an S6-IM rig as shown in Appendix B, controlled using the FOT approach are used for discussion here. The solid line represents the theoretical results while the diamond point is used in the figures to indicate the experimental results. The vertical dashed line represents the rated speed while the horizontal dashed line represents the voltage limit. Since the line-to-line voltages are normalized to the maximum line-to-line voltage for healthy S6-1N, there are two voltage limits depending

on the neutral configuration, with the limit for S6-1N being 1 p.u. and limit for S6-2N being 0.866 p.u. as explained in Section 5.1.

Figure 5.5 shows the results for healthy operation while Figure 5.6 and Figure 5.7 show the line-to-line voltages for 1 OPF with 2N and 1N respectively. Meanwhile, fault scenarios for 2 OPFs in the case of 2a and 2b with 2N and 1N are shown in Figure 5.8 to Figure 5.9 and Figure 5.10 to Figure 5.11 respectively. Figure 5.12 shows the case of 2c with S6-1N.

Furthermore, the line-to-line voltages for 3 OPFs with 2N and 1N are shown in Figure 5.13 and Figure 5.14. Based on Figure 5.5 to Figure 5.14, most of the post-fault cases hit the current limit first before reaching the voltage limit except for case 2b with 2N. The main reason for this happened due to the effect from the fault occurred at two different windings, a_1 and a_2 .

Special attention should also be given to case 1 OPF, 2 OPFs for case 2a and 2c with S6-1N whereby the maximum line-to-line voltages nearly hit the voltage limit which is more likely due to the θ - subspace.

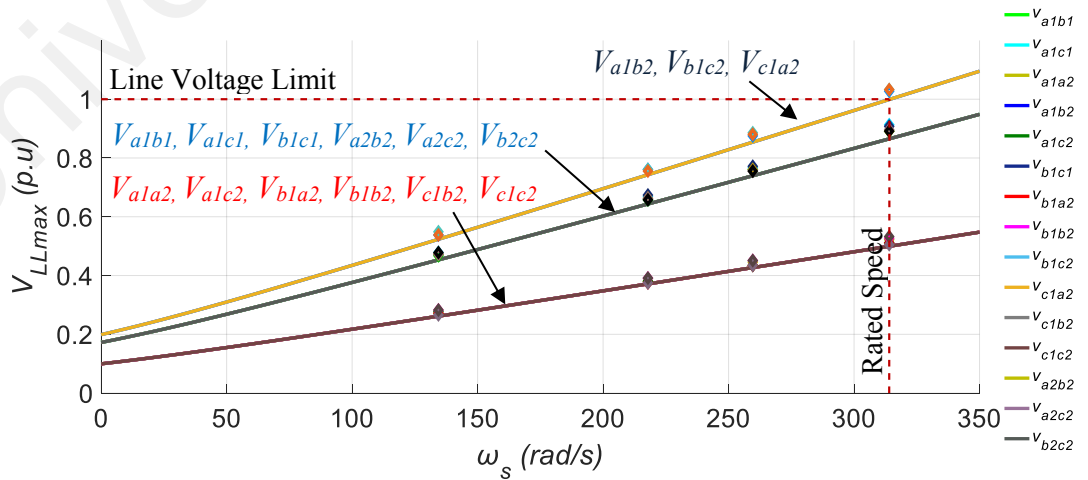


Figure 5.5: Voltage limit under different ω_s at rated ω_{slip} and rated current in healthy operation

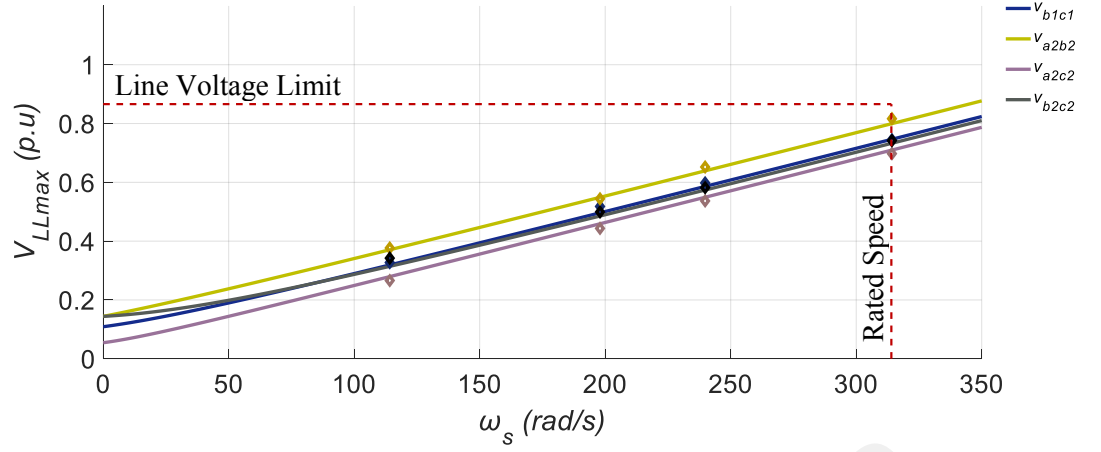


Figure 5.6: Voltage limit under different ω_s at rated ω_{slip} and rated current in 1 OPF with 2N operation

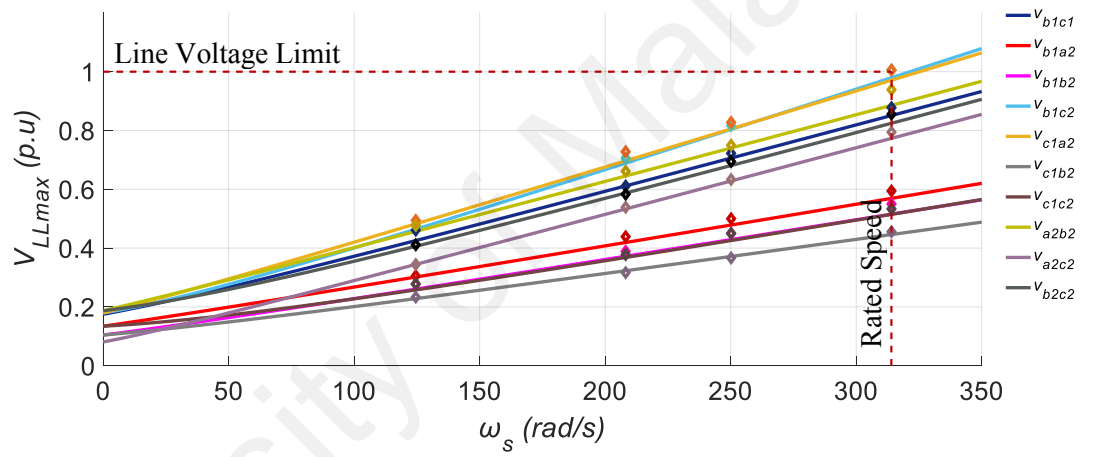


Figure 5.7: Voltage limit under different ω_s at rated ω_{slip} and rated current in 1 OPF with 1N operation

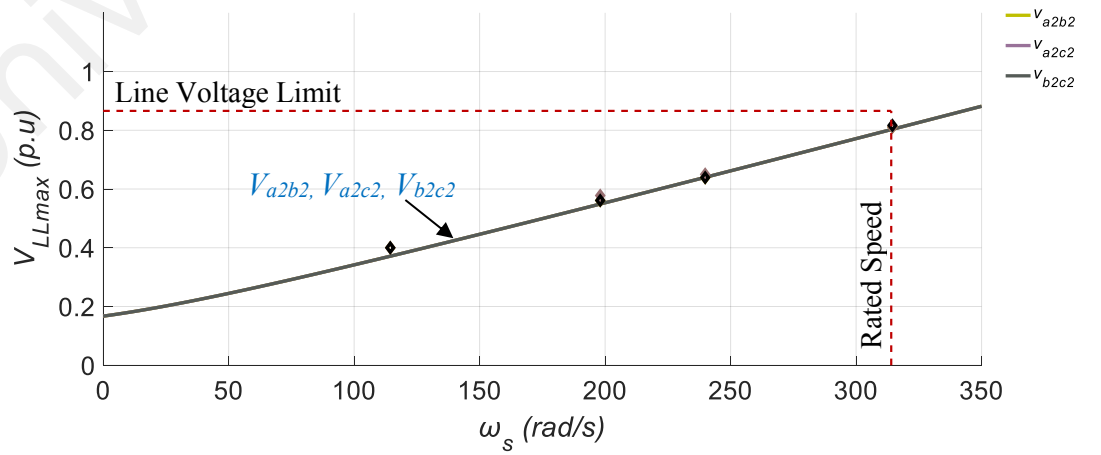


Figure 5.8: Voltage limit under different ω_s at rated ω_{slip} and rated current in 2 OPFs (case 2a) with 2N operation

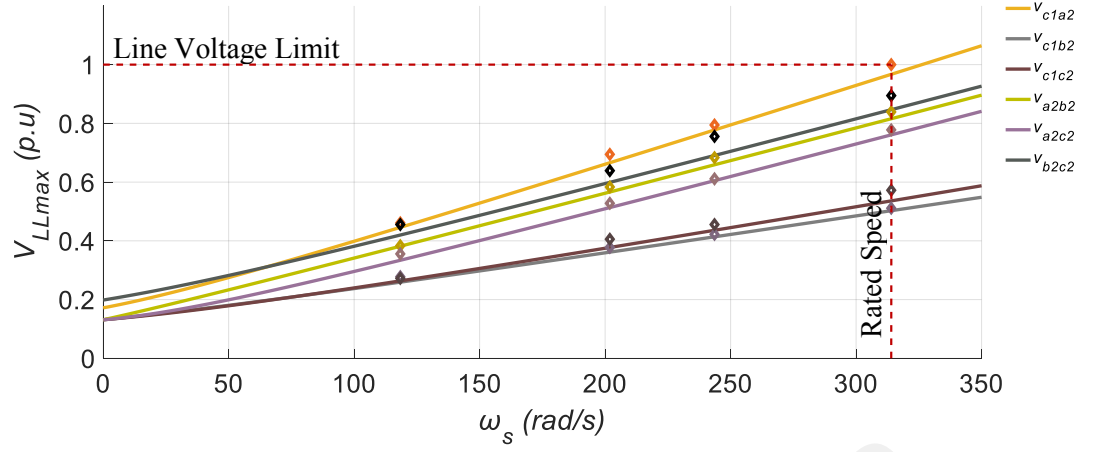


Figure 5.9: Voltage limit under different ω_s at rated ω_{slip} and rated current in 2 OPFs (case 2a) with 1N operation

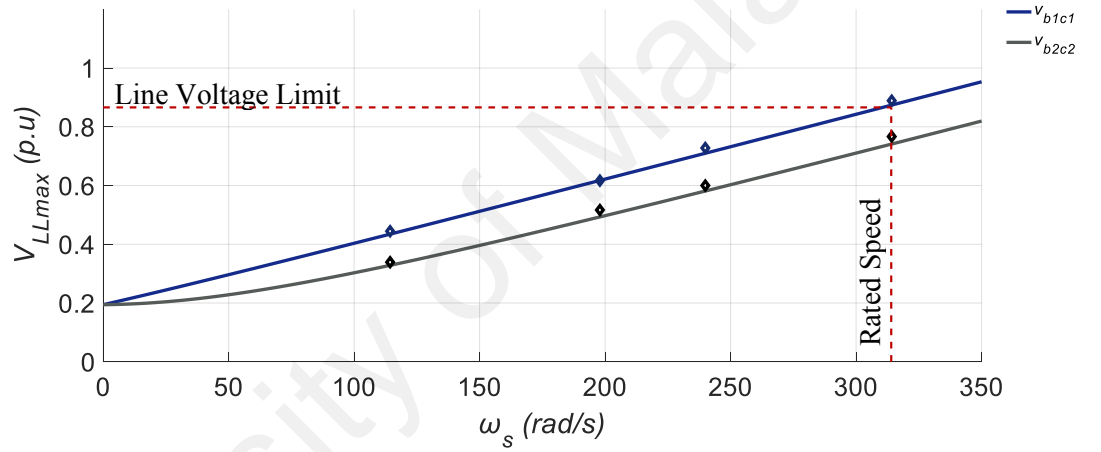


Figure 5.10: Voltage limit under different ω_s at rated ω_{slip} and rated current in 2 OPFs (case 2b) with 2N operation

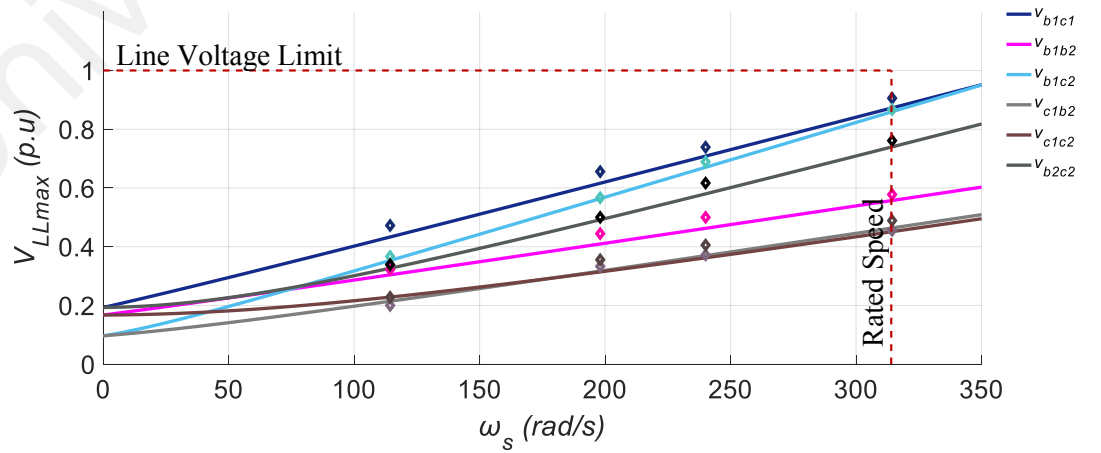


Figure 5.11: Voltage limit under different ω_s at rated ω_{slip} and rated current in 2 OPFs (case 2b) with 1N operation

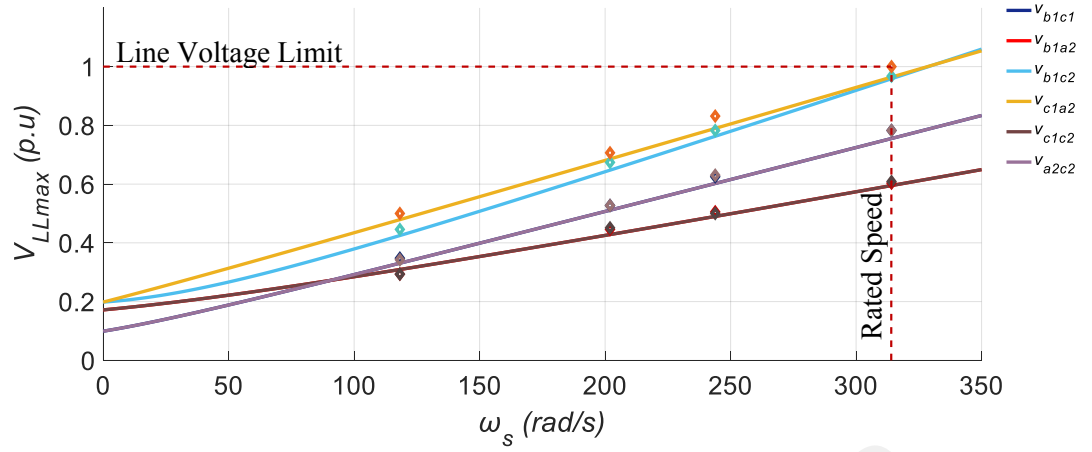


Figure 5.12: Voltage limit under different ω_s at rated ω_{slip} and rated current in 2 OPFs (case 2c) with 1N operation

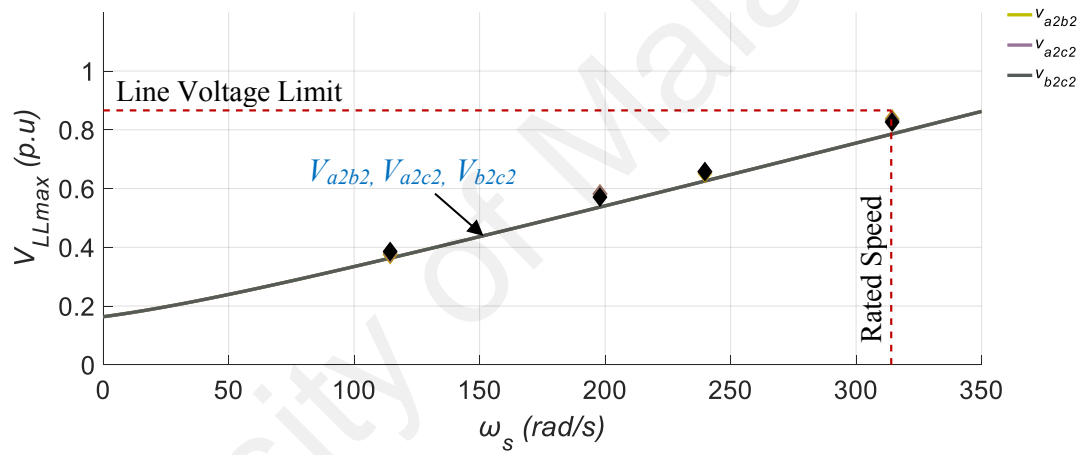


Figure 5.13: Voltage limit under different ω_s at rated ω_{slip} and rated current in 3 OPFs (case 3a) with 2N operation

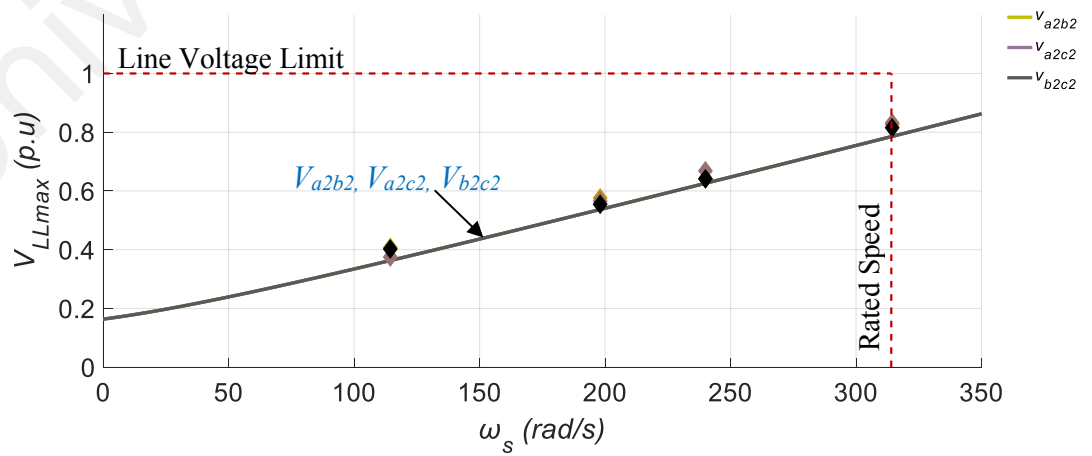


Figure 5.14: Voltage limit under different ω_s at rated ω_{slip} and rated current in 3 OPFs (case 3a) with 1N operation

The experimental results are in agreement with the theoretical line-to-line voltages, with error less than 2% confirming the validity of the derived equations in Chapter 4. Looking at the results from Figure 5.5 to 5.14, it is found that the synchronous frequency ω_s has a profound effect on the magnitude of the line-to-line voltages. Moreover when the ω_s increases, all the line-to-line voltages increase, such that the maximum line-to-line voltage will occur around the maximum ω_s .

5.4.2 Voltage against Slip Frequency, ω_{slip}

To further illustrate the variations of line-to-line voltage against slip frequency, ω_{slip} for post-fault S6-1N, experimental results for fault scenarios up to 3 OPFs were also conducted. In the post-fault control, the flux current i_{ds} maintained at its rated value of 1.3 A, while the synchronous frequency, ω_s is set as given in (5.2) at 314 rad/s and i_{qs} reflecting the torque is given by (5.3). The results are recorded in ControlDesk.

Figure 5.15 shows the results for healthy operation while Figure 5.16 and Figure 5.17 show the line-to-line voltages for 1 OPF with 2N and 1N respectively. Meanwhile, fault scenarios for 2 OPFs in the case of 2a and 2b with 2N and 1N are shown in Figure 5.18 to Figure 5.19 and Figure 5.20 to Figure 5.21 respectively. Figure 5.22 shows the case 2c with S6-1N. Meanwhile, Figure 5.23 and Figure 5.24 show the cases of 3 OPFs with 2N and 1N respectively.

Similar to the previous section, the solid line represents the theoretical results while the diamond point is used in the figures to indicate the experimental results. The maximum slip frequency, $\omega_{slipmax}$ from equation (5.6) will determine the current limit with respect to the OPF scenarios. Meanwhile, the voltage limit is defined based on neutral configurations. In what follows, the vertical dashed line represents the rated values based on fault scenarios with derating factor, a indicating the current limit while the horizontal dashed line represents the voltage limit.

As expected, the experimental results coincide with the theoretical results. With rated synchronous frequency ω_s , most of the maximum line voltages for fault scenarios hit the current limit first before reached the voltage limit excluding case 2b with 2N. The main reason for this happened due to the effect from the fault occurred at two different windings, a_1 and a_2 . It can also be observed that the maximum line-to-line voltages for 1 OPF, 2 OPFs for case 2a and 2c with S6-1N nearly hit the voltage limit due to the effect from θ - subspace.

It is worth highlighting that, for voltage against slip frequency, ω_{slip} , there is some tendency of the medium line-to-line voltages to be higher than the large line-to-line voltages. The main reasons for this happened due to the effect from the x - y and θ -components which result in the ω_{slip} on line-to-line voltages are not equal.

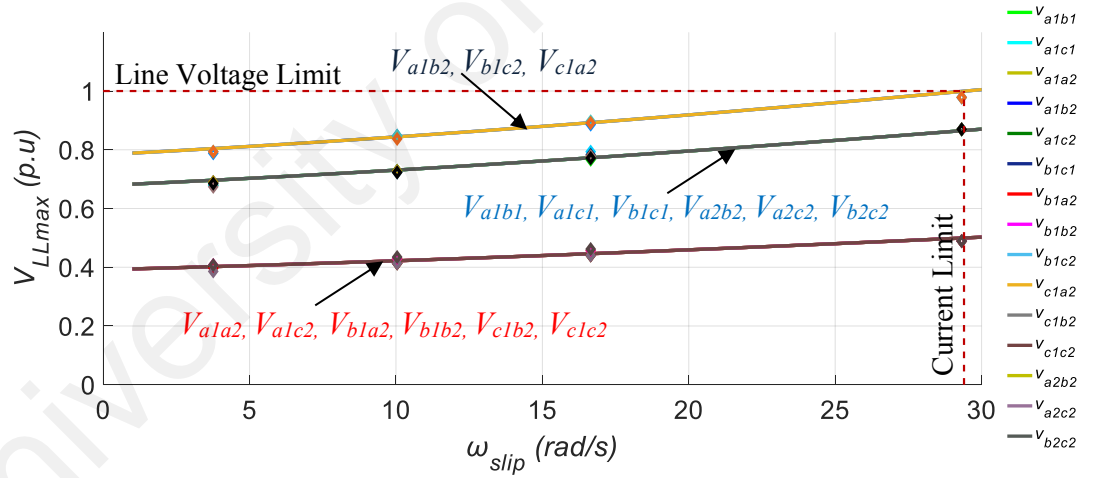


Figure 5.15: Voltage limit under different ω_{slip} at rated ω_s and rated current in healthy operation

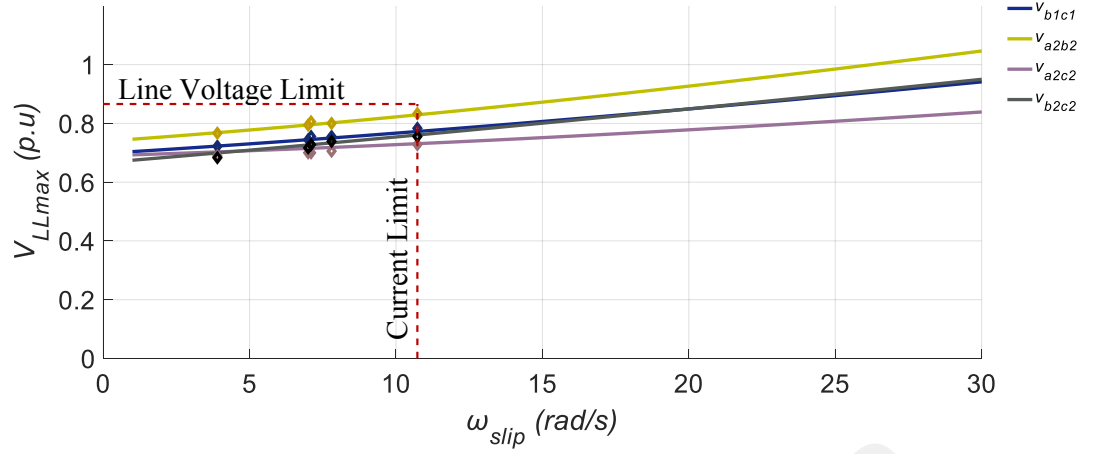


Figure 5.16: Voltage limit under different ω_{slip} at rated ω_s and rated current in 1 OPF with 2N operation

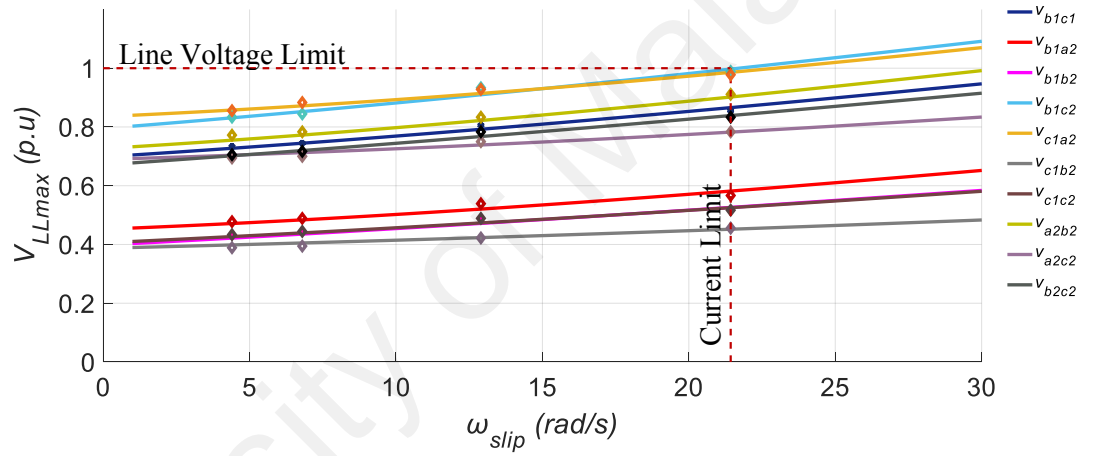


Figure 5.17: Voltage limit under different ω_{slip} at rated ω_s and rated current in 1 OPF with 1N operation

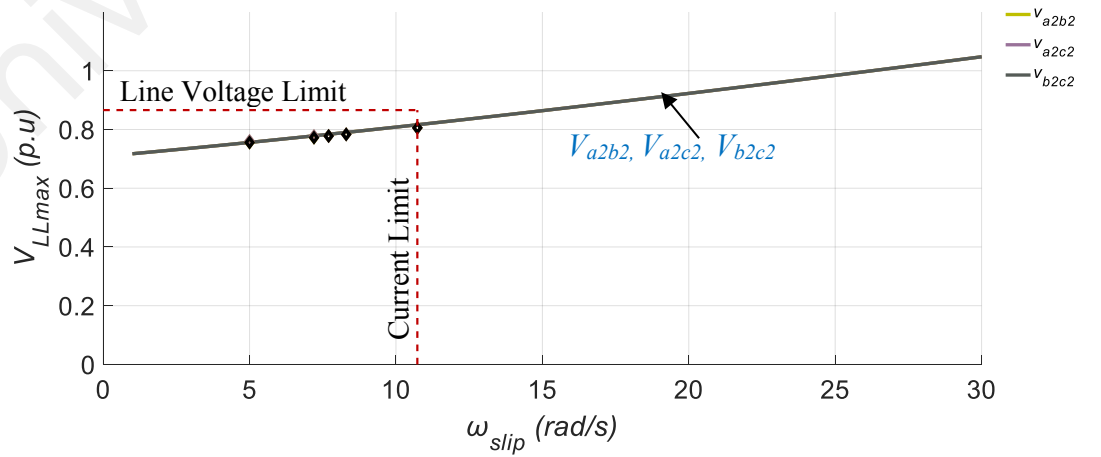


Figure 5.18: Voltage limit under different ω_{slip} at rated ω_s and rated current in 2 OPFs (case 2a) with 2N operation

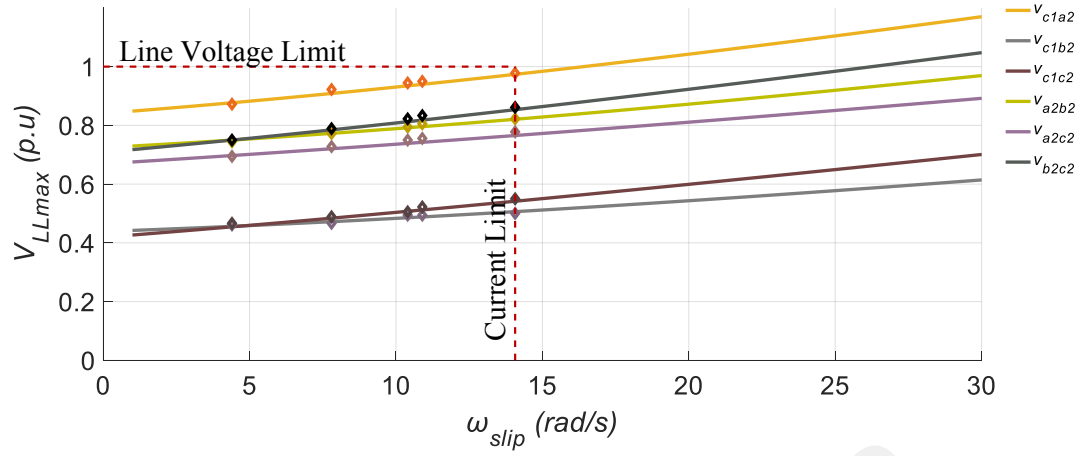


Figure 5.19: Voltage limit under different ω_{slip} at rated ω_s and rated current in 2 OPFs (case 2a) with 1N operation

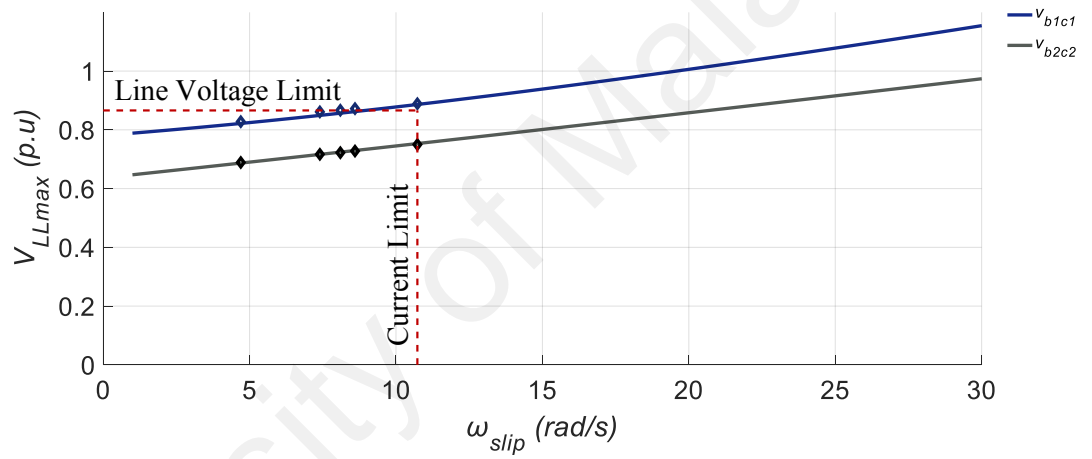


Figure 5.20: Voltage limit under different ω_{slip} at rated ω_s and rated current in 2 OPFs (case 2b) with 2N operation

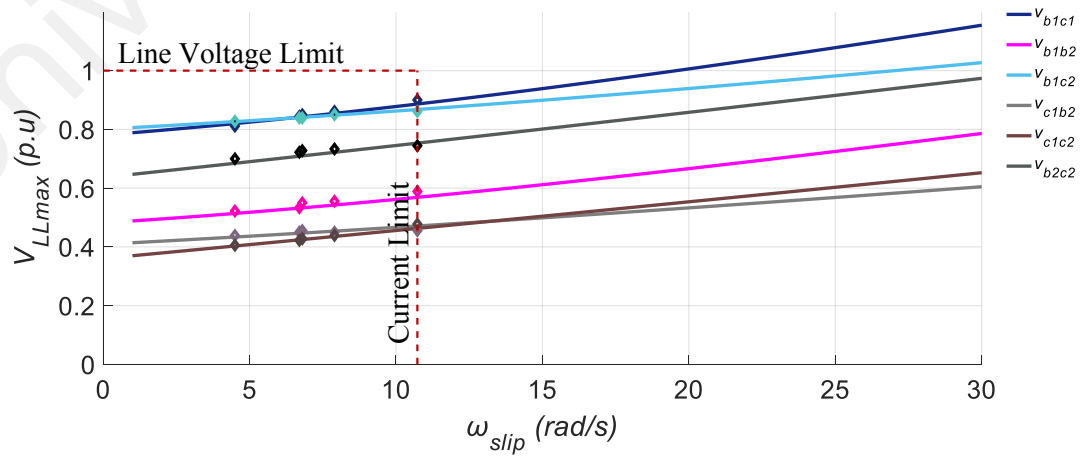


Figure 5.21: Voltage limit under different ω_{slip} at rated ω_s and rated current in 2 OPFs (case 2b) with 1N operation

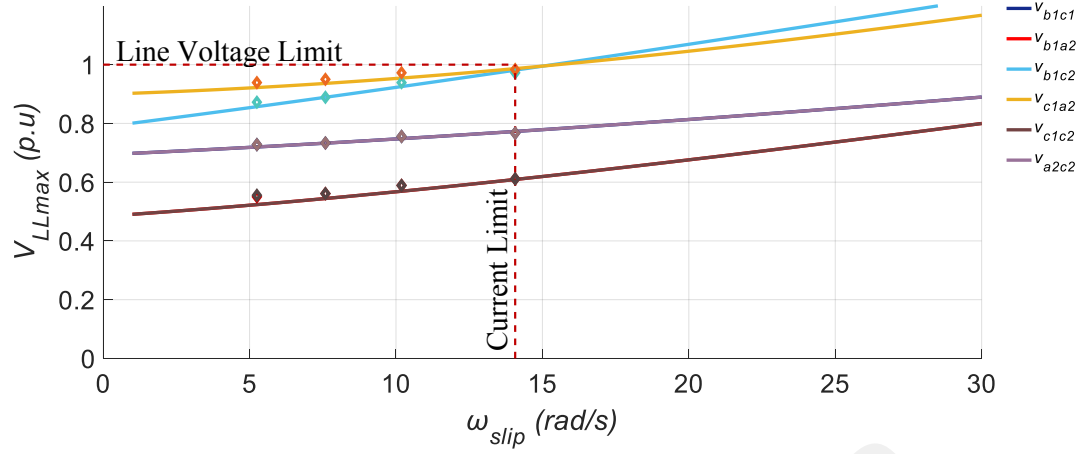


Figure 5.22: Voltage limit under different ω_{slip} at rated ω_s and rated current in 2 OPFs (case 2c) with 1N operation

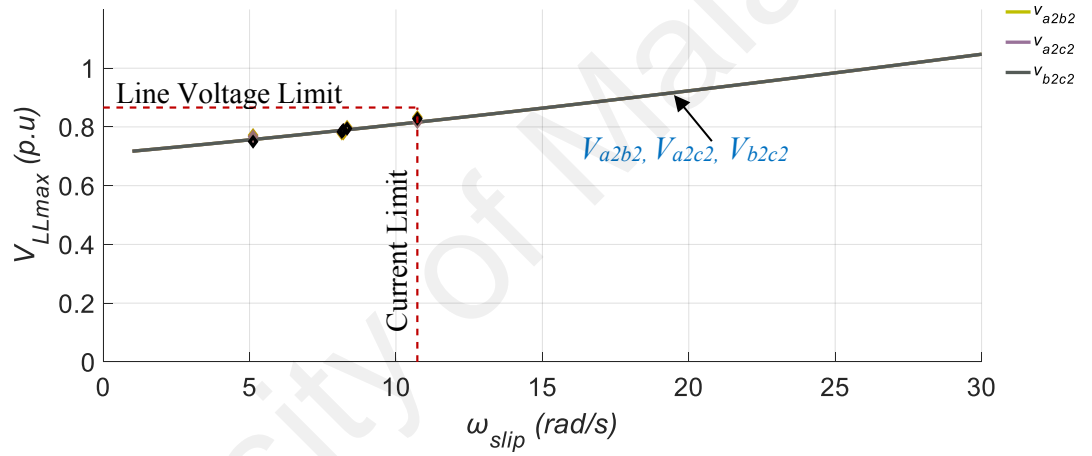


Figure 5.23: Voltage limit under different ω_{slip} at rated ω_s and rated current in 3 OPFs (case 3a) with 2N operation

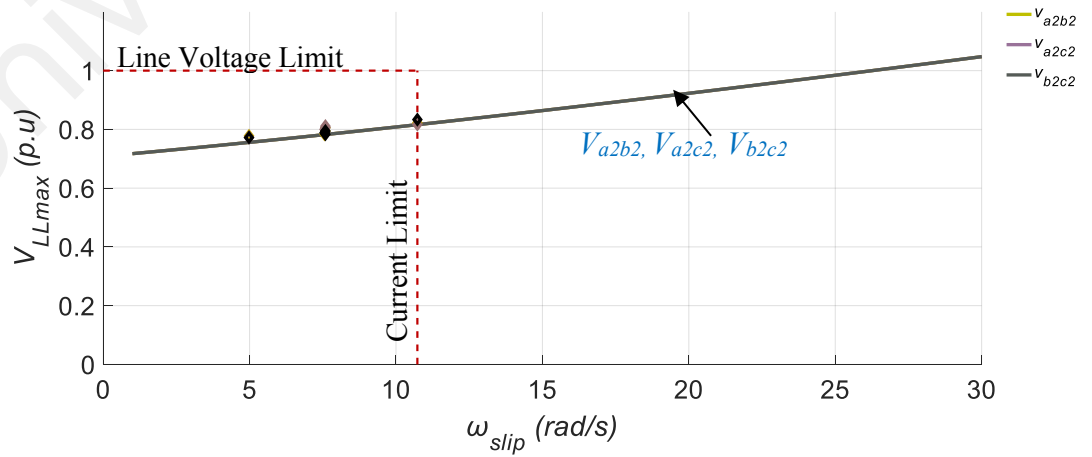


Figure 5.24: Voltage limit under different ω_{slip} at rated ω_s and rated current in 3 OPFs (case 3a) with 1N operation

Similar to ω_s , increasing ω_{slip} increases the line-to-line voltages monotonously but the increment is less profound compared to ω_s . The limit for ω_{slip} represents the current limit for the post-fault machine, where the maximum phase current should be limited to the rated phase current. Based on the line-to-line voltages plots, it can be concluded that the current limit is the dominant limiting factor for the S6 machine studied. Even though the line-to-line voltages increases after OPF, the current limit will force the machine to operate at lower slip frequency, hence lower line-to-line voltages.

For healthy operation running at rated current (see Figure 5.25(a)-left plot), the maximum line-to-line voltage is around 0.866 p.u. as shown in Figure 5.25(b)-left plot. This agrees with the theoretical voltage limit for 2N connection which is 0.866 p.u. For 1OPF, the line-to-line voltages increase significantly with the maximum line-to-line voltage, V_{a2b2} , exceeds well above the 0.866 p.u. limit (see Figure 5.26).

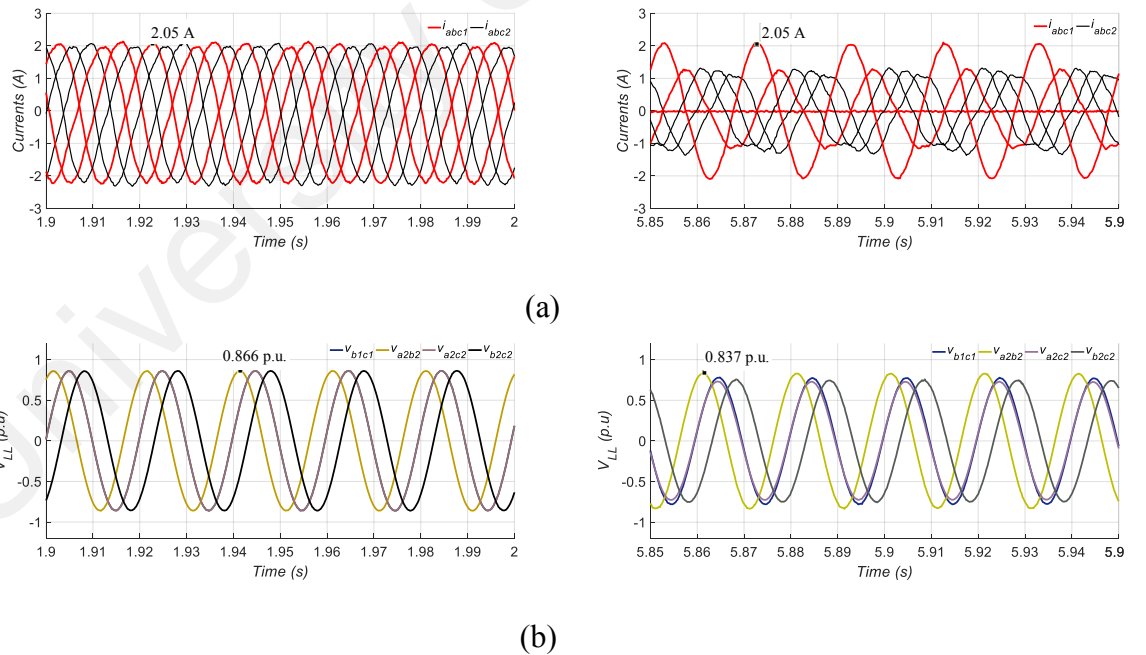


Figure 5.25: Healthy (left plot) and 1 OPF (right plot) for S6-2N. From top to bottom: (a) phase currents; (b) line voltages

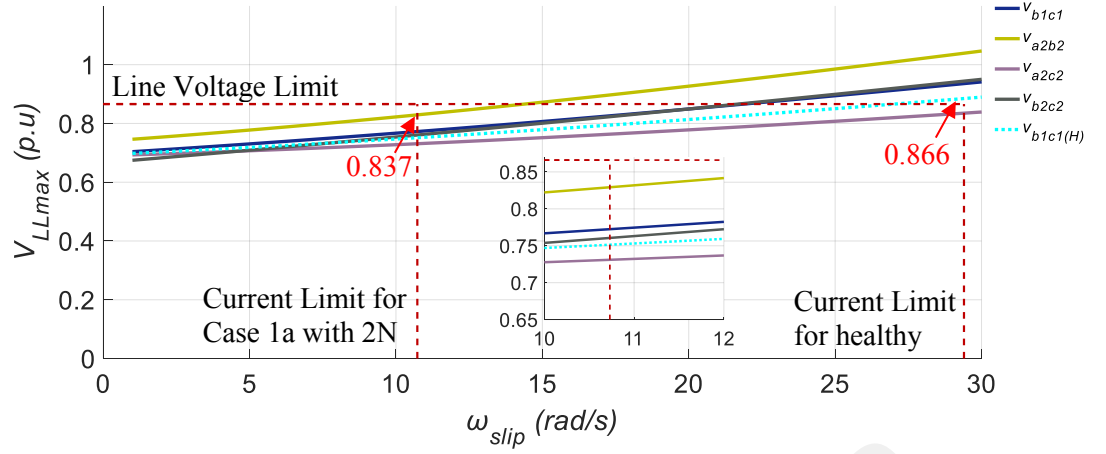


Figure 5.26: Comparison of current and voltage limit for 1 OPF with 2N and healthy at rated current

However, due to the current limits, S6-2N with 1OPF can only operate up to a maximum ω_{slip} of 10.73 rad/s to keep the maximum current at the rated value of around 2.05A (see Figure 5.25(a)-right plot). Hence, for 1OPF with 2N, the maximum allowable line-to-line voltage is only around 0.837 p.u. as shown in Figure 5.25(b)-right plot because the current limit is reached before the voltage limit.

Meanwhile, in some cases, the voltage limit is reached before the current limit. Figure 5.27 depicted the 2 OPFs for case 2b with S6-2N. From Figure 5.27(a), the rated phase currents recorded around 2.05A. The modulating signals and the line voltages are shown in Figure 5.27(b) and (c) respectively. At rated current, the maximum line voltage, i.e. V_{b1c1} , is found to be 0.903 p.u. (as indicated in Figure 5.20 as well), which exceeds the voltage limit of 0.866 p.u. However, the increment is only 3.9 %, which can be easily mitigated by having a higher DC-link voltage reserve margin.

It is worth noting that the line-to-line voltages can increase at different rates with the increase in ω_s and ω_{slip} during post-fault operation. Intuitively, the line-to-line voltages from the large voltage group in Table 5.1 should be the maximum line-to-line voltage during the post-fault operation. However, this is not always the case. Due to the different

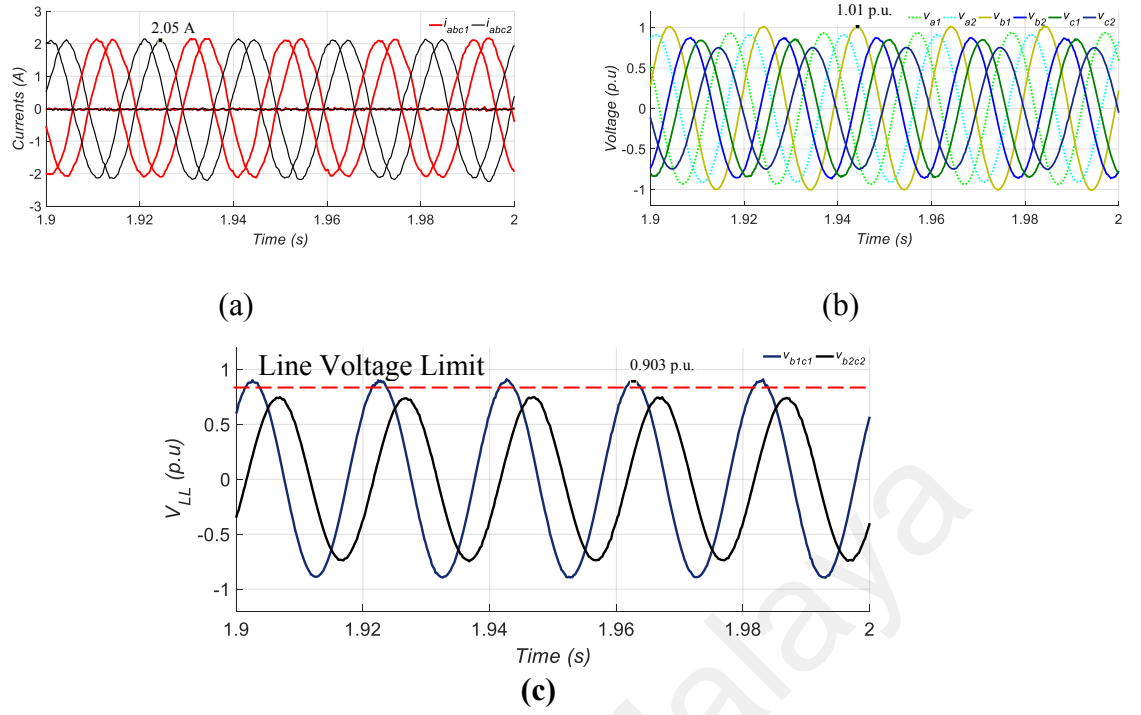


Figure 5.27: 2 OPFs (case 2b) for S6-2N: (a) rated phase currents; (b) modulating signals (c) line voltages

Table 5.4: Maximum line-to-line voltages in case 2c with 1N under different ω_{slip}

ω_{slip} (rad/s)	V_{c1a2} (p.u)	V_{b1c2} (p.u)
10	0.9322 $\angle 182^\circ$	0.9026 $\angle 76^\circ$
14	0.9651 $\angle 187^\circ$	0.9598 $\angle 83^\circ$
16	0.9827 $\angle 188^\circ$	0.9876 $\angle 86^\circ$
18	1.0000 $\angle 189^\circ$	1.0134 $\angle 88^\circ$
30	1.1427 $\angle 190^\circ$	1.1970 $\angle 94^\circ$

rate of magnitude increase, it is possible one of the large line-to-line voltages to be larger than the rest (as in the case 2c with 1N) or even for medium line-to-line voltage to be larger than the large line-to-line voltage (as in the case 2b with 1N). In order to fully identify the voltage limit, all the possible line-to-line voltages need to be determined for all possible range of operations, as it is done here in this Chapter. To illustrate the impact of operating point, particularly ω_{slip} , on the maximum line-to-line voltage, the case 2c with 1N is discussed here.

Table 5.4 compares the two large line-to-line voltages, namely V_{c1a2} and V_{b1c2} , at different ω_{slip} for case 2c with S6-1N running at rated ω_s . At lower ω_{slip} , V_{c1a2} is the highest line voltage followed by V_{b1c2} . At ω_{slip} around 16 rad/s, the line voltage V_{b1c2} cross-over V_{c1a2} to become

the maximum line voltage. This is due to the fact that OPF distorts the rated line voltages differently. This distorting can be viewed as the addition of voltage vectors (which is a function of x - y and/or 0 + 0 - voltages) to the healthy line voltages (Lee & Sul, 2014).

To illustrate the effect of the additional voltage vectors to the rated line voltages, the voltage vector representation of line-to-line voltages of the healthy (dotted line) with the faulted S6-IM under scenario 2c with 1N (solid line) for different ω_{slip} of 10 rad/s and 30 rad/s are depicted in Figure 5.28 and Figure 5.29 respectively. The resultant post-fault line voltage vector should be the vector sum of the healthy vector with an additional voltage vector. Table 5.5 gives a summary on the numerical values of the line-to-line voltages in Figure 5.28 and Figure 5.29 to aid the discussion here.

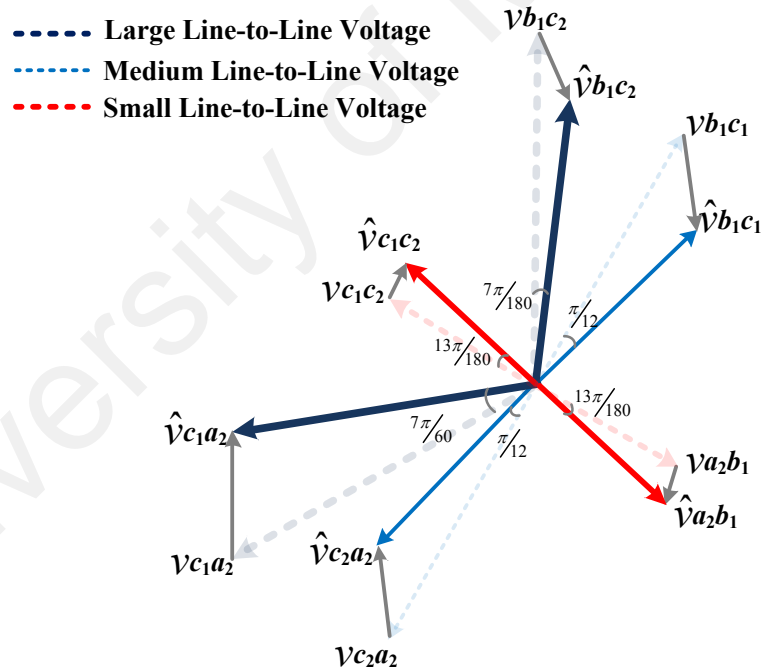


Figure 5.28: Line-to-line voltage vector representation of symmetrical six-phase induction machine in healthy (named without hat) and post-fault (named with hat) for case 2c with 1N at rated ω_s and rated $\omega_{slip} = 10$ rad/s.

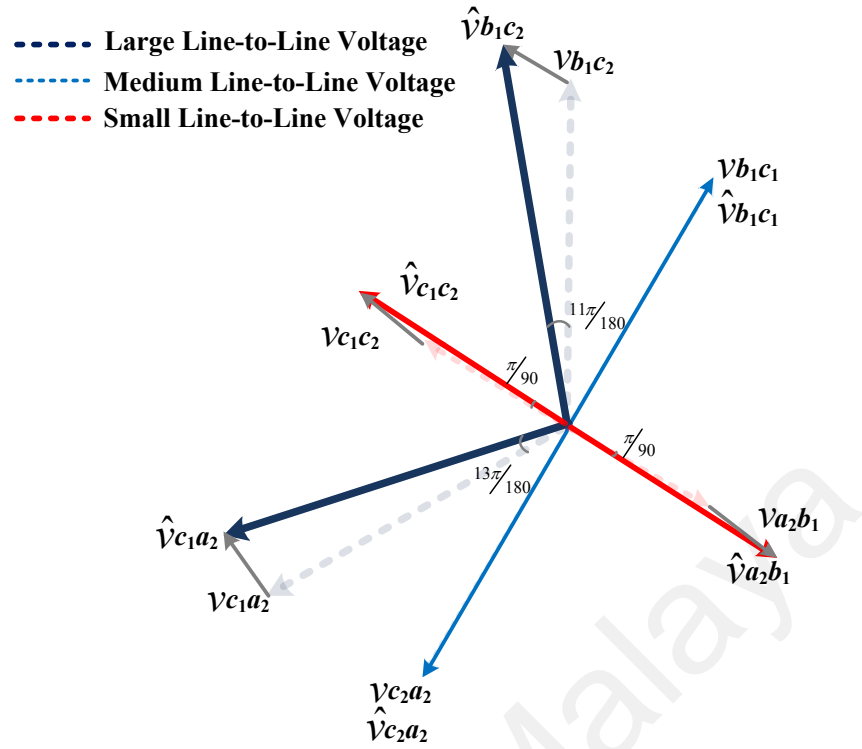


Figure 5.29: Line-to-line voltage vector representation of symmetrical six-phase induction machine in healthy (named without hat) and post-fault (named with hat) for case 2c with 1N at rated ω_s and rated $\omega_{slip} = 30$ rad/s.

Table 5.5: Maximum line-to-line voltages comparison between $\omega_{slip}=10$ rad/s and $\omega_{slip}=30$ rad/s in case 2c with 1N

ω_{slip} (rad/s) V_{LL} (p.u)	10	30
V_{b1c1}	0.7308 <38°	0.8702 <53°
V_{b1a2}	0.5549 <130°	0.7823 <141°
V_{b1c2}	0.9026 <76°	1.1970 <94° (highest)
V_{c1a2}	0.9322 <182° (highest)	1.1427 <190°
V_{c1c2}	0.5549 <130°	0.7828 <141°
V_{a2c2}	0.7308 <38°	0.8702 <53°

From Figure 5.28 at ω_{slip} 10 rad/s, it can be observed that magnitudes of the post-fault line voltage decreased compared to the healthy magnitude which recorded at $0.9026 < 76^\circ$ for V_{b1c2} and $0.9322 < 182^\circ$ for V_{c1a2} . When ω_{slip} is increased to 30 rad/s, the magnitudes of the large line-to-line voltage are larger than their healthy magnitude. Furthermore, V_{b1c2} has “crossed-over” V_{c1a2} to become the highest large line-to-line voltage at ω_{slip} 30 rad/s.

5.5 Conclusions

In this chapter, the voltage limits on the post-fault S6-IM is investigated. Using the post-fault current references and machine parameters determined in the preceding chapters, the theoretical line-to-line voltages for the S6 induction machine under different OPF scenarios and neutral configurations can be calculated from the machine equations. It is demonstrated that the operating point, particularly the synchronous frequency ω_s and slip frequency ω_{slip} , has a profound impact on the maximum line-to-line voltage. This, in turn, affects the voltage limit issue of the S6 machine. It should be highlighted here that unlike current limits, the conclusions on the voltage limit is highly dependent on the machine parameters. While the method presented here can be easily adopted for other S6 machines (or, as a matter of fact, other multiphase machines), the conclusions cannot be directly extended to other S6 machines due to the variations in machine parameters.

For the S6 machine studied, it was found that voltage limit is not violated in almost all fault scenarios, apart from case 2b configured with 2N. Even for the case of 2b configured with 2N, the maximum line-to-line voltage is found to be only 3.9% higher than the rated voltage limit and can easily be mitigated with a higher DC-link voltage margin. Since the voltage limits are not exceeded, the S6 machine will be able to run up to rated speed under all OPF scenarios considered. This also indicates that the post-fault performance of the machine is mainly determined by the current limits only.

In a nutshell, the findings that can be highlighted from the voltage limit study are:

1. The line-to-line voltage is a function of ω_s and ω_{slip} , where an increase in ω_{slip} or ω_s results in a monotonous increase in the line-to-line voltages. Thus, the maximum line-to-line voltage can be determined at the maximum ω_s and ω_{slip} .

2. The rate of increase in the magnitude of the line-to-line voltages can differ depending on the neutral configuration and OPFs. In order to identify the maximum line-to-line voltage (hence the voltage limit), all the post-fault line-to-line voltages need to be evaluated.
3. For the S6 machine studied in the project, it is clearly seen from the results that most of the fault scenarios hit the current limit first before reaching the voltage limit. Only one post-fault case hit the voltage limit before the current limit which is case 2b configured with 2N and can easily be mitigated with a higher DC-link voltage margin. This implies that the current limit is the main limiting factor for the post-fault operation of the S6-IM used in the project.

CHAPTER 6: CONCLUSIONS AND FUTURE WORKS

6.1 Conclusions

This thesis presents a study of the fault-tolerant capability of a star-connected S6-IM with single and two isolated neutrals considering both current and voltage limits.

In Chapter 3, post-fault current limits of S6-IM have determined for OPFs up to three open phases. Subsequently, comparisons of post-fault performance are made for S6-IM configured with single and two isolated neutrals under different OPFs. Then, the post-fault performance of S6-IM is compared to those of other commonly used six-phase machines, i.e. the A6 and D3 IMs. Even though the performance depends on the conditions of each specific case, the unified analysis allows extracting some general conclusions:

- i. Type of six-phase machine (S6): Compared to A6 and D3, S6 has higher post-fault capability in 1N, achieving a maximum post-fault current of 77.1% under 1 OPF and $\geq 50\%$ for all 2 OPFs scenarios.
- ii. Type of neutral connection (1N/2N): 1N provides better fault-tolerant capability than 2N in all scenarios. The improvement is relevant under 1 OPF scenario, minor with 2 OPFs and allows operating in all scenarios with 3 OPFs.
- iii. Type of fault scenario (1/2/3 OPFs): the scenario with 1 OPF clearly promotes the use of S6-1N. In scenarios with 3 OPFs, the post-fault operation is unfeasible in 2N (except case 3a) and provides only marginal current/torque in 1N.

In Chapter 4, machine parameters estimation using a closed-loop control waveform curve fitting technique for S6-IM has been presented. Machine voltage equations for the stationary of α - β , x - y and 0 + 0 - subspaces have been derived from the mathematical model of the induction motor. It was demonstrated that the machine parameters estimated using

the proposed method can accurately predict the line-to-line voltages under different loads and speeds.

In Chapter 5, the performance for fault-tolerant S6-IM is evaluated in terms of voltage limits. The significance of machine parameters and different operating points with possible range of ω_s and ω_{slip} are needed to determine the maximum line-to-line voltage. To validate the theoretical discussion, both voltage and current limits are executed experimentally to the independent cases of faulted S6-IM.

The concluding remarks for voltage limits on post-fault S6-IM are:

- i. The maximum line-to-line voltages are a function of machine parameters and different operating points.
- ii. For the S6 machine considered, the current limit hit the limit before reached the voltage limit under most OPF scenarios. For the case 2b configured with 2N, the maximum line-to-line voltage only exceeds the rated line-to-line voltage by 3.9%, which is not significant. This indicates that the post-fault performance of this S6 machine is mainly decided by the current limit.
- iii. The maximum line-to-line voltage is not necessarily the large line-to-line voltage. There is a tendency of cross-over conditions between the large and medium line-to-line voltages.

In a nutshell, this thesis has provided a complete view on the fault-tolerant capability of star-connected S6-IM considering current and voltage limits. This additional knowledge will be helpful for researchers to better understand the fault-tolerant capability of multiphase drives in applications such as electric vehicles, off-shore wind farms, more-electric aircraft, etc., where the reliability of drives is of great concern.

6.2 Future Works

Fault-tolerant control is still a topic of an ongoing investigation. There are some possible directions related to the control of multiphase machines that need to be discovered. Further research on the topic exposes could include:

1) Other optimization criteria based on different modes of operation for post-fault currents;

Although there are two main control modes, maximum torque (MT) and minimum loss (ML), there is still a gap in the optimization criteria such as full-range minimum loss (FRML) that can be enhanced to symmetrical six-phase and dual-three phase induction machine.

2) Extension of voltage limit analysis to symmetrical six-phase induction machine (S6-IM) using minimum loss (ML) mode;

The voltage limit plays an important constraint for post-fault control as the voltage limit will have a direct impact on the speed limit. The analysis of the DC-link voltage reserve enables the controller to operate in a post-fault operation without going into the over-modulation region. It is interesting to see the effect of voltage limitations if minimum loss (ML) is used rather than maximum torque (MT) and its effect on the considered cases.

3) Extension of voltage limit analysis to dual three-phase induction machine (D3-IM) and asymmetrical six-phase induction machine (A6-IM) using maximum torque (MT) and minimum loss (ML) mode;

While comprehensive studies for the S6 induction machine have been assured in this thesis, the discussion on the impact of voltage limits on the faulted D3 and A6 induction machine is yet to be discovered. In light of this, extending the concept

of voltage limits to other types of six-phase machine can provide a unified analysis including different neutral connections, modes of operation and fault scenarios.

4) Extension of current derating method

The behavior of current that being derated can give impact to the voltage limits. In this thesis, i_{ds} is set to be rated whilst i_s is set to be derated. The investigation of rated flux current together with a min-max injection to achieve minimum modulating signal has been applied to a S6-IM only. The same methods can be applied to the other multiphase machines considering current derating methods such as both i_{ds} and i_{qs} that need to be derated together.

REFERENCES

- Abdel-Khalik, A. S., Ahmed, S., Elserougi, A. a., & Massoud, A. M. (2015). Effect of stator winding connection of five-phase induction machines on torque ripples under open line condition. *IEEE/ASME Transactions on Mechatronics*, 20(1), 580–593. <http://doi.org/10.1109/TIE.2013.2242417>
- Abdel-Khalik, A. S., Elgenedy, M. A., Ahmed, S., & Massoud, A. M. (2016). An Improved Fault Tolerant Five-Phase Induction Machine Using A Combined Star/Pentagon Single Layer Stator Winding Connection. *IEEE Transactions on Industrial Electronics*, 63(1), 618 – 628. <http://doi.org/10.1109/TIE.2015.2426672>
- Abdel-Khalik, A. S., Hamad, M. S., Massoud, A. M., & Ahmed, S. (2017). Postfault Operation of a Nine-Phase Six-Terminal Induction Machine Under Single Open-Line Fault. *IEEE Transactions on Industrial Electronics*, 65(June), 1084–1096. <http://doi.org/10.1109/tie.2017.2733471>
- Abdel-Khalik, A. S., Hamdy, R. a., Massoud, A. M., & Ahmed, S. (2018). Postfault control of scalar (V/f) controlled asymmetrical six-phase induction machines. *IEEE Access*, 6, 59211–59220. <http://doi.org/10.1109/ACCESS.2018.2874133>
- Abdel-Khalik, A. S., Masoud, M. I., Ahmed, S., & Massoud, A. (2014). Calculation of derating factors based on steady-state unbalanced multiphase induction machine model under open phase(s) and optimal winding currents. *Electric Power Systems Research*, 106, 214–225. <http://doi.org/10.1016/j.epsr.2013.08.015>
- Abdel-Khalik, A. S., Massoud, A. M., & Ahmed, S. (2018). Effect of DC-Link Voltage Limitation on Postfault Steady-State Performance of Asymmetrical Six- Phase Induction Machines. *IEEE Transactions on Industrial Electronics*, DOI: 10.11. <http://doi.org/10.1109/TIE.2018.2795529>
- Alberti, L., & Bianchi, N. (2012). Experimental Tests of Dual Three-Phase Induction Motor Under Faulty Operating Condition. *IEEE Transactions on Industrial Electronics*, 59(5), 2041–2048. <http://doi.org/10.1109/TIE.2011.2171175>
- Andresen, B., & Birk, J. (2007). A high power density converter system for the Gamesa G10x 4 , 5 MW Wind turbine. *Proc. European Conf. on Power Electronics and Applications EPE*, 1–8. <http://doi.org/10.1109/EPE.2007.4417312>
- Ashoush, a., Gadoue, S. M., Abdel-Khalik, a. S., & Mohamadein, a. L. (2011). Current optimization for an eleven-phase induction machine under fault conditions using genetic algorithm. *SDEMPED 2011 - 8th IEEE Symposium on Diagnostics for Electrical Machines, Power Electronics and Drives*, (4), 529–534. <http://doi.org/10.1109/DEMPED.2011.6063674>
- Baneira, F., Doval-Gandoy, J., Yepes, A. G., Lopez, O., & Perez-Estevez, D. (2017). Comparison of Postfault Strategies for Current Reference Generation for Dual Three-Phase Machines in Terms of Converter Losses. *IEEE Transactions on Power Electronics*, 32(11), 8243–8246. <http://doi.org/10.1109/TPEL.2017.2691401>

- Barcaro, M., Bianchi, N., & Magnussen, F. (2009). Analysis and tests of a dual three-phase 12-slot 10-pole permanent magnet motor. *2009 IEEE Energy Conversion Congress and Exposition*, 3587–3594. <http://doi.org/10.1109/ECCE.2009.5316094>
- Barcaro, M., Bianchi, N., & Magnussen, F. (2010). Analysis and Tests of a Dual Three-Phase 12-Slot. *IEEE Transactions on Industry Applications*, 46(6), 2355–2362. <http://doi.org/10.1109/TIA.2010.2070784>
- Barrero, F., & Duran, M. J. (2016). Recent Advances in the Design, Modeling, and Control of Multiphase Machines - Part II. *IEEE Transactions on Industrial Electronics*, 63(1), 459–468. <http://doi.org/10.1109/TIE.2015.2448211>
- Baudart, F., Dehez, B., Matagne, E., Telteu-nedelcu, D., Alexandre, P., & Labrique, F. (2012). Torque Control Strategy of Polyphase Permanent-Magnet Synchronous Machines With Minimal Controller Reconfiguration Under Open-Circuit Fault of One Phase. *IEEE Transactions on Industrial Electronics*, 59(6), 2632–2644. <http://doi.org/10.1109/TIE.2011.2170393>
- Bennett, J. W., Mecrow, B. C., Atkinson, D. J., & Atkinson, G. J. (2011). Safety-critical design of electromechanical actuation systems in commercial aircraft. *IET Electric Power Applications*, 5(1), 37. <http://doi.org/10.1049/iet-epa.2009.0304>
- Bermudez, M., Gonzalez-Prieto, I., Barrero, F., Guzman, H., Duran, M. J., & Kestelyn, X. (2016). Open-Phase Fault-Tolerant Direct Torque Control Technique for Five-Phase Induction Motor Drives. *IEEE Transactions on Industrial Electronics*, 0046(c), 1–1. <http://doi.org/10.1109/TIE.2016.2610941>
- Bermudez, M., Gonzalez-Prieto, I., Barrero, F., Guzman, H., Duran, M. J., & Kestelyn, X. (2017). Open-Phase Fault-Tolerant Direct Torque Control Technique for Five-Phase Induction Motor Drives. *IEEE Transactions on Industrial Electronics*, 64(2), 902–911. <http://doi.org/10.1109/TIE.2016.2610941>
- Bianchi, N., Bolognani, S., & Pr , M. D. (2008). Impact of Stator Winding of a Five-Phase Permanent-Magnet Motor on Postfault Operations. *IEEE Transactions on Industrial Electronics*, 55(5), 1978–1987. <http://doi.org/10.1109/TIE.2008.920645>
- Bojoi, R., Cavagnino, a., Tenconi, a., & Vaschetto, S. (2016). Control of shaft-line-embedded multiphase starter/generator for aero-engine. *IEEE Transactions on Industrial Electronics*, 63(1), 641–652. <http://doi.org/10.1109/TIE.2015.2472637>
- Cao, W., Mecrow, B. C., Atkinson, G. J., Bennett, J. W., & Atkinson, D. J. (2012). Overview of Electric Motor Technologies Used for More Electric Aircraft (MEA). *IEEE Transactions on Industrial Electronics*, 59(9), 3523–3531. <http://doi.org/10.1109/TIE.2011.2165453>
- Cavagnino, A., Li, Z., Tenconi, A., & Vaschetto, S. (2013). Integrated Generator for More Electric Engine: Design and Testing of a Scaled-Size Prototype. *IEEE Transactions on Industry Applications*, 49(5), 2034–2043. <http://doi.org/10.1109/TIA.2013.2259785>
- Che, H. S., Abdel-Khalik, A. S., Dordevic, O., & Levi, E. (2017). Parameter Estimation of Asymmetrical Six-Phase Induction Machines Using Modified Standard Tests.

IEEE Transactions on Industrial Electronics, 64(8), 6075–6085.
<http://doi.org/10.1109/TIE.2017.2677349>

- Che, H. S., Duran, M. J., Levi, E., Jones, M., Hew, W., & Rahim, N. A. (2014). Postfault Operation of an Asymmetrical Six-Phase Induction Machine With Single and Two Isolated Neutral Points. *IEEE Transactions on Power Electronics*, 29(10), 5406–5416. <http://doi.org/10.1109/TPEL.2013.2293195>
- Che, H. S., Duran, M., Levi, E., Jones, M., Hew, W. P., & Rahim, N. a. (2013). Post-fault operation of an asymmetrical six-phase induction machine with single and two isolated neutral points. *2013 IEEE Energy Conversion Congress and Exposition*, (2), 1131–1138. <http://doi.org/10.1109/ECCE.2013.6646832>
- Che, H. S., & Hew, W. P. (2016). Dual three-phase operation of single neutral symmetrical six-phase machine for improved performance. *IECON 2015 - 41st Annual Conference of the IEEE Industrial Electronics Society*, 1176–1181. <http://doi.org/10.1109/IECON.2015.7392259>
- Che, H. S., Levi, E., Jones, M., Duran, M. J., Hew, W. P., & Rahim, N. A. (2014). Operation of a six-phase induction machine using series-connected machine-side converters. *IEEE Transactions on Industrial Electronics*, 61(1), 164–176. <http://doi.org/10.1109/TIE.2013.2248338>
- Che, H. S., Levi, E., Jones, M., Hew, W., & Rahim, N. A. (2014). Current Control Methods for an Asymmetrical Six-Phase Induction Motor Drive. *IEEE Transactions on Power Electronics*, 29(1), 407–417. <http://doi.org/10.1109/TPEL.2013.2248170>
- Diab, M. S., Elserougi, A. a., Abdel-Khalik, A. S., Massoud, A. M., & Ahmed, S. (2016). A Nine-Switch-Converter-Based Integrated Motor Drive and Battery Charger System for EVs Using Symmetrical Six-Phase Machines. *IEEE Transactions on Industrial Electronics*, 63(9), 5326–5335. <http://doi.org/10.1109/TIE.2016.2555295>
- Diallo, D., Benbouzid, M. E. H., & Makouf, A. (2004). A Fault-Tolerant Control Architecture for Induction Motor Drives in Automotive Applications. *IEEE Transactions on Vehicular Technology*, 53(6), 1847–1855. <http://doi.org/10.1109/TVT.2004.833610>
- Ditmanson, C., Hein, P., Kolb, S., Mölck, J., & Bernet, S. (2014). A New Modular Flux-Switching Permanent-Magnet Drive for Large Wind Turbines. *IEEE Transactions on Industry Applications*, 50(6), 3787–3794. <http://doi.org/10.1109/TIA.2014.2322135>
- Dujic, D., Iqbal, A., Levi, E., Dujic, D., Iqbal, A., Levi, E., ... Liverpool, L. (2007). A Space Vector PWM Technique for Symmetrical Six-Phase Voltage Source Inverters A Space Vector PWM Technique for Symmetrical Six-Phase Voltage Source Inverters. *EPE Journal (European Power Electronics and Drives Journal)*, 17(1), 24–32. <http://doi.org/10.1080/09398368.2007.11463639>
- Duran, M., Gonzalez, I., Bermudez, M., Barrero, F., Guzman, H., & Arahall, M. (2016). Optimal Fault-tolerant Control of Six-phase Induction Motor Drives with Parallel Converters. *IEEE Transactions on Industrial Electronics*, 63(1), 629–640. <http://doi.org/10.1109/TIE.2015.2461516>

- Duran, M. J., Gonzalez-Prieto, I., Rios-Garcia, N., & Barrero, F. (2018). A Simple, Fast, and Robust Open-Phase Fault Detection Technique for Six-Phase Induction Motor Drives. *IEEE Transactions on Power Electronics*, 33(c), 547–557. <http://doi.org/10.1109/TPEL.2017.2670924>
- Eldeeb, H. M., Abdel-Khalik, A. S., & Hackl, C. M. (2019). Postfault Full Torque-Speed Exploitation of Dual Three-Phase IPMSM Drives. *IEEE Transactions on Industrial Electronics*, 66(October), 6746–6756. <http://doi.org/10.1109/TIE.2018.2880698>
- Fall, O., Ky, N., Frédéric, J., Letellier, P., Semail, E., & Kestelyn, X. (2016). Variable speed control of a 5-phase permanent magnet synchronous generator including voltage and current limits in healthy and open-circuited modes. *Electric Power Systems Research*, 140, 507–516. <http://doi.org/10.1016/j.epsr.2016.05.024>
- Fu, J. R., & Lipo, T. A. (1994). Disturbance-Free Operation of a Multiphase Current-Regulated Motor Drive with an Opened Phase. *IEEE Transactions on Industry Applications*, 30(5), 1267–1274. <http://doi.org/10.1109/28.315238>
- Ginart, A. E., Kalgren, P. W., Roemer, M. J., Brown, D. W., & Abbas, M. (2010). Transistor diagnostic strategies and extended operation under one-transistor trigger suppression in inverter power drives. *IEEE Transactions on Power Electronics*, 25(2), 499–506. <http://doi.org/10.1109/TPEL.2009.2026750>
- Gjerde, S. S., Olsen, P. K., Ljøkelsøy, K., & Undeland, T. M. (2014). Control and Fault Handling in a Modular Series-Connected Converter for a Transformerless Wind Turbine. *IEEE Transactions on Industry Applications*, 50(2), 1094–1105. <http://doi.org/10.1109/TIA.2013.2272032>
- Gjerde, S. S., & Undeland, T. M. (2012). A Transformerless Generator-Converter Concept making feasible a 100 kV Low Weight Offshore Wind Turbine Part II - The Converter. *IEEE Energy Conversion Congress and Exposition ECCE*, 253–260.
- Gonzalez-Prieto, I., Duran, M. J., Barrero, F., Bermudez, M., & Guzman, H. (2017). Impact of Postfault Flux Adaptation on Six-Phase Induction Motor Drives with Parallel Converters. *IEEE Transactions on Power Electronics*, 32(1), 515–528. <http://doi.org/10.1109/TPEL.2016.2533719>
- Gonzalez-Prieto, I., Duran, M. J., & Barrero, F. J. (2017). Fault-Tolerant Control of Six-Phase Induction Motor Drives with Variable Current Injection. *IEEE Transactions on Power Electronics*, 32(10), 7894–7903. <http://doi.org/10.1109/TPEL.2016.2639070>
- Gonzalez-Prieto, I., Duran, M. J., Che, H. S., Levi, E., Bermúdez, M., & Barrero, F. (2016). Fault-Tolerant Operation of Six-Phase Energy Conversion Systems With Parallel Machine-Side Converters. *IEEE Transactions on Power Electronics*, 31(4), 3068–3079. <http://doi.org/10.1109/TPEL.2015.2455595>
- Guzman, H., Barrero, F., & Duran, M. J. (2015). IGBT-Gating Failure Effect on a Fault-Tolerant Induction Motor Drive. *IEEE Transactions on Industrial Electronics*, 62(1), 15–20. <http://doi.org/10.1109/TIE.2014.2331019>

- Guzman, H., Duran, M. J., Barrero, F., Bogado, B., & Toral, S. (2014). Speed Control of Five-Phase Induction Motors With Integrated Open-Phase Fault Operation Using Model-Based Predictive Current Control Techniques. *IEEE Transactions on Industrial Electronics*, 61(9), 4474–4484. <http://doi.org/10.1109/TIE.2013.2289882>
- Guzman, H., Duran, M. J., Barrero, F., Zarri, L., Bogado, B., Gonzalez Prieto, I., & Arahal, M. R. (2016). Comparative study of predictive and resonant controllers in fault-tolerant five-phase induction motor drives. *IEEE Transactions on Industrial Electronics*, 63(1), 606–617. <http://doi.org/10.1109/TIE.2015.2418732>
- Huang, X., Goodman, A., Gerada, C., Fang, Y., & Lu, Q. (2012). Design of a Five-Phase Brushless DC Motor for a Safety Critical Aerospace Application. *IEEE Transactions on Industrial Electronics*, 59(9), 3532–3541. <http://doi.org/10.1109/TIE.2011.2172170>
- Jacobina, C. B., Azevedo, C. C. De, Silva, C. R., Lima, A. M. N., & Silva, E. R. C. (2002). On-line Estimation of the Stator Resistance of a Six-phase Induction Machine. *Conference Record of the 2002 IEEE Industry Applications Conference. 37th IAS Annual Meeting (Cat. No.02CH37344)*, 2(6), 746–751 vol.2. <http://doi.org/10.1109/IAS.2002.1042643>
- Jung, E., Yoo, H., Sul, S., Choi, H.-S., & Choi, Y.-Y. (2012). A Nine-Phase Permanent-Magnet Motor Drive System for an Ultrahigh-Speed Elevator. *IEEE Transactions on Industry Applications*, 48(3), 987–995. <http://doi.org/10.1109/TIA.2012.2190472>
- Kianinezhad, R., Nahid-Mobarakeh, B., Baghli, L., Betin, F., & Capolino, G.-A. (2008). Modeling and Control of Six-Phase Symmetrical Induction Machine Under Fault Condition Due to Open Phases. *IEEE Transactions on Industrial Electronics*, 55(5), 1966–1977. <http://doi.org/10.1109/TIE.2008.918479>
- Lee, W. J., & Sul, S. K. (2014). DC-link voltage stabilization for reduced DC-link capacitor inverter. *IEEE Transactions on Industry Applications*, 50(1), 404–414. <http://doi.org/10.1109/TIA.2013.2268733>
- Levi, E. (2008). Multiphase Electric Machines for Variable-Speed Applications. *IEEE Transactions on Industrial Electronics*, 55(5), 1893–1909. <http://doi.org/10.1109/TIE.2008.918488>
- Levi, E., Barrero, F., & Duran, M. (2015). Multiphase Machines and Drives - Revisited. *IEEE Transactions on Industrial Electronics*, 63(1), 1–1. <http://doi.org/10.1109/TIE.2015.2493510>
- Levi, E., Bojoi, R., Profumo, F., Toliyat, H. A., & Williamson, S. (2007). Multiphase induction motor drives – a technology status review. *IET Electric Power Applications*, 1(no. 4), 489–516. <http://doi.org/10.1049/iet-epa>
- Levi, E., Dujic, D., Jones, M., & Grandi, G. (2008). Analytical determination of DC-bus utilization limits in multiphase VSI supplied AC drives. *IEEE Transactions on Energy Conversion*, 23(2), 433–443. <http://doi.org/10.1109/TEC.2008.921557>

- Locment, F., Semail, E., & Kestelyn, X. (2008). Vectorial Approach-Based Control of a Seven-Phase Axial Flux Machine Designed for Fault Operation. *IEEE Transactions on Industrial Electronics*, 55(10), 3682–3691. <http://doi.org/10.1109/TIE.2008.925313>
- Mengoni, M., Zarri, L., Tani, A., Gritli, Y., Serra, G., Filippetti, F., & Casadei, D. (2014). On-Line Detection of High-Resistance Connections in Multiphase Induction Machines. *IEEE Transactions on Power Electronics*, 8993(c), 1–1. <http://doi.org/10.1109/TPEL.2014.2357439>
- Nelson, R. H., & Krause, P. C. (1974). Induction machine analysis for arbitrary displacement between multiple winding sets. *IEEE Transactions on Power Apparatus and Systems*, PAS-93(4), 841–848. <http://doi.org/10.1109/TPAS.1974.293983>
- Pantea, A., Yazidi, A., Betin, F., Taherzadeh, M., Carrière, S., Henao, H., & Capolino, G. A. (2016). Six-Phase Induction Machine Model for Electrical Fault Simulation Using the Circuit-Oriented Method. *IEEE Transactions on Industrial Electronics*, 63(1), 494–503. <http://doi.org/10.1109/TIE.2015.2493727>
- Parsa, L., & Toliyat, H. A. (2007). Fault-Tolerant Interior-Permanent-Magnet Machines for Hybrid Electric Vehicle Applications. *IEEE Transactions on Vehicular Technology*, 56(4), 1546–1552.
- Riveros, J. A., Yepes, A. G., Barrero, F., Doval-gandoy, J., Bogado, B., Lopez, O., ... Levi, E. (2012). Parameter Identification of Multiphase Induction Machines With Distributed Windings — Part 2 : Time-Domain Techniques. *IEEE Transactions on Energy Conversion*, 27(4), 1067–1077. <http://doi.org/10.1109/TEC.2012.2219862>
- Ryu, H., Kim, J., & Sul, S. (2006). Synchronous-Frame Current Control of Multiphase Synchronous Motor Under Asymmetric Fault Condition Due to Open Phases. *IEEE Transactions on Industry Applications*, 42(4), 1062–1070. <http://doi.org/10.1109/TIA.2006.876074>
- Sayed-Ahmed, A., & Demerdash, N. A. O. (2012). Fault-Tolerant Operation of Delta-Connected Scalar- and Vector-Controlled AC Motor Drives. *IEEE Transactions on Power Electronics*, 27(6), 3041–3049. <http://doi.org/10.1109/TPEL.2011.2176556>
- Semail, E., Locment, F., Ensam, L. E. P., & Xiv, B. L. (2008). Fault Tolerant Multiphase Electrical Drives : The Impact of Design. *Eur. Phys. J. - Appl. Phys.*, 43(2), 159–163. <http://doi.org/10.1049/ic:20070028>
- Shamsi-Nejad, M.-A., Nahid-Mobarakeh, B., Pierfederici, S., & Meibody-Tabar, F. (2008). Fault Tolerant and Minimum Loss Control of Double-Star Synchronous Machines Under Open Phase Conditions. *IEEE Transactions on Industrial Electronics*, 55(5), 1956–1965. <http://doi.org/10.1109/TIE.2008.918485>
- Shao, L., Hua, W., Dai, N., & Shao, L. (2016). Mathematical Modeling of a 12-Phase Machine for Wind Power Generation. *IEEE Transactions on Industrial Electronics*, 63(1), 504–516.

- Simões, M. G., & Vieira, P. (2002). A High-Torque Low-Speed Multiphase Brushless Machine — A Perspective Application for Electric Vehicles. *IEEE Transactions on Industrial Electronics*, 49(5), 1154–1164. <http://doi.org/10.1109/TIE.2002.803241>
- Subotic, I., Bodo, N., Levi, E., & Jones, M. (2015). Onboard Integrated Battery Charger for EVs Using an Asymmetrical Nine-Phase Machine. *IEEE Transactions on Industrial Electronics*, 62(5), 3285–3295. <http://doi.org/10.1109/TIE.2014.2345341>
- Sulligoi, G., & Tassarolo, A. (2009). Modeling, Simulation and Experimental Validation of a Generation System for Medium-Voltage DC Integrated Power Systems. *IEEE Transactions on Industry Applications*, 129–134.
- Sulligoi, G., & Tassarolo, A. (2013). Design and development of a medium-voltage dc generation system. *IEEE Ind. Appl. Mag.*, 19(19), 47–55. <http://doi.org/10.1109/MIAS.2012.2215643>
- Tani, A., Mengoni, M., Zarri, L., Serra, G., & Casadei, D. (2012). Control of Multiphase Induction Motors With an Odd Number of Phases Under Open-Circuit Phase Faults. *IEEE Transactions on Power Electronics*, 27(2), 565–577. <http://doi.org/10.1109/TPEL.2011.2140334>
- Tousizadeh, M., Che, H. S., Abd Rahim, N., Selvaraj, J., & Ooi, B. T. (2018). Performance Comparison of Fault-Tolerant Three-Phase Induction Motor Drives Considering Current and Voltage Limits. *IEEE Transactions on Industrial Electronics*, 66(4), 2639–2648. <http://doi.org/10.1109/TIE.2018.2850006>
- Tousizadeh, M., Che, H. S., Selvaraj, J., Abd Rahim, N., & Ooi, B. T. (2018). Fault-Tolerant Field Oriented Control of Three-Phase Induction Motor based on Unified Feed-forward Method. *IEEE Transactions on Power Electronics*, 34(8), 7172–7183. <http://doi.org/10.1109/TPEL.2018.2884759>
- Xue, X., Zhao, W., Zhu, J., Liu, G., Zhu, X., & Cheng, M. (2013). Design of Five-Phase Modular Flux-Switching Permanent-Magnet Machines for High Reliability Applications. *IEEE Transactions on Magnetics*, 49(7), 3941–3944. <http://doi.org/10.1109/TMAG.2013.2244201>
- Yepes, A. G., Riveros, J. A., Jones, M., & Levi, E. (2012). Parameter Identification of Multiphase Induction Machines With Distributed Windings — Part 1 : Sinusoidal Excitation Methods. *IEEE Transactions on Energy Conversion*, 27(4), 1056–1066. <http://doi.org/10.1109/TEC.2012.2220967>
- Zarri, L., Mengoni, M., Gritli, Y., Tani, A., Filippetti, F., Serra, G., & Casadei, D. (2013). Detection and Localization of Stator Resistance Dissymmetry Based on Multiple Reference Frame Controllers in Multiphase Induction Motor Drives. *IEEE Transactions on Industrial Electronics*, 60(8), 3506–3518. <http://doi.org/10.1109/TIE.2012.2235393>
- Zhang, G., Hua, W., Cheng, M., & Liao, J. (2016). Design and Comparison of Two Six-Phase for EV / HEV Applications. *IEEE Transactions on Industrial Electronics*, 63(1), 481–493. <http://doi.org/10.1109/TIE.2015.2447501>

- Zhao, Y., & Lipo, T. A. (1996a). Modeling and control of a multi-phase induction machine with structural unbalance - Part I. *IEEE Transactions on Energy Conversion*, 11(3), 570–577. <http://doi.org/10.1109/60.537009>
- Zhao, Y., & Lipo, T. A. (1996b). Modeling and control of a multi-phase induction machine with structural unbalance - Part II. *IEEE Transactions on Energy Conversion*, 11(3), 578–584. <http://doi.org/10.1109/60.537028>
- Zheng, L., Fletcher, J. E., & Williams, B. W. (2006). Current Optimization for a Multi-Phase Machine under an Open Circuit Phase Fault Condition. *Power Electronics, Machines and Drives, 2006. The 3rd IET International Conference on*, 2, 414–419.
- Zhou, H., Zhao, W., Liu, G., Cheng, R., & Xie, Y. (2017). Remedial Field-Oriented Control of Five-Phase Fault-Tolerant Permanent-Magnet Motor by Using Reduced-Order Transformation Matrices. *IEEE Transactions on Industrial Electronics*, 64(1), 169–178. <http://doi.org/10.1109/TIE.2016.2599501>
- Zhou, Y., Lin, X., & Cheng, M. (2016). A Fault-Tolerant Direct Torque Control for Six-Phase Permanent Magnet Synchronous Motor with Arbitrary Two Opened Phases Based on Modified Variables. *IEEE Transactions on Energy Conversion*, 31(2), 549–556. <http://doi.org/10.1109/TEC.2015.2504376>

LIST OF PUBLICATIONS AND PAPERS PRESENTED

Journal Paper

1. W.N.W.A. Munim, Mario J. Duran, Hang Seng Che, Mario Bermúdez, Ignacio Gonzáles-Prieto, Nasrudin Abd Rahim, 2017. A Unified Analysis of the Fault Tolerance Capability in Six-phase Induction Motor Drives. *IEEE Trans. on Power Electronics*. vol. 32, no. 10, pp. 7824-7836.
2. W.N.W.A. Munim, Mahdi Tousizadeh, Hang Seng Che, 2019. Effects of Zero-Sequence Transformations and Min-Max Injection on Fault-Tolerant Symmetrical Six-Phase Drives with Single Isolated Neutral. *Journal of Power Electronics*, vol. 19, no. 4, pp. 968-979.

Conference Paper

3. W.N.W.A. Munim, Hang Seng Che, Wooi Ping Hew, 2016. Fault Tolerant Capability of Symmetrical Multiphase Machines under One Open-Circuit Fault. In *4th IET International Conference on Clean Energy and Technology Conference (CEAT) 2016*, Kuala Lumpur. pp. 1-6.